THREE-DIMENSIONAL COMBUSTION CALCULATIONS

AND GRAPHIC DISPLAY

By

TZER-KUN LIN

Bachelor of Science
National Taiwan Cheng Kung University
Tainan, Taiwan, Republic of China
1985

Master of Science
Oklahoma State University
Stillwater, Oklahoma
1990

Submitted to the Faculty of the
Graduate College of the
Oklahoma State University
in partial fulfillment of
the requirements for the Degree of
DOCTOR OF PHILOSOPHY
December, 1995

THREE-DIMENSIONAL COMBUSTION CALCULATIONS

AND GRAPHIC DISPLAY

Thesis Approved :

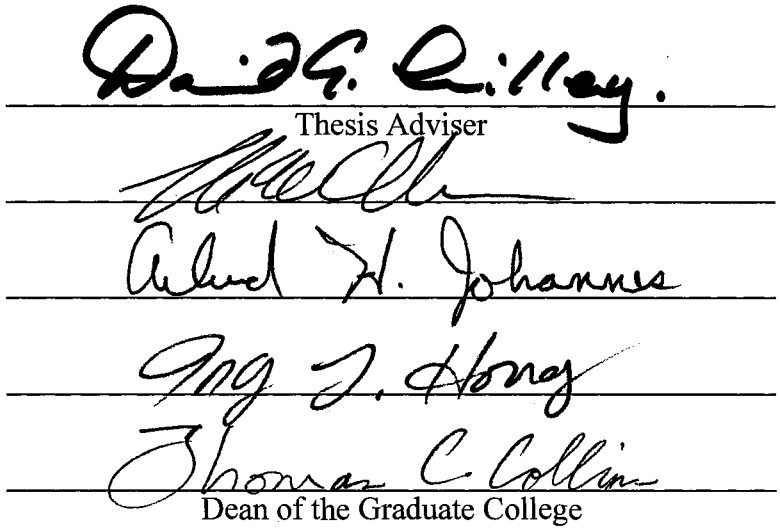

Thesis Adviser

Dean of the Graduate College

ACKNOWLEDGMENTS

I would like to express my sincere appreciation to my adviser, Dr. David G. Lilley, for his valuable suggestions and advice throughout the progress of this research. Further advice and criticism of my committee members, Dr. Ing T. Hong, Dr. Frank W. Chambers and Dr. Arland H. Johannes, are greatly acknowledged.

Moreover, I would like to express my sincere gratitude to my close friends who provided suggestions and assistance for this study : Dr. Ming-Chun Dong, Dr. Lap-Mou Tam. Dr. Ye Tian, Dr. Jiaqi Cai and Mr. Wen-Cheih Tang.

Special gratitude and appreciation is expressed to my loving wife, Chian-Huat Lee, for her support, understanding, and sacrifices throughout this whole process. I deeply appreciate the encouragement and financial support given by my parents, Mr. Lin Ging-Long and Mrs. Lin Chang Li-Hua, and my parents-in-law, Mr. Lee Khing-Piang and Mrs. Lee Juan Guan-Ayeng.

Finally, I would like to thank the School of Mechanical and Aerospace Engineering for the financial support during these four and half years of study.

TABLE OF CONTENTS

Chapter **Page**

LIST OF TABLES

LIST OF FIGURES

Figure **Page**

Figure **Page**

Figure **Page**

Figure **Page**

NOMENCLATURE

A	Area
$\mathbf{C}_p$	Specific heat
D	Divergence term in the FDE for the continuity equation
d	Jet diameter, or Equivalent jet diameter
f	Combined quantity, $f = m_{fu} - m_{air} / i$
$\mathbf{f}_\rho$	Under-relaxation factor for density
FUX~FUZ	Convection terms in FDEs for u, v, w, and s equaitons
$\mathbf{g_x}$, $\mathbf{g_y}$, $\mathbf{g_z}$	Gravitational forces in x, y and z-directions
$\mathbf{H_{fu}}$	Heat of combustion
h	Stagnation enthalpy
i	Air/Fuel stoichiometric ratio by mass (AFRs)
k	Turbulence kinetic energy per unit mass
k_u	Jet spread paramter
K_u	Jet decay parameter
m	Mass fraction
M	Molecular weight

$\mathbf{P}$	Pressure
$\mathbf{R}$	Universal gas constant
$\mathbf{R_{fu}}$, $\mathbf{R_{air}}$	Mean reaction rate of fuel and air
$\mathbf{s}$	Jet species mass fraction, or Mixture fraction
$\mathbf{S_\Phi}$	Source of general Φ variable
$\mathbf{S^u}$, $\mathbf{S^v}$, $\mathbf{S^w}$, $\mathbf{S^s}$	Linearized source terms for u, v, w and s equations
$\mathbf{T}$	Temperature
$\mathbf{t}$	Time
$\mathbf{U_{sec}}$	Inlet velocity of secondary flow
$\mathbf{U_{jet}}$	Inlet velocity of co-flowing jet
$\mathbf{V_{jet}}$	Inlet velocity of cross-flowing jet
$\mathbf{u, v, w}$	Velocity components in x, y and z directions

Greek Letters

ζ	Coefficient for upstream (donor cell) differencing
ε	Turbulence dissipation rate
Γ	Exchange coefficient in Eq. (3.1)
Δ	Increment symbol for x, y and z grid sizes, or time
∇	Laplacian operator
μ	Constant dynamic viscosity
ν_t	Turbulent kinematic viscosity

ρ	Density (constant or variable)
σ_s	Prandtl-Schmidt number, taken as 0.7
ϕ	General flow field variable
ω	Relaxation factor for over-relaxation and under-relaxation

Subscripts

e, w, n, s, i, o	Surfaces representing six sides of a cell; east, west, north, south, inner and outer surfaces
ni, no, nw, ne	
sw, se, si, so	
iw, ie, ow, oe	Locations of densities over a cell
fu, ox, pr, air	Fuel, oxygen, product and air
c, m	center and maximum
sec, jet	Secondary surrounding and jet flows, respectively
st	Stoichiometric
old, new	Old and new values of density

Superscripts

‘	New value at time $t + \Delta t$
( )	Blank subscript; old value at time t

CHAPTER I

INTRODUCTION

1.1 Three Dimensional Flow Prediction in Jets and Flames

The theoretical computation of jets and flames in co-flowing or cross-flowing streams has attracted increasing interest in combustion aerodynamics and aerothermochemistry. The requirement of increased mixing and combustion efficiency from a variety of devices in the chemical process industries has led to the need for economical and improved methods of prediction and calculation for fully three dimensional jet flows involving chemical reaction. In practical situations, system design requires costly and lengthy experimental procedures. However, it can be greatly facilitated by the availability, interpretation and understanding of calculations obtained by the use of mathematical models. For mixing problems without chemical reaction, uniform fluid distribution after the mixing of different gases is often a requirement for the operation of chemical processing equipment such as reactors, mixers, burners and heat exchangers.

Another problem associated with three-dimensional calculations is how to reduce the vast amount of computed data into easily assimilated forms. The vector display of velocities taken from two-dimensional slices through a three-dimensional mesh is not

always sufficient to form a clear picture of the complete flow pattern. Reconstructing a composite three-dimensional mental picture from a collection of two-dimensional slices is an alternative and more efficient means of displaying data.

This study is concerned with a method which, in a computer program, solves the fully three-dimensional time-dependent flow equations in cartesian coordinates. The domain is chosen via inspection of the symmetry planes associated with this situation of a round jet injection into a co-flowing stream. The idea is to simulate the mixing and possibly burning of the jet fluid with surrounding co-flowing or cross-flowing stream, and illustrate parameter effects on the flowfields. An effective three-dimensional perspective color graphic display is needed to make complex results involving hundreds of numbers easy to comprehend.

1.2 Background

Even though many practical flowfields are in axisymmetric two-dimensional flows in cylindrical polar coordinates, there are needs for fully three-dimensional flow predictions in ducts of non-circular section and non-axisymmetric boundary conditions. In practical situations there are many phenomena of this kind, for example in furnace and process industries, axisymmetric transient reciprocating engines, gas turbine combustors, downstream of the primary zone, and many combustors having air multi-inlets at discrete lateral injection locations.

If the flow does not exhibit transient features and has a predominant direction, then simplifying boundary layer approximations may be applied to reduce the complexity

of governing equations, and a forward-march solution procedure may be applied in the appropriate direction. However, if the flow exhibits transient features and does not have a predominant direction in three space directions, then a time-march solution procedure is needed since the governing equations are parabolic in the time direction, and a fully three-dimensional marching procedure must be used. This is the procedure undertaken here.

Mathematically, if the steady state is of prime importance, the governing equations are elliptic in character and a relaxation method of solution is appropriate if solving directly for the steady-state; they are parabolic in time and a marching method of solution in the time direction is appropriate if solving for the steady state via the time evolution of the transient flow process. This is the approach taken here.

1.3 Objective of the Present Study

The computer code, a version of the SOLA [1] technique, has been appropriately modified and extended so as to obtain predicted results of interest. Density variations, turbulent flow and combustion are now permitted. Density and velocity differences may exist between the primary jet (to be taken as air, methane or propane, etc.) and surrounding stream (to be taken as air), and reaction occurs in the form of physically-controlled diffusion flames where unburned fuel and oxygen cannot co-exist at the same location at the same time. A constant density 3-D laminar flow version of this code forms the starting point of this study.

The specific objectives of the present study are to simulate the mixing of the jet fluid with surrounding flow and the simple chemically reacting system of physically-controlled diffusion flames, and gain quantitative knowledge of jets and flames. The objectives of the present research are identified as :

1. To investigate flowfield predictions of jets mixing in stagnant, co-flowing and cross-flowing surroundings.
2. To investigate flowfield predictions of diffusion flames in co-flowing and cross-flowing surroundings.
3. To incorporate a turbulence model into the existing computer code, illustrating this inclusion with the two-equation k-ε model.
4. To develop an effective three dimensional perspective color graphic display for visualizing calculation results.
5. To apply the resulting computer program to practical flow problems. The simulations and accuracy of the developed computer program will be assessed via comparisons with the presently available experimental data.

1.4 Outline of the Thesis

Chapter I of this seven-chapter report is the introduction. The computations of three-dimensional flowfields with and without combustion are briefly addressed. The objectives of present study are stated in details.

Both experimental and theoretical studies of other research on three-dimensional nonreacting and reacting flows are reviewed in Chapter II. The experimental findings,

mathematical modeling efforts and computational methods are summarized in this Literature Review chapter.

Chapter III provides the governing equations, combustion simulation, numerical formulation and solution procedure adopted in the computer program of calculation.

The developments of the color graphic display are described in Chapter IV. First, the general arrangement and function are introduced, and then data file format and graph construction are documented in detail.

Applications and validations of the developed computer program are discussed in Chapter V. Six test cases are chosen and presented. Assessments are conducted by comparing the predicted results with experimental data (if available) for the first four of the test cases. The last two test cases serve to illustrate applications of the code to problems of interests to combustion engineers.

Chapter VI is the closure of this study. The conclusions of the present investigation are summarized and the recommendations for future work are briefly stated.

Tables and figures appear in Appendices A and B, respectively.

CHAPTER II

LITERATURE REVIEW

The flowfield characteristics of non-reacting and reacting flows in jets and flames have been important subjects of various experimental and numerical investigations in a variety of applications. Numerous studies about them currently exist. Recently, fully three-dimensional flows have attracted interest and been studied in depth in the field of combustion aerodynamics.

2.1 Theoretical Studies of Three-Dimensional Flow

The most useful theoretical resources that constitute the structure of the present work in the computer simulation are from the two textbooks by Gupta and Lilley [2], and by Beer and Chigier [3]. These two texts provide the detailed information of mixing and combustion processes, turbulence modeling, several numerical solution schemes of two-dimensional and three-dimensional flows, and other complexities to more practical situations. Though quite general, these can also serve as leading guides for the extension of the present study to more complex cases.

Spalding [4] numerically solved for the mixing and chemical reaction in steady confined turbulent flames, where a mixing length version of the eddy-break-up model of premixed combustion was used. Together with premixed flames, the characteristics of

turbulent diffusion flames are well presented with graphical concepts so that the structure of diffusion flames can be easily understood.

An excellent summary of combustion modeling, a review of mathematical models of turbulent flames, was also presented by Spalding [5]. He reviewed the problem of predicting turbulent diffusion flame phenomena, with special reference to the turbulent diffusion flames and the confined pre-mixed flame downstream of a flame-holder. Attention was also given to means of describing instantaneous and time-average states, and to the distinctions between the micro-scale aspects of the two flame types which permit. Concluding remarks to the turbulent combustion are of special interest to ones who are interested in the simulation of practical combustion systems.

Vatistas et al. [6] provided basic concepts for numerical prediction of fully three-dimensional transient chemically-reacting flowfields in cylindrical coordinates, without detailed turbulence modeling, which is one of the bases on which the present study is based in the simulation of chemical reaction, finite difference equations, and the solution technique.

Chigier [7] presented a review over the overall interaction between fluid mechanics and combustion, which describes the very broad spectrum of combustion systems and identifies the special role played by fluid mechanics in controlling and influencing the combustion process. Since most practical combustion systems have turbulent flows and are mixing controlled, understanding of the detailed flow structure within combustion chambers will be aided by this review paper.

2.2 Experimental Measurements

Wohl et al. [8] conducted an experiment study for diffusion flames in laminar and turbulent flows rising vertically from a tube, where laminar flames with velocities above 2 fps and turbulent flames with velocities above 100 fps were investigated. Their experimental data and photographs, together with the general theory of diffusion flames and flame structure, are particularly useful to numerical investigators because physical structures and phenomena of diffusion flames are clearly shown with ready explanations.

Kremer [9] used the experimental burner with variable slot width and length to study plane, isothermal turbulent air jets and a vertically burning, plane turbulent city-gas flame. The measurements include momentum and nozzle gas-mass fluxes distributions with air and fuel jets which serves to evaluate momentum and mass transfer coefficients appearing in the Richardt's similarity theory.

Experiments on turbulent circular jets issuing vertically into a cross-flow (with velocities ranged from 20 to 30 fps), both for heated unheated jets (hotter than the free stream) were made by Kamotani and Greber [10] in a 28 inch square cross section wind tunnel with the jet nozzle of diameter of 0.25 inch. Longitudinal and transverse distributions of velocity, temperature, and turbulence intensity were presented for different ratios of the jet momentum flux to the freestream momentum flux. They concluded that the jet velocity and temperature trajectories are mainly determined by the jet-to-crossflowing momentum ratio, and that a pair of vortices forms behind the jet soon after it emerges from the nozzle and strongly interacts with the jet.

The effects of velocity ratios of jets to external flow was experimentally investigated by Kent and Bilger [11]. They measured concentrations, temperatures, velocities, and turbulence levels, under the conditions that buoyancy effects are negligible and that the flames are essentially unconfined because the tunnel cross section is large enough. They concluded that the velocity field is very sensitive to the concentration field in the outer part of the flow, where the density gradients and fluctuations are steepest.

Velocity field measurements were made by Fearn and Weston [12] to relate the velocity field to empirical values for the strength and location of the pair of contra-rotating vortices associated with the jet. The experimental investigation was conducted in a wind tunnel with the test section of 14.5 ft by 21 ft in dimensions. Test section air speeds ranged from 100-170 feet per second (fps). The jet of air was formed by a converging nozzle designed to provide a flat velocity profile at the 4 inch diameter nozzle exit. They found that the vortex pair is formed very close to the jet orifice as relatively concentrated vortices with an initial strength that is directly proportional to the speed of the jet at the orifice and to the diameter of the jet.

So far, two texts, one is written by Libby and Williams [13] and the other is written by Schetz [14], provide numerous valuable materials of jet mixing and reacting flows, which are also of great use to the present study.

2.3 Predictions of Three-Dimensional Flow

Spalding [5] calculated concentration fluctuations for an axisymmetric round turbulent jet injected into stagnant surroundings of substantially the same density, where

the RMS (Root-Mean Square) fluctuating concentration was supposed to obey a parabolic differential equation containing terms for convection, diffusion, generation, and dissipation. The profiles of concentration fluctuations and related quantities are compared with previous experimental data.

Pantankar and Spalding [15] presented the development of a computer program (called Mammoth If) for the prediction of the flow, heat transfer, and combustion process in 3-D furnaces, where the mathematical model involves the solution of the differential equations for momentum, continuity, chemical species concentrations, stagnation enthalpy, radiation fluxes, turbulence quantities, and concentration of particles in various size ranges. Their conclusions showed that substantial progress had been made towards the development of a mathematical model for the transfer of heat in furnaces. However, they suggested further research on the validation of the mathematical model and the elementary processes of radiation absorption, particle-size growth, etc., which the more complex of the furnace calculations will require as an input.

Abou et al. [16] developed a numerical technique for solving 3-D turbulent reacting flows of diffusion flames in two kinds of rectangular furnaces (Gaz de France and IFRF). They employed the turbulence model of the two-equation variety and a flux model for the thermal radiation. They calculated distributions of velocity, temperature, and H_2O concentrations in axial and lateral locations, and compared these with previous experimental data. Their two validation tests show that predictions and experiments are in good agreement.

Another valuable prediction of turbulent chemically-reacting flows of diffusion flames was made by Edelman and Harsha [17] in an axisymmetric chamber for the reactions of H_2 jets with air streams, with emphasis on the detailed prediction of reacting jet flows coupling models of turbulent mixing process with a detailed finite-rate kinetics scheme. Several turbulence models of a reacting hydrogen-air jet are presented, with the comparison of predicted results to previous works. They recommended a two-equation turbulence model because that the accuracy of the one-equation model depends on a judicious choice of the turbulence length scale distribution. Also, an efficient kinetics calculation for a hydrocarbon system using the quasiglobal concept is discussed, and results obtained with an advanced quasiglobal model for the higher hydrocarbons are described.

Birch et al. [18] investigated both numerically and experimentally the use of 3-D compressible parabolic turbulent flow analysis for the design of an internal mixer for jet noise suppression. Three flows, a full-scale free mixer, a full-scale lobed mixer, and a model-scale lobed mixer, were selected and studied. Contour maps of the nozzle exit velocity and total temperature distributions are presented well for each of the three mixers. Their numerical analysis shows fair agreement with model-scale test as a simulation of the full-scale flow.

Using a two-dimensional axisymmetric boundary layer code, Ha and Lilley [19] conducted numerical experiments on turbulent non-reacting round free jets in co-flowing streams, with the PML (Prandtl Mixing Length) turbulence model. Results of the parametric study are presented to show the influences of several parameters on the

flowfield, which are effects of PML parameters, Schmidt numbers, surrounding-to-jet velocity ratios, and surrounding-to-jet density ratios. Their predicted results confirm previous findings fairly well, and the PML model of turbulence is shown to be adequate for simulation of the mixing problem of boundary-layer type flows.

A prediction of turbulent 3-D jet flows in co-flowing and cross-flowing streams in a rectangular duct was reported by Karki et al. [20], in which computations were performed with two numerical schemes for convection terms, Power-law and Flux-spline schemes, on two grid systems, coarse and fine grid systems. Discussions of the accuracy of computations and the comparison of velocity profiles with previous experimental results are included in details. Numerical schemes for 2-D and 3-D laminar and turbulent flows are also provided with several test cases.

Ha and Lilley [21] extended their previous work [22] to deal with a simple chemical reaction (premixed flames) with typical hydrocarbon fuels burning in air, where dissociation effects are included in a simple manner. Results showing the effects of strategic parameters on the resulting jets in co-flowing surroundings are tabulated, plotted, and discussed. They confirmed and extended the limited theoretical deductions available from previous empirical data.

Weathers [23] conducted a numerical investigation of 3-D turbulent, buoyant air flows of constant density in a rectangular room, with the imposition of wall functions and low-Reynolds model in conjunction with the k-ε turbulence model. He presented the results in graphical ways and compared with experimental flow patterns, for various investigation parameters (flow rates, flow types, wall boundary conditions, and inlet

profiles). Results show, in general, better consistency with experimental flow patterns when using the low-Reynolds k-ε model and approximated non-uniform inlet velocity profiles.

2.4 Turbulence Modeling

The first move towards a model of turbulence can be attributed to Boussinesq [24]. He suggested that the effective turbulent shear stress, arising from the cross-correlation of fluctuating velocities, could be replaced by the product of the mean velocity gradient and a quantity termed the "turbulent viscosity". The introduction of ν_t provides a framework for constructing a turbulence model; for there remains the task of expressing the turbulent viscosity in terms of known or calculable quantities.

The simplest of all turbulence models are known as algebraic models. These models and variants were proposed by Prandtl [25], Von Kármán [26], Clauser [27], Mellor [28] and many others. These models use the Boussinesq eddy-viscosity approximation to compute the Reynolds stress tensor as the product of an eddy viscosity and the mean strain-rate tensor. For computational simplicity, the eddy viscosity is often computed in terms of a mixing length that is analogous to the mean free path in a gas. Because the eddy viscosity and mixing length depend upon the particular flow under consideration they must be specified in advance. These models will work well only for the flows for which they have been fine tuned. There is very little hope of extrapolating beyond the established data base for which an algebraic model is calibrated.

The turbulence models based upon the equation for the turbulence kinetic energy have became the cornerstone of modern turbulence modeling research. There are two types of turbulence energy models, one-equation models and two-equation models, which both retain the Boussinesq eddy-viscosity approximation; but differ in one important respect.

One-equation models are incomplete as they relate the turbulence length scale to some typical flow dimension. Such models were proposed and derived by Prandtl [29], Kolmogorov [30], Nee and Kovaszay [31], Bradshaw et al. [32], Baldwin and Barth [33], and several others. In most circumstances, one-equation models are only marginally superior to the mixing-length model.

By contrast, two-equation models provide an equation for the turbulence length scale and are thus complete. By far, the most popular two-equation model is the k-ε model. The earliest development efforts based on this model were those of Chou [34], Davidov [35], and Harlow and Nakayama [36]. The central paper is published by Jones and Launder [37] and the model is so well known that is often referred to as the standard k-ε model. Improved accuracy is obtained in comparison to less-complicated models. Researchers investigating some of the primary two-equation models have discovered that only the k-ε model yields experimentally substantiated results for regions far from solid boundaries or walls [38]. For the other models to match the results, it was found necessary to replace some of the constants with empirical functions which added to the complexity of the models.

Since the emergence of the k-ε turbulence model, numerous researchers have introduced modifications to the basic models, particularly in an attempt to accurately predict near-wall and low-Reynolds number turbulent flow with varying degrees of success. They are Lam and Bremhorst [39] , Dutoya-Michard [40], Hassid-Poreh [41] and many others, see Ref. [42].

In this study, consideration is given to the simulation of unconfined jets and flames in co-flowing and cross-flowing streams. The standard k-ε model is used in this study. This turbulence models review is for information. The present study identifies how the k-ε two-equation model of turbulence may be incorporated into the framework of the 3-D computational code. Incorporation of more advanced turbulence models into the computer codes can be implemented in later studies.

CHAPTER III

DEVELOPMENT OF THREE DIMENSIONAL COMBUSTION FLOW CALCULATION PROGRAM (3DCC)

3.1 Governing Equations

In the modeling and prediction of mixing and combustion flowfields, the problem is simulated by simultaneous nonlinear partial differential equations. These equations express mathematically appropriate conservation laws for mass, momentum, species diffusion, turbulent kinetic energy and turbulence dissipation rate. Each of these transport equations contains similar terms for the convection, diffusion (via effective flux term) and source terms of a general flowfield variable ϕ. Introduction of turbulent exchange coefficients Γ_ϕ and the usual turbulent diffusion-flux laws provides a similarity in the form among all the governing partial differential equations. This similarity allows them to be put in the common form and solved in a similar manner in cartesian coordinates as :

$$\frac{\partial}{\partial t}(\rho\phi)+\frac{\partial}{\partial x}(\rho u\phi)+\frac{\partial}{\partial y}(\rho v\phi)+\frac{\partial}{\partial z}(\rho w\phi)=\nabla\left(\Gamma_\phi\nabla\phi\right)+S_\phi \qquad (3.1)$$

where ϕ is one of the dependent variables (1, u, v, w, k, ε and s), and the corresponding values of the exchange coefficient Γ_ϕ and the source term S_ϕ are indicated in Table 1-a

and 1-b for turbulent jet flows simulated via a constant large viscosity and a two-equation turbulence model, respectively.

Note that u, v and w are velocity components in the x, y and z directions (respectively); k is turbulent kinetic energy; ε is turbulence dissipation rate; and s is the mass fraction of jet species m_{jet} of density ρ_{jet}. Figure 1 shows a schematic of the physical problem for a two-fluid (or two-species) situation, where the two fluids are referred to as "jet" and "sec" (secondary). The local mass fraction m_{jet} (equal to the variable s) of fluid of density ρ_{jet} allows the local density to be found using

$$m_{jet} + m_{sec} = 1 \tag{3.2}$$

$$\rho = m_{jet}\rho_{jet} + m_{sec}\rho_{sec} \tag{3.3}$$

when the jet and surrounding have different densities. Here, m_{sec} and ρ_{sec} stand for mass fraction and density of secondary fluid. In the combustion simulation used in this study, a three-component situation is used with a three-fluid simulation and Eqs. (3.2) and (3.3) are replaced as described in section 3.2. Figure 2 shows a schematic of the domain overlaid with a uniform rectangular grid system.

On the question of turbulence modeling, turbulent flow has two primary characteristics, random and chaotic fluctuations in the fluid's velocity, and intense mixing on the macroscopic level. These fluctuations and mixing create a fluid motion so complex that the exact details of the motion are indeterminable by a direct analytic approach. Therefore, solutions are usually concerned only with the time-averaged effects of turbulent flow. Thus, a turbulence model means a set of equations which, when solved

with the mean-flow equations, allows calculation of the relevant correlations and so simulates the behavior of real fluids in important respects.

Numerous models have been introduced through years, with varying degrees of success. The success of a model is determined by the following criteria :

1. Width of applicability - The model must be capable of being implemented to serve over the complete range of geometries and other parameters for the problem.
2. Accuracy - The model must be capable of providing solutions which are within tolerable bounds of accepted experimental results.
3. Simplicity and economy - Although computational capabilities have significantly increased, overly-complex models may increase the manpower and required computing time beyond the limits of feasibility.

For the predictions of turbulence flow, standard texts indicate that the time-mean behavior or certain turbulent jet flows may be simulated via a constant large viscosity. This is the approach taken when the turbulence model option is not chosen in the finally-developed program. That such a value is appropriate for a round turbulent free jet and is well known [2, 24, 25]. It is asserted that the turbulent viscosity in a round free jet in stagnant surroundings is approximately constant and given by

$$\nu_t = 0.00196\ (x + a)\ u_m \tag{3.4}$$

in terms of station maximum axial velocity U_m. In terms of jet initial velocity u_{jet}, and correcting for the co-flowing velocity u_{sec} and cross-flowing velocity V_{jet}, it is anticipated that this can be written for the present study as

$$\nu_t = 0.00196 \cdot A \cdot (u_{jet} - u_{sec}) \cdot d \qquad \text{for co-flowing flows,} \qquad (3.5a)$$

$$\nu_t = 0.00196 \cdot A \cdot V_{jet} \cdot d \qquad \text{for cross-flowing flows,} \qquad (3.5b)$$

where A is an empirical constant (equal to approximately 6.8 found in experiments for jet flows into stagnant surroundings of the same density, see Ref. [19]) and d is the jet diameter. Other experimenters discussed in Ref. [19] quote values of A from 5.9 to 6.4 depending upon jet exit conditions. An indication of how susceptible computed results are to this choice of value given to the constant turbulent viscosity may be found via computer experimentation.

To define the effective exchange coefficients Γ_ϕ in the standard k-ε turbulence model, the turbulent or eddy viscosity concept, given in Reynolds transport equations, may be suitably generalized to the multi-component system equations. The flux-gradient transport laws of Newton, Fourier and Fick for momentum, heat and mass transfer provided most useful unifying assumptions. In the multi-component flow case, the analogy in the form to the single-component flow leads to the effective exchange coefficient μ (effective viscosity) and Γ_ϕ being defined. These effective exchange coefficients are composed of laminar and turbulent parts :

$$\mu = \mu_{lam.} + \mu_{turb.} \qquad (3.6)$$

$$\Gamma_\phi = \Gamma_{\phi\,lam.} + \Gamma_{\phi\,turb.} \qquad (3.7)$$

To describe the turbulent transport, the standard two-equation k-ε turbulence model (which is widely used for turbulence prediction because it is moderate in complexity and is considered to be superior to other models having a similar degree of complexity) is used, whereby the turbulent viscosity, $\mu_{turb.}$, is calculated from

$$\mu_{turb.} = C_\mu \rho \frac{k^2}{\varepsilon} \tag{3.8}$$

and two differential equations are solved for the two turbulence quantities k and ε. Schmidt numbers for these two turbulence equations are generally taken as

$\sigma_k = 1.0$

$\sigma_\varepsilon = 1.3$

and the final turbulence constant is taken as

$C_\mu = 0.09$

The kinetic energy and dissipation rate at the inlet are determined form the following equations which were recommended by Ref. [45] :

$$k_{in} = \frac{3}{2} I_u^2 U_{in}^2 \tag{3.9}$$

$$\varepsilon_{in} = \frac{k_{in}^{1.5}}{\lambda H} \tag{3.10}$$

where I_u = turbulence intensity of the U velocity taken as 0.15 (15%)

λ = the length scale taken as 0.03 (3%)

H = the characteristic dimension of the flow passage

Different values of k_{in} and ε_{in} have been shown to have little effect on the results of simulations [43].

3.2 Combustion Simulation

The conservation equations of stagnation enthalpy and chemical species mass fraction are not completely closed forms since the density and mass rate of creation or destruction of species are unknown. The values must specified prior to the solution of the

equations, so that introduction of chemical reaction model and thermodynamic considerations provide the necessary extra information to close the system.

In a multi-component system, simplifications can be introduced through the use of the concept of a simple chemically-reacting system (SCRS) to reduce the number of chemical species equations to solve [2]. The SCRS is defined as follows :

1. To reduce the number of chemical species PDEs, consideration is given to a simplified main exothermic reaction between just two species (fuel and air), combining with a stoichiometric air/fuel mass ratio of i to form product plus release of energy by fuel burning, which a finite rate chemistry assumption. Only the fuel is supposed to possess a heat of combustion H_{fu}(J/kg).

$$1\ \text{kg fuel} + i\ \text{kg air} \longrightarrow (1+i)\ \text{kg product} + H_{fu} \tag{3.11}$$

$$h = C_p T + H_{fu}\, m_{fu} + V^2/2 \tag{3.12}$$

$$m_{fu} + m_{air} + m_{pr} = 1 \tag{3.13}$$

For a simple chemical reaction, the rates of reaction of fuel and air are closely related; for every 1 kg of fuel burning , i kg of air also burns. Thus,

$$R_{fu} = R_{air} / i \tag{3.14}$$

and the combined concentration quantity may readily be deduced by eliminating the source term from the governing PDEs for fuel and air.

$$f = m_{fu} - m_{air} / i \qquad \text{(conserved property)} \tag{3.15}$$

2. The exchange coefficients are equal to each other at each point.

$$\Gamma_{fu} = \Gamma_{air} = \Gamma_{pr} = \Gamma_h = \Gamma_f = \mu / \sigma_i \tag{3.16}$$

3. The specific heats C_p of all species are equal to each other, and independent of T.

Most furnace and engine flames are physically-controlled diffusion flames, which means that their outward characteristics, such as temperature distribution, can be computed without knowledge of the detailed reaction-kinetic constants. When fuel and air are injected separately, the rate of mixing and therefore the total rate of controlling process are slow in comparison to the rate of reaction that the chemical-kinetic process can achieve as the completion of the reaction process. Therefore, thermodynamic equilibrium prevails throughout and a further simplification to the mathematical simulation is possible because unburned fuel and air can not co-exist at the same position at the same time. Hence the mixture consists of either fuel and products, or air and products at any position in the flowfield. In expression of the combined concentration quantity f, it is

$f \geq 0$; $m_{air} = 0$ and $m_{fu} = f$

$f \leq 0$; $m_{fu} = 0$ and $m_{air} = -i \cdot f$

The flame region is very thin and occurs over the surface where f = 0. The reaction problem is now essentially a two-component system and hence solution of just two PDEs for f and h characterizes the problem. That is,

$$m_{pr} = 1 - m_{ox} - m_{fu} \tag{3.17}$$

$$T = (h - H_{fu} m_{fu} - V^2/2) / C_p \tag{3.18}$$

$$\rho = P M / (R T) \tag{3.19}$$

where m_{ox} ($= 0.232\, m_{air}$) and m_{fu} are deduced from f

$$\frac{1}{M} = \sum_j \frac{m_j}{M_j} \tag{3.20}$$

R = universal gas constant

Now, consideration is given to a fast reacting SCRS in a steady flow process in which fuel and air enter via separate inlets, then mix and react in an adiabatic impervious combustor and exit through a common outlet. If the kinetic energy contribution to h is neglected, i.e. $h = C_p T + H_{fu} m_{fu}$, then m_{fu}, m_{air}, m_{pr}, h and T are all linearly related to the single variable f, inlet and outlet conditions are derived as follows :

Inlet fuel;

$m_{fu} = 1$
$m_{air} = 0$
$T = T_{fu}$
$h = h_{fu} = C_p T_{fu} + H_{fu} m_{fu}$
$f = m_{fu} = 1$
$s = 1$

Inlet air;

$m_{fu} = 0$
$m_{air} = 1$
$T = T_{air}$
$h = h_{air} = C_p T_{air}$
$f = -m_{air}/ i = -1/i$
$s = 0$

where s is defined as the mixture fraction via the normalized value of f, i.e.

$$s = \frac{f - f_{air}}{f_{fu} - f_{air}} = \frac{m_{fu} - m_{air}/i + 1/i}{1 + 1/i} \tag{3.21}$$

so that its value is 0 in the inlet air stream and 1 in the inlet fuel stream. By the linearity between f and h in these circumstances, s is also related to h, via

$$s = \frac{h - h_{air}}{h_{fu} - h_{air}} \tag{3.22}$$

The s_{st} value corresponding to the stoichiometric f = 0 value is simply

$$s_{st} = \frac{1}{1 + i} \tag{3.23}$$

where i is the stoichiometric air/fuel mass ratio.

The mixture fraction s can then be written in terms of s_{st} as :

$$s = s_{st} (i\, m_{fu} - m_{air} + 1) \tag{3.24}$$

And corresponding h_{st} and T_{st} at the stoichiometric(f = 0) values are :

$$s_{st} = \frac{h_{st} - h_{air}}{h_{fu} - h_{air}} = \frac{1}{1+i} \tag{3.25}$$

from which

$$\begin{aligned} hst &= h_{air} + s_{st} (h_{fu} - h_{air}) \\ &= C_p T_{air} + S_{st} (C_p T_{fu} + H_{fu} - C_p T_{air}) \\ &= s_{st} (C_p T_{fu} + H_{fu} + i C_p T_{air}) \end{aligned} \tag{3.26}$$

and hence

$$T_{st} = s_{st} (T_{fu} + i T_{air} + H_{fu} / C_p) \tag{3.27}$$

which is the Adiabatic Flame Temperature (AFT).

The linear relationship between the instantaneous mass fractions of fuel and oxidant and s is shown in Figures 3 and 4 for the nonreacting flow ($H_{fu} = 0$) and reacting flow ($H_{fu} \neq 0$), respectively. These figures are specific examples for the case of the inlet temperatures of the fuel and air streams being 300 K and 450 K, respectively. The magnitudes will change if the inlet temperatures and/or the specific heat C_p is changed. The computer program takes proper account of the parameters and calculation based on the above equations, not the specific values from Figures 3 and 4. These are all related to mixture fraction (s) and hence the flame is actually divided into two regions :

1. The first region of the flame is the one where the oxidant and the products co-exist, i.e.

$$0 < s < s_{st}$$
$$m_{fu} = 0$$
$$m_{air} = (s_{st} - s) / s_{st}$$
$$T = \frac{T_{air}(s_{st} - s) + T_{st}\, s}{s_{st}} \tag{3.28}$$

2. The second region is the one where the fuel and the products co-exist, i.e.

$$s_{st} < s < 1$$
$$m_{air} = 0$$
$$m_{fu} = (s - s_{st}) / (1 - s_{st})$$
$$T = \frac{T_{fu}(s - s_{st}) + T_{st}\,(1 - s)}{1 - s_{st}} \tag{3.29}$$

3.3 Numerical Formulation

The rectangular three-dimensional region to be considered is divided into rectangular cell divisions, with uniform Δx, Δy and Δz spacings. This solution domain is complemented by a layer of cell on all sides, so as to allow easy simulation of the required boundary conditions. These fictitious cells increase the total number of cells in each direction. Figure 2 illustrates the total mesh arrangement with a coarse grid, showing 20, 8 and 8 internal cell divisions in directions x, y and z, respectively. Appropriate specification of the spacings and I, J, K limits can assign the solution domain size. Also, the inlet velocities and species mass fractions can be specified on the cells with I=1 via observation of the zy-section and inlet plane information required from Fig. 2. Figure 5 portrays a single cell and shows the location of each field variable p, u, v, w

and s relative to this (I,J,K)-cell. Notice that p and s are cell centered. Velocities are located on the faces of the cell such that appropriate pressure gradients in their differential equations are readily found.

Notice that in Fig. 5 that the u, v and w velocities are located, respectively, on the right, top and back faces of the cell, touching the I+1, j+1, and k+1 cells, respectively. Emphasizing this

u_{ijk} = x-direction velocity located at center of right face of the (i,j,k)-cell touching the (i+1,j,k)-cell

v_{ijk} = y-direction velocity located at center of top face of the (i,j,k)-cell touching the (i,j+1,k)-cell

w_{ijk} = z-direction velocity located at center of back face of the (i,j,k)-cell touching the (i,j,k+1)-cell

Notice also that normal velocities lie directly on the physical boundaries of the solution domain, while the tangential velocities and pressure are displaced half a cell interval inside the flowfield. In this way the exterior fictitious cells are particularly convenient when applying the boundary conditions.

Figures 1 and 2 also represent the physical problem of the application of the 3-D procedure to the flowfield downstream of the injection of a jet (with velocity $U = U_{jet}$ and jet fluid mass fraction s = 1) into a secondary flow jet (with velocity $U = U_{sec}$ and s = 0). This specification occurs in the boundary conditions section of the computer code.

Finite difference equations simulating the problem are set up and solved by way of a time-march process applied to cells within the flow domain of interest. Cells touching the boundary thus utilize the value on the boundary (in the case of a normal velocity) or values half a cell distant beyond the boundary (in the case of tangential velocities and jet species mass fraction s).

Interior normal velocity calculations take the zero normal wall values, the given normal inlet values, on the yet-to-be-determined outlet values as appropriate boundary conditions during their calculations. Interior tangential velocity calculations use the fictitious values which are placed in the surrounding layer of complementary cells. Specification of these is after each time-step and after each sweep of the cells during the pressure iteration. With a coarse grid near wall boundaries, free-slip boundary conditions are appropriate for tangential velocities, and external values are set equal to their associated immediately interior values. On the other hand, with a fine grid computing through the boundary layer near wall boundaries, no-slip boundary conditions are appropriate and the tangential velocities and external values are set equal to the negative of their associated immediately interior values.

Specification of normal velocities at an outflow boundary often poses a problem, as it can have detrimental upstream influence. One might merely impose the zero-normal gradient or continuative condition and set these values equal to their immediately upstream values. When primary interest is being focused on the final steady-state solution, it has been found that a suitable constant may be added to each such extrapolated value, with advantage to the rapidity of convergence. This constant value is

chosen so as to make the total outlet flux equal to the total inlet flux, thus ensuring the requirement of a macroscropic mass balance. Outlet boundary specification is imposed only after each time-step and not after each pass through the mesh during the pressure-velocity iteration.

At planes of symmetry the usual zero normal velocity and free-slip tangential velocity specification are applicable. In the present problem, this applies to the top, bottom, front and back faces of the flow domain.

3.4 Solution Procedure

Finite difference representations are required of the governing partial differential equations. The usual intuitive estimates of one-sided first-derivatives, centered first-derivatives and centered second-derivatives are used in representing terms in the momentum equations. The symbols ϕ^o and ϕ are used to denote values of the general variable ϕ at the old time-level t and the new time-level $t+\Delta t$, respectively. Simple explicit time-stepping equations are deducible that enable one such forward time-step to be accomplished. Thus, starting from initial field values throughout the domain of interest, a time-march process is used so as to advance toward the final steady-state solution, which is usually of special interest as opposed to the en route calculations. In Eq. (3.1) the time-derivatives are approximated by forward one-sided derivatives; most spatial derivatives are approximated by central differences based on values at time-level t. Special techniques are required in computational fluid dynamics, however, in the

representation of the convection terms, and a certain amount of upstream differencing is required.

The difference equations representing the partial differential equations may be written explicitly as :

$$\phi = \phi^o + \Delta t\ (....) \tag{3.30}$$

where ϕ = u, v, w, k, ε and m_j. Convection, diffusion and source terms occur in the parentheses on the right hand side. These terms are obtained in a straightforward but tedious manner as 3-D versions of the 2-D versions given in Ref. [1]. In all these forward marching equations, donor cell differencing is used with the convection terms. In this, a coefficient α takes a constant value between 0 and 1, so giving the desired amount of upstream differencing. A value of 0 gives merely central differencing as in the original MAC code and numerical instability problems arise; a value of 1 gives the full upstream or donor cell method which, although less accurate, is stable provided among other things that the fluid is not allowed to pass through more than one cell in one time-step.

Although Eq. (3.28) accomplishes one forward time-step based on conservation of momentum principles, the newly calculated velocities will not, in general, satisfy the continuity requirement. This continuity condition is imposed by iteratively adjusting the cell pressure and the cell's six local normal velocities. Pressure and velocity update iteration continues until the cell mass flow balances of all the cells are less than some prescribed small positive quantity. After this continuity equation is sufficiently well satisfied, the values are accepted as new-time values and preparation for the next step of the time-march can begin.

3.5 Output Data File for Results and Graphics

During the calculation stage, pressure p and mass fraction s and most other variables are cell-centered, while velocities u, v, and w are located on the faces of the cell. The main output file for results is typically called 3DCC.OUT. It contains headings, input data and tabular data of the results. The other output file contains results of the calculation in a form readable directly by the color graphic display program 3DGD, which is described in Chapter IV. The data sent into the file to be read by the color graphic display program are consistently at the same locations. This requires simple interpolation so that all variables are given values at the extreme corner of each cell. Thus all variables to be plotted are located at the same (x, y, z) points covering the solution domain. The data file with these values is typically called 3DCC.DAT and is read directly by the color graphic display program 3DGD.

CHAPTER IV

DEVELOPMENT OF COLOR GRAPHIC DISPLAY PROGRAM

4.1 General arrangement / User's Guide

The graphic display program 3DGD (3-D Graphics Display) has been written (in C++ programming language) primarily with a view to maximizing ease of use and ease of interpretation of the three-dimensional flowfield calculation results. Ease of use is achieved by having an interactive user interface which permits easy specification of the particular data file to use and easy specification of display parameters. Ease of interpretation is enhanced by the availability of generating color-coded line contours and contour maps.

When 3DGD is activated, the user is given an integrated enviroment shown as Figure 6. The menu bar at the top is the primary access to the menu commands. The only time the menu bar is not visible is when the user viewing the graphic information. If a menu command is followed by an ellipsis mark (...), choosing the command displays a dialog box. A dialog box is a convient way to view and set multiple options. If the command is followed by an arrow (↓), the command leads to another menu (a pop-up menu). A command without either an ellipsis mark or an arrow indicates that once the user chooses it, that action occurs.

The menus in the menu bar and its menu commands are described as following :

1. File menu The File menu lets the user open a prepared data file to read and lets the user quit the program.

   a) Open The File|Open command displays a file-selection dialog box as shown in Figure 7 for the user to select a data file to open and read. The dialog box contains an input box, a file list, buttons labeled Open, and Cancel, and an information panel describes the selected file. The user can type in either a full file name or a file name with wildcards, which filters the file list to match the user's specifications. Pressing (↓) key will let the user to choose a file specification from a history list of file specifications entered earlier.

   b) Change dir The File|Change Dir command lets the user specify a drive and a directory to make current. The current directory is the one 3DGD uses to look for data files. The Change Directory dialog box is shown as Figure 8.

   c) Quit The File|Quit command exits 3DGD, removes it from memory, and returns to the DOS command line.

2. View menu The View menu lets the user choose one of the two types of color coded illustrations, which are either "Line Contours" or "Contour Maps". Then the pop-up sub-menu will appear to allow the users to choose cross-section planes in either yx-planes or yz-planes. After viewing, pressing any key will exit the graphic mode and return to the integrated environment for further action. Figure 9 shows the View menu and its menu items with pop-up sub-menus.

3. Variables menu The Variables menu lets the user choose among currently available variables, like dimensionless u, v, w, s, and p, within the opened data file.

   a) Choose The Variables|Choose command displays the Variable selection dialog box shown as Figure 10, which lets the user choos among listed data groups.

4. Change menu The Change menu displays the "Graphic Display Option" dialog box, which allows the user to change the numerical interval value for the color contour levels and specify the desired location of cross-section planes for plotting. The user can select the item to change with mouse click on the input box and input with desired numerical value, and then choose "OK" button to finish the modification task.

5. Display The Display menu lets the user specify color display or gray-scaled display for graph itself and notation text. This feature is useful to get gray-scaled picture when color printer is not available.

   a) Character The Display|Character menu command displays the "Color/Mono Option" dialog box shown as Figure 12 Part (a), which allows the user to choose display option for notation text .

   b) Graphic The Display|Graphic menu command displays the "Color/Mono Option" dialog box shown as Figure 12 Part (b), which allows the user to choose display option for contour lines and maps.

4.2 Input Data File Format

The execution of the three dimensional combustion flow calculation program essentially generates two output files as described in Section 3.5. One of these files, called 3DCC.DAT contains results of calculation in a form which is read directly by the color graphic display prgoram 3DGD. This data file 3DCC.DAT is written in an ASCII (American Standard Code for Information Interchange) format. Although data files of this type take more storage space and accessing time as compared with files of binary type, it can be accessed by most other programs as necessary.

A typical data file is listed in Appendix C. The first line in the typical data file starts with three integer and three real numbers which represent numbers of cells (including surrounded fictitious cells) and solution domain sizes in x, y and z direction of the three dimensional region, respectively. The following lines are numbers which indicate each grid location in x direction in sequence. Then the respective grid locations in y and z direction are listed as well. The rest of the data file is composed of data groups from calculated result. For each data group, heading of the calculation variable is written at the first line while variable values are listed point by point throughout the three dimensional region.

4.3 Graph Construction

The color graphics program 3DGD reads the prepared file 3DCC.DAT to obtain the locations x, y, z and values of the variables u, v, w, p, s at these locations. The task of 3DGD is to present this information pictorially on the monitor, including drawing color-

coded lines of constant values (iso-lines) or color shading between these lines. The chosen variable is shown graphically at three longitudinal slices or four lateral cross-section planes via either color-coded line contours or contour maps in yx-planes or yz-planes, respectively. Each cross-section plane is shown in the three dimensional view at the top of the figure with two dimensional line contours or contour maps shown below. The desired location of each cross-section plane within the three dimensional solution domain can be easily specified by the user as necessary. This flexible feature provides the user with a comprehensive insight into the problem and is especially useful during the debugging stage of the application. By default, the color scale indicator is ranged from 0.0 to 1.0 and re-used for values above 1.0 and below 0.0 with the same indicated interval. Modification with regard to scaling may be necessary, and the equal-spaced interval value could be easily specified by the user.

Basically, the graphic interpretation on the monitor requires two dimensional translation and scaling to effect the mapping from solution coordinates (x,y) to screen coordinates (X,Y). Then the equations of the two dimensional transformation can be written as :

$$X = D_x + S_x \cdot x \tag{4.1}$$

$$Y = D_y + S_y \cdot y \tag{4.2}$$

where (D_x , D_y) are translation factors and (S_x , S_y) are scaling factors.

Inside the 3DGD program code, two subroutines named WINDOW and VIEW are written for the arrangement of two dimensional translation and scaling factors. The

WINDOW subroutine takes four arguments which are X_{min}, Y_{min}, X_{max} and Y_{max} to define a rectangular region in the screen coordinates shown as Figure 13. Notice that the direction of Y axis is downward. On the other hand, the VIEW subroutine defines the same region in the solution coordinates with another four arguments which are x_1, y_1, x_2, and y_2 shown in Figure 13 as well. Therefore, we can write the two dimensional transformation factors for translation and scaling as :

$$S_x = \frac{X_{min} - X_{max}}{x_1 - x_2} \cdot GS_x \tag{4.3}$$

$$S_y = -\frac{Y_{min} - Y_{max}}{y_1 - y_2} \cdot GS_y \tag{4.4}$$

$$D_x = X_{min} - x_1 \cdot S_x \tag{4.5}$$

$$D_y = Y_{min} - y_1 \cdot S_y \tag{4.6}$$

Note that, except for the high resolution mode which is setup to have square pixels, the characteristics of personal computer displays are such that unit pixel dimensions are different along the x and y axes. Therefore, the GS_x and GS_y factors are applied to obtain the same unit length in both axes as necessary.

Based on the two dimensional mapping, the cross-section plane within the three dimensional fluid region will be plotted on the screen by filling it with color pixels, each different color signifying the range within which the local value of the chosen variables lies. Consider the point which lies within a grid cell, whose area is Δx x Δy, as sketch in Figure 14. The grid point at the lower left corner of the cell is designated (i,j) in index notation. Lines passing through the considered point divide the cell into four rectangular

regions of areas A_1, A_2, A_3, and A_4 as marked in the figure following the clockwise direction. The value of the chosen variable at that point can be interpolated from the values at the four corners of the containing cell, which are already known from the calculation results. It can easily be verified that, when linear interpolation is used, the variable value at the point (x,y) is

$$\phi_{(x,y)} = \frac{A_1 \cdot \phi_{i,j} + A_2 \cdot \phi_{i,j+1} + A_3 \cdot \phi_{i+1,j+1} + A_4 \cdot \phi_{i+1,j}}{\Delta x \cdot \Delta y} \tag{4.7}$$

The four areas are the weighting factors, and they are computed from the lengths l_x and l_y according to Figure 14. After $\phi_{(x,y)}$ has been found, the remaining task is to convert this value to a particular color. The whole range of this value is equally divided into subranges, the size of each subrange is user-specified interval δ. In the computer program we assign colors represented by numbers according to the following table.

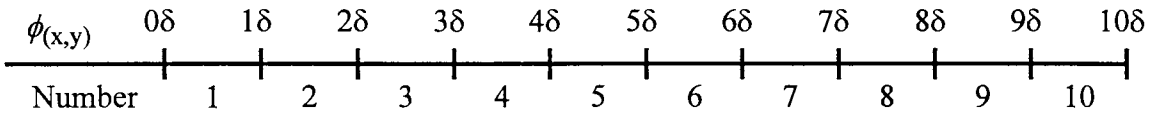

For a given value of $\phi_{(x,y)}$, the corresponding subrange number is obtained by first calculating the numerical value of $(1+ \phi_{(x,y)}/\delta)$ and then truncating it after the decimal point. This number determines the color to be plotted on the screen. Note that such a color scale is re-used for values above 10δ and below 0δ. By analogy, a graph can be constructed having the whole value range of chosen variable subdivided into any desired number of color scales.

To plot the whole cross-section plane with color contour map, we start from the point at the left bottom corner, compute the local value of the chosen variable at that point and convert it into respective color, and then print the color pixel on the screen by mapping from local coordinates to screen coordinates. After it is plotted, the procedure is repeated point by point throughout the whole region. To draw the color contour lines of constant values (iso-lines), we have to search for all suspect points where the local value matches with pre-selected constant values, and then plot those points with pixels on the screen to form an iso-line. The procedure is repeated until all pre-selected contour lines are drawn.

CHAPTER V

APPLICATIONS AND DISCUSSION

Several test applications of the computer code 3DCC are now described. They are listed in Tables 2, 3 and 4. Test cases 1 through 4 are identified in Table 2 with complete input data given in Table 3. Application of the calculation program to general 3-D flows with chemical reaction is accomplished via simulation of diffusion flames from co-flow and cross-flow fuel injection situations identified in Table 4. These two situations are called Test Cases 5 and 6, respectively. For each case, turbulence simulation is via use of the standard two-equation (k-ε) model except for Test case 3 which addresses the use of the "constant viscosity model of turbulence".

5.1 Test Case 1 : Free Jet of Air into Stagnant Surroundings with Different Density

5.1.1 Problem Description

The validation of the present code for turbulent inert mixing free jets in variable density situations is addressed in Test Case 1 as shown in Figure 15. Here density differences exist between the jet and surrounding flows. Ha and Lilley [22] provide a lengthy review of the situation and present predictions using a boundary layer jet mixing

CHAPTER V

APPLICATIONS AND DISCUSSION

Several test applications of the computer code 3DCC are now described. They are listed in Tables 2, 3 and 4. Test cases 1 through 4 are identified in Table 2 with complete input data given in Table 3. Application of the calculation program to general 3-D flows with chemical reaction is accomplished via simulation of diffusion flames from co-flow and cross-flow fuel injection situations identified in Table 4. These two situations are called Test Cases 5 and 6, respectively. For each case, turbulence simulation is via use of the standard two-equation (k-ε) model except for Test case 3 which addresses the use of the "constant viscosity model of turbulence".

5.1 Test Case 1 : Free Jet of Air into Stagnant Surroundings with Different Density

5.1.1 Problem Description

The validation of the present code for turbulent inert mixing free jets in variable density situations is addressed in Test Case 1 as shown in Figure 15. Here density differences exist between the jet and surrounding flows. Ha and Lilley [22] provide a lengthy review of the situation and present predictions using a boundary layer jet mixing

computer code. The decay of the axial velocity on the centerline has been plotted versus the downstream distance for this free jet. They computed these flows for the axisymmetric jet mixing situation by solving the boundary layer equations using the standard Prandtl mixing length model of turbulence. They investigated jet spread and decay parameter effects by making various production runs; their results confirmed previous experimental findings about the jet development, and extended knowledge to more practical situations.

Consider a round jet, with velocity U_{jet}, emerging into surroundings which may be co-flowing in the same direction as the main flow, with velocity U_{sec}. Then, in usual notation, velocity maximum values along the axis are given by

$$\frac{U_m - U_{sec}}{U_{jet} - U_{sec}} = K_u \frac{D_{jet}}{X + a}$$

where K_u is the jet decay parameter.

The equation is valid with constant K_u when $U_{sec} = 0$ beyond the central core region ($X/D_{jet} > 6$). Here "a" is the apparent jet origin distance upstream of the jet exit. It is permissible to set a = 0 with only slight error, as may previous authors do. In fact, the distance a is very susceptible to precise nozzle exit profiles and surrounding flow conditions. The ransverse profile is given via jet spread parameter k_u by

$$\frac{U - U_{sec}}{U_m - U_{sec}} = e^{-k_u(\frac{r}{X+a})^2}$$

valid in the similarity zone of $X/D_{jet} > 10$ approximately.

Jet half-angle (angle sub-tended at the apparent origin by the axis and a line connecting the half-velocity ($U-U_{sec})/(U_m-U_{sec}) = 0.5$ lateral locations) also help to characterize the flow development :

$$\tan \alpha_{0.5} = \frac{r_{0.5}}{X + a}$$

The jet half-angle is known to be invariant with axial distance X when $U_{sec} = 0$, but to decrease with X when the surroundings are co-flowing with nonzero velocity. Thus the jet decay and spread parameters K_u, k_u and α are very important values to be used in clarifying jet flow features and comparing predicted results with experimental data.

In this test case, the "constant viscosity model of turbulence" is used to illustrate its predictive capability. That is, Eq.(3.5) is used to specify the constant turbulent viscosity value to be used throughout the flowfield. For constant density of the jet and its co-flowing stream, A = 6.604 was found to give good agreement with the experimental data. However, for the variable density case, it was found necessary to reduce the value of the parameter A according to :

$\rho_{sec} / \rho_{jet} = 1.0;$ $\quad A = 6.604$

$\rho_{sec} / \rho_{jet} = 0.5;$ $\quad A = 4.568$

$\rho_{sec} / \rho_{jet} = 0.25;$ $\quad A = 3.264$

where these values were found via computer experiment.

5.1.2 Some Results About Density Ratio Effect

Figure 16 illustrates the density effect (ρ_{sec}/ρ_{jet}=1, 0.5, and 0.25) of a round jet into stagnant surroundings. The lower density surroundings produce less decay of the axial velocity along the centerline in the downstream direction. This is expected, since there is less drag on the main jet flow from the lower density surroundings. Inspection of Figure 16 reveals that the calculated results are in quite good agreement with the previous numerical investigation by Ha and Lilley [22], which themselves are consistent with previous experimental data.

The effect of density differences between jet and surrounding fluid on axial velocity decay constant K_u and jet half-angle α are portrayed in Figure 17 and 18 respectively. Key development parameters have been deduced from predicted results at the axial location X/D_{jet} = 20. It is seen that higher values of surrounding density have lower values of K_u and higher values of α. These are associated with faster decay and wider spread of velocity in the flowfield.

Flowfield illustrations given for different density ratios ρ_{sec}/ρ_{jet}=0.25, 0.5, and 1.0 are for the case of the jet in the stagnant surroundings. Figure 19 Parts (a) and (b) illustrates the mixing when the co-flowing stream is stagnant with density ratio ρ_{sec}/ρ_{jet}=0.25. The dimensionless axial velocity U is shown at three longitudinal slices and four lateral cross-sections via gray-scaled contour plots in yx-planes and yz-planes, respectively. Each cross-section plane is shown in the 3-D view at the top of the figure with 2-D contour plots shown below. In Part (a) of the figure, longitudinal slodes A, B, C are located at 0.0, 1.1, 2.2 jet diameters (approximately) to the side of the jet centerline.

Regarding Part (a), the portrait shows a rectangular longitudinal slice of aspect ratio 5:1. There has been a coordinate compression of 17 percent in the x-direction. The length in fact is 0.36 m and the height is 0.06 m. Of course, for scenic purposes at the screen display, the aspect ratio is adjusted to fit in the pre-set display region for viewing purposes. In Part (b) of the figure, lateral cross-sections A, B, C and D are located approximately at 7, 16, 25, and 34 jet diameters downstream of the jet injection location. Regarding Part (b), the portrait shows a rectangular cross-section of aspect ratio 20:13. There has been a coordinate compression of 35 percent in the y-direction. The width in fact is 0.06 m and the height is 0.06 m. The gray scale indicator is ranged from 0.0 to 1.0 and re-used for values above 1.0 and below 0.0 with the same indicated interval. Figure 20 and 21 show calculated values of axial velocity when the surrounding-to-jet density ratio is ρ_{sec}/ρ_{jet}= 0.5 and 1.0, respectively. These may be compared with and contrasted to corresponding data given in Figure 19 which was for the case with ρ_{sec}/ρ_{jet}=0.25. The predictions illustrate the reduced rate of entrainment and a narrower jet mixing region when the surrounding has a lower density value. A longer thinner jet mixing region results, and progressively so as the surrounding density decreases.

5.2 Test Case 2 : Free Jet of Air into Co-flowing Secondary Flow of Air

5.2.1 Problem Description

For this test case as shown in Figure 22, a free jet issuing into co-flowing surrounding streams is simulated to predict the jet flow characteristics. Several studies

[3, 14, 22, 55-57] have documented experimental evidence about jets in co-flowing streams. When the jet and surroundings have the same density, flowfields differ according to the ratio of secondary to jet velocities. The effect of the velocity ratio $VR=U_{sec}/U_{jet}$ (secondary to jet velocity ratio) is particularly important, since its value is known to affect the downstream development and lateral spread. This study is basically that of an unconfined jet emerging into an infinite co-flowing stream; 'free slip' boundary conditions are applied at the sides of the domain which are located approximately 6 jet diameters to the side of the jet. From the entrainment point of view the jet is essentially unconfined, see Ref. [2].

5.2.2 Secondary to Jet Velocity Ratio Effect

Figure 23 illustrates the current predicted effect of surrounding co-flowing velocities ($VR = U_{sec}/U_{jet} = 0$, 0.25 and 0.5) on the axial velocity maximum decay. Notice that the one with higher surrounding co-flowing velocity produces less decay of the axial velocity along the centerline in the downstream direction. The calculated results show good agreement with the experimental data by Beer and Chigier [3].

The predicted half-velocity line (a line connecting the half-velocity $(U-U_{sec}) / (U_m-U_{sec}) = 0.5$ lateral locations) along the jet axis for a free jet in stagnant surroundings is shown in Figure 24, with the data predicted previously by Ha and Lilley [22]. Hence the Figure 25 illustrates the predicted and theoretical transverse profiles of velocity for a free jet in stagnant surroundings at the downstream location $X/D_{jet} = 20$, where the

predicted profile curve shows fairly good agreement with the theoretical curves. Here the constant k_u has the values between 82 and 92, see Refs [3, 22].

The effect of velocity differences between jet and surrounding fluid on axial velocity decay constant K_u and jet half-angle α are portrayed in Figures 26 and 27 respectively. Key development parameters have been deduced from predicted results at the axial location $X/D_{jet} = 20$. It is seen that lower values of surrounding velocity have lower values of K_u and higher values of α. These are associated with faster decay and wider spread of velocity in the flowfield.

Flowfield illustrations now given for different velocity ratios VR = 0, 0.25 and 0.5 are for the case of the same density in the jet and its surroundings. Figure 28 Parts (a) and (b) illustrates the mixing when the co-flowing stream is stagnant (that is, VR=0 and U_{sec}=0). The dimensionless axial velocity U is plotted as the 3DGD display. In Part (a) of the figure, longitudinal A, B, C are located at 0.0, 1.1, 2.2 jet diameters (approximately) to the side of the jet centerline. Regarding Part (a), the portrait shows a rectangular longitudinal slice of aspect ratio 5:1. There has been a coordinate extraction of 10 percent in the x-direction. The length in fact is 0.272 m and the height is 0.06 m. In Part (b) of the figure, lateral cross-sections A, B, C and D are located approximately at 4, 10, 17 and 24 jet diameters downstream of the jet injection location. Regarding Part (b), the portrait shows a rectangular cross-section of aspect ratio 20:13. There has been a coordinate compression of 35 percent in the y-direction. The width in fact is 0.06 m and the height is 0.06 m.

Figure 29 and 30 show calculated values of axial velocity when the secondary-to-jet velocity ratio is VR= 0.25 and 0.5, respectively. This may be compared with and contrasted to corresponding data given in Figure 28 which was for the stagnant surroundings case. The predictions illustrate the reduced rate of entrainment and a narrower jet mixing region when the secondary flow has a nonzero velocity. A longer thinner jet mixing region results. However, with the normalization used (division by U_{jet}) higher velocities are seen in the figures in the surrounding region. These and other predictions are extremely informative in understanding the mixing characteristics of any particular 3-D situation.

5.3 Test Case 3 : Free Jet of Air into Cross-flowing Secondary Flow of Air

5.3.1 Problem Description

As the third test case, the new code is employed to predict a turbulent jet in a cross flow in a large square cross section wind tunnel, which was studied experimentally by Kamotani and Greber [10] in a 28 inch square cross section subsonic wind tunnel. They measured velocity by a hot wire anemometer, the mean flow direction by a small yaw angle meter and temperature by an iron-constantan thermocouple. Their measurements were performed over the ratios of 15 to 60 of the jet momentum flux to the free stream momentum flux (called the momentum ratio, $J = \rho_{jet} U_{jet}^2 / \rho_{sec} U_{sec}^2$) for both heated and for unheated jets.

For the prediction of this flowfield in the computer code, a small portion around the jet inlet of the actual is considered as the solution domain with all free-slip BCs, as shown in Figure 31. The treatment of an enclosed (or confined) jet, such as a jet issuing into a duct, is based on the assumption that the rate of entrainment of the jet is unaffected by the enclosure and that the development of the jet is determined by its momentum flux; this simple assumption gives good agreement with experiment when the jet nozzle diameter is smaller than 1/10 of the duct diameter, see Ref. [3].

5.3.2 Some Results

The case of the momentum ratio J = 59.6 is simulated here for this prediction and compared with the experimental data. Figure 32 shows the comparison of the predicted maximum temperature centerline locations with the experimental data points along the downstream distance. The prediction results via constant viscosity and k-ε turbulence model for turbulent flow are both in good agreement with the experiment, though some discrepancies appear at the upstream locations $X/D_{jet} < 5$, either. However, the calculation via k-ε turbulence model shows a little improvement in that region. The comparison of the predicted maximum velocity centerline locations with the experimental values is shown in Figure 33. The calculation via constant viscosity shows the same trend as the experiment but shows rather higher values than the experimental data. However the calculation via k-ε turbulence model shows good agreement with the experimental data. Note that the jet temperature and velocity trajectories shown in

Figures 32 and 33 are the locus of the maximum temperature and velocity in the plane of symmetry. This is the most common measure of the jet trajectory used in experiments.

Figure 34 Parts (a) and (b) illustrates the temperature distribution for a jet in a cross-flowing flow. The temperature distribution is shown at three longitudinal slices and four lateral cross-sections via gray-scaled contour plots in yx-planes and yz-planes, respectively. Each cross-section plane is shown in the 3-D view at the top of the figure with 2-D contour plots shown below. In Part (a) of the figure, longitudinal A, B, C are located at 0, 4, 8 jet diameters (approximately) to the side of the jet centerline. Regarding Part (a), the portrait shows a rectangular longitudinal slice of aspect ratio 5:1. There has been a coordinate compression of 74 percent in the y-direction. The length in fact is 0.1651 m and the height is 0.127 m. In Part (b) of the figure, lateral cross-sections A, B, C and D are located approximately at 1, 7, 14 and 21 jet diameters downstream of the jet injection location. Regarding Part (b), the portrait shows a rectangular cross-section of aspect ratio 20:13. There has been a coordinate compression of 68 percent in the y-direction. The width in fact is 0.0635 m and the height is 0.127m. The gray scale indicator ranges from 0.01 to 0.1. These cross-sectional views provide better visualization of jet development and spread in cross-flowing flow.

5.4 Test Case 4 : Diffusion Flames of a Hydrogen Jet in a Co-flowing Stream of Air

5.4.1 Problem Description

Test case 4 applies the present code to turbulent diffusion flames which have been previously studied experimentally by Kent and Bilger [11]. They conducted experiments in a square wind tunnel of 0.36 x 0.305 x 1.8m, for turbulent diffusion flames of a round jet (d=7.62 mm) of hydrogen in a co-flowing stream of air.

A small portion around the jet inlet of the large wind tunnel is chosen as the solution domain (as shown in Figure 35) for the prediction of turbulent diffusion flames, since the tunnel cross-section is large enough as compared to the jet diameter so that the flames can be considered to be essentially unconfined from turbulent entrainment view point.

5.4.2 Some Results

The downstream development of the unburned hydrogen volumetric fractions is presented in Figure 36 and 37 which are resulted from calculations via constant viscosity and k-ε turbulence model for turbulent flow, respectively. The two lines represent the predictions with velocity ratio VR=0.2 and 0.1. The calculated hydrogen levels in Figure 36 which resulte from the constant viscosity simulation are a little lower than the corresponding experimental measurements. Qualitatively the results show the correct trend, but the diffusion-controlled flame has exhibited overly-fast chemical reaction of the injected fuel. This is highly dependent upon the rate of mixing. Constrastly, the

calculated hydrogen levels in Figure 37 which is resulted from k-ε turbulence model simulation shows good agreement with experimental result.

Figure 38 Parts (a) and (b) illustrates the mixing and diffusional chemical reaction when the center hydrogen jet is injected with a velocity five times the magnitude of the secondary air flow (VR=0.2). The dimensionless axial velocity U is shown at three longitudinal slices and four lateral cross-sections via gray-scaled contour plots in yx-planes and yz-planes, respectively. In Part (a) of the figure, longitudinal A, B, and C are located at 0.0, 1.25 and 2.5 jet diameters (approximately) to the side of the jet centerline. Regarding Part (a), the portrait shows a rectangular longitudinal slice of aspect ratio 5:1. There has been a coordinate compression of 40 percent in the x-direction. The length in fact is 0.396 m and the height is 0.0473 m. In Part (b) of the figure, lateral cross-sections A, B, C and D are located approximately at 12, 24, 38, and 52 jet diameters downstream of the jet injection location. Regarding Part (b), the portrait shows a rectangular cross-section of aspect ratio 20:13. There has been a coordinate compression of 35 percent in the y-direction. The width in fact is 0.0473 m and the height is 0.0473 m. Figure 39 shows the corresponding contour plots of temperature for the same velocity ratio case as Figure 38. The highest temperature is observed at the diffusion flame envelope-with no unburned fuel outside this flame region and no oxygen inside this flame region. Figure 40 and 41 show calculated values of axial velocity and temperature when the jet-to-secondary velocity ratio VR=0.1. These may be compared with and contrasted to corresponding data given in Figures 38 and 39 which were for the lower velocity ratio

case of VR=0.2. Inspection of the figures reveals that velocities and temperatures are higher in the larger flame zone than the previous case.

5.5 Test Case 5 : Diffusion Flames of a Methane Jet in a Co-flowing Stream of Air

5.5.1 Problem Description

Application of the calculation program to general 3-D flows with chemical reaction is considered using the as schematic and problem description given in Figure 42. A free jet of methane (CH_4) emerges into a co-flowing stream of air with chemical reaction simulated via the diffusion flame concept. Three simulation runs have been made to show the effect of changing U_{sec} (surrounding secondary velocity of air) while retaining other parameters at their base values. These three simulations are identified as VR(velocity ratio)=U_{sec}/U_{jet}= 0.1, 0.3 and 0.5 and other parameters used are given in Table 4.

5.5.2 Some Results

Figure 43 shows clearly the effects of the surrounding secondary velocities on centerline velocity decay. The calculation results illustrate the slower downstream centerline velocity decay when the velocity ratio VR= U_{sec}/U_{jet} is higher. Figure 44 and 45 show the effects on downstream development of centerline temperature distribution and unburned fuel fraction, respectively. The results illustrate good qualitative trend on

downstream development of centerline flames where lower temperature and higher unburned fuel fraction are observed when the velocity ratio U_{sec}/U_{jet} is higher. However, the quantitative results are not expected as previous predictions done by other researcher [22] while experimental results are unavailable. Such discrepancy can be affected by the use of different turbulence model and convergence criterion for calculation.

Figures 46~48 illustrate the mixing and diffusional chemical reaction when the center methane jet is injected with a velocity ten times the magnitude of the surrounding air flow (VR=0.1). The corresponding contour plots of the dimensionless axial velocity U, unburned fuel mass fraction and temperature distribution are shown as the 3DGD format. Figures 49~51 and 52~54 show the corresponding contour plots of the same three variables for the velocity ratio VR=0.3 and 0.5, respectively. These may be compared with and contrasted to corresponding data given in Figure 46~48 which were for the lower velocity ratio case of VR=0.1. The examination of these figures reveals that the calculated results for diffusion flames concur with previous literature concepts : near the jet inlet, the effect of a co-flowing stream is merely to reduce the speed and delay the decay of the jet [21,47]; but further downstream the jet flow becomes escalated slightly by coming into the core of the "very thin flame region" which occurs over the surface where S (concentration or mixture fracture) and T (temperature) approaches their Stoichiometric values. Further inspection of the figures reveals that the velocities and temperatures are higher in the larger flame zone when the velocity ratio is lower.

5.6 Test Case 6 : Diffusion Flames of a Methane Jet in a Cross-flowing Stream of Air

5.6.1 Problem Description

For this test case, the calculation program is applied to general 3-D cross-flow with chemical reaction as shown in Figure 55 with schematic and problem description. A free jet of methane (CH_4) emerges into cross-flowing stream of air with chemical reaction simulated via the diffusion flame concept. Three simulation runs have been made to show the effect of changing U_{sec} (surrounding secondary velocity of air) while retaining other parameters at their base values. These three simulations are identified as VR(velocity ratio) = U_{sec}/V_{jet}= 0.3, 0.4 and 0.5 and other parameters used are given in Table 4.

5.6.2 Some Results

Figure 56 shows clearly the effects of the cross-flowing secondary velocities on maximum velocity centerline location. The calculation results illustrate the jet trajectory is deflected more when the velocity ratio VR= U_{sec}/V_{jet} is higher. Figure 57~58 illustrate the mixing and diffusional chemical reaction when the turbulent methane jet is injected with a velocity approximately three times the magnitude of the cross-flowing air flow (VR=0.3). The corresponding contour plots of the unburned fuel mass fraction and temperature distribution are shown as the 3DGD format. Figures 59~60 and 61~62 show the corresponding contour plots of the same variables for the velocity ratio VR=0.4 and

0.5, respectively. These may be compared with and contrasted to corresponding data given in Figure 57~58 which were for the lower velocity ratio case of VR=0.3.

CHAPTER VI

CLOSURE

6.1 Conclusions

Mathematical simulation and color graphic display capability have been developed for nonreacting (mixing) and reacting (simple diffusion flames) flowfields in a 3-D rectangular solution domain. The 3-D calculation program 3DCC has been developed for variable density jet mixing and diffusion flame simulation in transient fully 3-D situations. Several test cases were chosen and confirmed the validity of the code. The effective 3-D perspective color graphic display program 3DGD has been developed to make complex calculation results easy to comprehend. Quantitative information of the specific variable and flowfield visualization are demonstrated via clear graphic display. Important specific results and discussion for each application in Chapter V are provided in each section. This chapter presents general conclusions and makes recommendations for future work. The following conclusions may be drawn from the confirmatory calculations and comparisons with the available experimental data :

1. The turbulence model simulated via constant viscosity was adequate for constant density free jet flow simulation.

2. Quality of the standard two-equation (k-ε) turbulence model vs. constant viscosity simulation has been identified for variable density and chemically reacting flows.
3. Flat radial profiles of all the variables at the inlet was sufficient to permit good simulation of the subsequent flowfield.
4. Grid refinement studies for the reacting jet indicated that a relatively coarse grid (26x14x14 internal cell coverage) provided adequate accuracy.
5. It is now possible to calculate fully 3-D flowfields with turbulence and chemical reaction.
6. The appropriate equations for adequate simulation of fully 3-D turbulent reacting flows have been identified, together with a technique for their solution.
7. A methodology for color graphic display of the results has been identified and successfully implemented.

6.2 Recommendations for Future Work

Further fundamental research should be extended in several areas to develop a more powerful and accurate simulation tool for 3-D flowfields with or without chemical reaction. They are briefly identified as follows :

1. A coordinates transformation scheme should be implemented to the current computer code for both rectangular and cylindrical polar coordinates.

2. The current computer code with uniform grid system should be extended to incorporate a nonuniform grid system which allows greater flexibility in grid and domain coverage. This would resolve the limitations of being incapable of simulating well complex solution domains, and would allow finer grids near the inlet and boundary surfaces.
3. A more advanced turbulence model could be incorporated for the potential capability of more precise flow simulation.
4. An intensive submodel validation and development effort should be continued for a finite reaction model to have the capability of simulation of premixed flames. In these flames, the current assumption of an infinitely fast chemical reaction for diffusion flames is invalid.
5. More realistically approximated velocity profiles at the inlet could be implemented to the current code so as to have better simulation of the flowfield.
6. Further application about the effects of inlet flow parameters on combustor flowfields can be continued and assessed versus experimental data.
7. The development of color graphic display program 3DGD can be continued to have features of a graphical user interface, real 3-D visualization and image procession.

REFERENCES

1. Hirt, C.W., Nichols, B.D. and Romero, N.C., "SOLA - A Numerical Solution Algorithm for Transient Fluid Flows," Los Alamos Scientific Laboratory, Report LA - 5852, New Mexico, 1975.

2. Gupta, A.K. and Lilley, D.G., Flowfield Modeling and Diagnostics, Abacus Press, Tunbridge Wells, England, 1985.

3. Beer, J.M. and Chigier, N.A., Combustion Aerodynamics, Applied Science, London, England, 1972.

4. Spalding, D.B., "Mixing and Chemical Reaction in Steady Confined Turbulent Flames," 13th Symposium (International) on Combustion, The Combustion Institute, Pittsburgh, 1971, pp. 649-657.

5. Spalding, D.B., "Concentration Fluctuations in a Round Turbulent Free Jet," Chemical Engineering Science, Vol. 26, 1971, pp. 3-25.

6. Vatistas, C.H., Lilley, D.G., and Rhode, D.L., "Basic Concepts for Numerical Prediction of Fully Three-Dimensional Chemically-Reacting Flowfields," Presented at Com. Inst./Canadian Section Meeting, Kingston, Ontario, Canada, May 3-4, 1979.

7. Chigier, N.A., "The Interaction between Fluid Mechanics and Combustion," Journal of Fluids Mechanics of Combustion Systems, The Fluids Engineering Conference, Boulder, Colorado, Jan. 22-23, 1981.

8. Wohl, K., Gazley, C., and Kapp, N., "Diffusion Flames," 3rd Symposium on Combustion, Flame and Explosion Phenomena, 1958.

9. Kremer, H., "Mixing in a Plane Free-Turbulent-Jet Diffusion Flames," 11th Symposium (International) on combustion, The Combustion Institute, 1967, pp. 799-806.

10. Kamotani, Y. and Greber, I., "Experiments on a Turbulent Jet in a Cross Flow," AIAA Journal, Vol. 10, 1972, pp. 1425-1429.

11. Kent, J.H. and Bilger, R.W., "Turbulent Diffusion Flames," 14th Symposium (International) on Combustion, The Combustion Institute, Pittsburgh, PA., 1973, pp. 615-625.

12. Fearn, R. and Weston, R.P., "Vorticity Associated with a Jet in a Cross Flow," AIAA Journal, Vol. 12, , 1974, pp. 1666-1671.

13. Libby, P.A. and Williams, F.A., Turbulent Reacting Flows, Springer-Verlag, Berlin, Heidelberg, 1980.

14. Schetz, J.A., "Injection and Mixing in Turbulent Flow," Progress in Astronautics and Aeronautics, Vol. 68, AIAA, 1980.

15. Pantankar, S.V. and Spalding, D.B., "A Computer Model for Three-Dimensional Flow in Furnaces," 14th Symposium (International) on combustion, The Combustion Institute, Pittsburgh, P.A., 1973, pp. 605-614.

16. Abou Ellail, M.M.M., Gosman, A.D., Lockwood, F.C., and Megahed, I.E.A., "Three-Dimensional Procedure for Combustion Chamber Flows," AIAA Paper 77-138, Los Angeles, Calif., Jan. 24-26, 1977.

17. Edelman, R.B. and Harsha, P.T., "Some Observations on Turbulent Mixing with Chemical Reactions," AIAA Paper 77-142, Los Angeles, Calif., Jan. 24-26, 1977.

18. Birch, S.F., Paynter, G.C., Spalding, D.B. and Tatchell, D.G., "Numerical Modeling of Three-Dimensional Flows in Turbofan Engine Exhaust Nozzles," Journal of Aircraft, vol. 15, No. 8, 1978, pp. 489-496.

19. Ha, S. and Lilley, D.G., "Jets in Co-flowing Streams," ASME Journal, Vol. 3, 1987, pp. 181-188.

20. Karki, K.C., Patankar, S.V., Runchal, A.K. and Mongia, H.C., "Improved Numerical Methods of Turbulent Viscous Recirculating Flows," Aerothermal Modeling Phase II Final Report, Report NASA CR-182169, NASA Lewis Research Center, June, 1988.

21. Ha, S. and Lilley, D.G., "Prediction of Jets and Flames in Co-flowing Streams," ASME International Computers in Engineering Conference, Santa Clara, CA, Aug. 18-22, 1991.

22. Ha, S. and Lilley, D.G., "Jets and Flames in Co-flowing Streams," AIAA/SAE/ ASME/ASEE 23rd Joint Propulsion Conference, AIAA Paper 87-1952, San Diego, Calif., June 29 - July 2, 1987.

23. Weathers, J.W., "A Study of Computational Fluid Dynamics Applied to Room Air flow," Master's Thesis, Oklahoma State University, 1992.

24. Boussinesq, J., "Théorie de l'Écoulement Tourbillant," Mem. Présentés par Divers Savants Acad. Sci. Inst. Fr., Vol. 23, 1887, pp. 46-50.

25. Prandtl, L., "Über die ausgebildete Turbulenz," ZAMM, Vol. 5, 1925, pp. 136-139.

26. Von Kármán, T.H., "Mechanische Ahnlichkeit und Turbulenz," Proc. 3rd Int. Congress Appl. Mech., Stocknolm, pt. 1, 1930, p. 85.

27. Clauser, F.H., "The Turbulent Boundary Layer," Adv. in App. Mech. IV, pt. 1, New York Academic Press, 1956.

28. Mellor, G.L., "Turbulent Boundary Layers with Arbitrary Pressure Gradients and Divergent or Convergent Cross flows," Dept. Aerospace and Mech. Sci., Princeton Univ., Rep. 755, 1966.

29. Prandtl, L., "Über ein neues Formelsystem für die ausgebildete Turbulenz," Nachrichten von der Akad. der Wissenschaft in Göttingen, 1945.

30. Kolomogrov, A.N., "Equations of Turbulent Motion of an Incompressible Turbulent Fluid," Izv. Akad. Nauk SSSR Ser Phys. VI, No.1-2, 1942, p. 56.

31. Nee, V.W. and Kovasznay, "The Calculation of the Incompressible Turbulent Boundary Layer by a Simple Theory," Proc. of AFOSR/IFP Conf. on Computation of Turbulent Boundary Layers, vol. I, Stanford University, 1968.

32. Bradshaw, P. et al, "Calculation of Boundary Layer Development Using the Turbulent Energy Equation," Journal of Fluid Mechanics, vol. 23, 1965, p. 31.

33. Baldwin, B. S. and Barth, T. J., " A One-Equation Turbulence Transport Model for High Reynolds Number Wall-Bounded Flows," NASA TM-102847.

34. Chou, P. Y., "On the Velocity Correlations and the Solution of the Equations of Turbulent Fluctuation," Quart. Appl. math., Vol. 3, 1945, p. 38.

35. Davidov, B. I., "On the Statistical Dynamics of an Incompressible Fluid," Doklady AN. SSSR, Vol. 136, 1961, p. 47.

36. Harlow, F. H. and Nakayama, P. I., "Transport of Turbulence Energy Decay Rate," LosAlamos Sci. Lab., University of California Report LA-3854, 1968.

37. Launder, B. E. and Spalding, D. B., Mathematical Models of Turbulence, Academic Press, London, 1974.

38. Launder, B. E. and Spalding, D. B., "The Numerical Computation of Turbulent Flows," Computer Methods in Applied Mechanics and Engineering, Vol. 3, 1974.

39. Lam, C. K. G. and Bremhorst, K. A., "Modified Form of k-ε Model for Predicting Wall Turbulence," ASME, Journal of Fluids Engineering, vol. 103, 1981, pp.456-460.

40. Dutoya, D. and Michard, P., "A Program for Calculating Boundary Layers Along Compressor and Turbine Blades," Numerical Methods in Heat Transfer, New York, 1981.

41. Hassid, S. and Poreh, M., "A Turbulent Energy Dissipation Model for Flows with Drag Reduction," ASME, Journal of Fluids Engineering, Vol. 100, 1978, pp. 107-112.

42. Wilcox, D.C., Turbulence Modeling for CFD, DCW Industries Inc., La Cañada, California, 1993.

43. Awbi, H.B., "Application of Computational Fluid Dynamics in Room Ventilation," Building and Environment, Vol. 24, No. 1, 1989.

44. Hinze, J.O., Turbulence, 2nd ed., McGraw-Hill, New York, 1975.

45. Gupta, A. K., Lilley, D. G. and Syred, N., Swirl Flows, Abacuss Press, Turbridge Wells, England, 1984.

46. Busnina, A.A. and Lilley, D.G., "Numerical Simulation of Swirling Flow in a Cyclone Chamber," Journal of Fluids Mechanics of Combustion Systems, The Fluids Engineering Conference, Boulder, Colorado, Jan. 22-23, 1987.

47. Forstall, W. and Shapiro, A.H., "Momentum and Mass Transfer in Co-axial Gas Jets," Trans. ASME J. of Appl. Mech., Vol. 72, 1950, pp. 399-408.

48. Harlow, F.H. and Welch, J.E., "Numerical Calculation of Time-Dependent Viscous Incompressible Flow," Physics Fluids 8, 1965.

49. Welch, J.E., Harlow, F.H., Shanon, J.P., and Daly, B.J., "The MAC Method : A Computer Technique for Solving Viscous, Incompressible, Transient Fluid Flow Problems Involving Free Surfaces," Los Alamos Scientific Laboratory, Report LA-3425, March 1966.

50. Hirt, C.W. and Cook, J.L., "Calculating 3-D Flows around Structures and Over Rough Terrain," Journal of Comp. Physics, Vol. 10, 1972, pp. 324-340.

51. Launder, B.E. and Spalding, D.B., Mathematical Models of Turbulence, Academic Press, London, England, 1972.

52. Lilley, D.G., "Three-Dimensional Flow Prediction for Industrial Mixing," ASME International Computers in Engineering conference, San Fransisco, C.A., July 31 - Aug. 3, 1988.

53. Patankar, S.V., Numerical Heat Transfer and Fluid Flow, Hemisphere Publishing Co., London, England, 1980.

54. Patankar, S.V. and Spalding, D.B., "A Calculation procedure for Heat, Mass, Momentum Transfer in Three-Dimensional Parabolic Flows," International Journal of Heat and Mass Transfer, Vol. 15, 1972.

55. Pai, S. I., "Fluid Dynamics of Jets", Van Nostrand, New York, 1954.

56. Abramovitch, G. N., "The Theory of Turbulent Jets," MIT Press, Cambridge, MA, 1963.

57. Rajaratnam, N., "Turbulent Jets", Elsevier, Amsterdam, Netherlands, 1976.

APPENDIX A

TABLES

TABLE 1-a. SOURCE TERMS AND EXCHANGE COEFFICIENTS IN EQ. (3.1)

(Turbulent jet flows are simulated via a large constant viscosity.)

ϕ	Γ_ϕ	S_ϕ
1	0	0
u	μ	$-\frac{\partial P}{\partial x}+\rho g_x+\mu\frac{1}{3}\frac{\partial}{\partial x}(\nabla\cdot V)+S^u$
v	μ	$-\frac{\partial P}{\partial y}+\rho g_y+\mu\frac{1}{3}\frac{\partial}{\partial y}(\nabla\cdot V)+S^v$
w	μ	$-\frac{\partial P}{\partial z}+\rho g_z+\mu\frac{1}{3}\frac{\partial}{\partial z}(\nabla\cdot V)+S^w$
S	$\frac{\mu}{\sigma_S}$	S^S

where certain quantities are defined as follows :

$$S^u=\frac{\partial\mu}{\partial x}\left(2\frac{\partial u}{\partial x}\right)+\frac{\partial\mu}{\partial y}\left(\frac{\partial u}{\partial y}+\frac{\partial v}{\partial x}\right)+\frac{\partial\mu}{\partial z}\left(\frac{\partial w}{\partial x}+\frac{\partial u}{\partial z}\right)-\frac{2}{3}\frac{\partial\mu}{\partial x}(\nabla\cdot V)$$

$$S^v=\frac{\partial\mu}{\partial x}\left(\frac{\partial v}{\partial x}+\frac{\partial u}{\partial y}\right)+\frac{\partial\mu}{\partial y}\left(2\frac{\partial v}{\partial y}\right)+\frac{\partial\mu}{\partial z}\left(\frac{\partial v}{\partial z}+\frac{\partial w}{\partial y}\right)-\frac{2}{3}\frac{\partial\mu}{\partial y}(\nabla\cdot V)$$

$$S^v=\frac{\partial\mu}{\partial x}\left(\frac{\partial v}{\partial x}+\frac{\partial u}{\partial y}\right)+\frac{\partial\mu}{\partial y}\left(2\frac{\partial v}{\partial y}\right)+\frac{\partial\mu}{\partial z}\left(\frac{\partial v}{\partial z}+\frac{\partial w}{\partial y}\right)-\frac{2}{3}\frac{\partial\mu}{\partial y}(\nabla\cdot V)$$

$$S^s=\frac{\partial\mu}{\partial x}\frac{\partial s}{\partial x}+\frac{\partial\mu}{\partial y}\frac{\partial s}{\partial y}+\frac{\partial\mu}{\partial z}\frac{\partial s}{\partial z}$$

σ_s = Prandtl-Schmidt number, taken as 0.7

TABLE 1-b. SOURCE TERMS AND EXCHANGE COEFFICIENTS IN EQ. (3.1)

(Turbulent jet flows are simulated via k-ε turbulence model.)

ϕ	Γ_ϕ	S_ϕ
1	0	0
u	μ	$-\frac{\partial P}{\partial x}+\rho g_x+\mu\frac{1}{3}\frac{\partial}{\partial x}(\nabla\cdot V)+S^u$
v	μ	$-\frac{\partial P}{\partial y}+\rho g_y+\mu\frac{1}{3}\frac{\partial}{\partial y}(\nabla\cdot V)+S^v$
w	μ	$-\frac{\partial P}{\partial z}+\rho g_z+\mu\frac{1}{3}\frac{\partial}{\partial z}(\nabla\cdot V)+S^w$
k	$\frac{\mu}{\sigma_k}$	$G_k - \rho\varepsilon$
ε	$\frac{\mu}{\sigma_\varepsilon}$	$\frac{1}{k}\left(C_1\varepsilon G_k - C_2\rho\varepsilon^2\right)$
S	$\frac{\mu}{\sigma_s}$	S^S

where certain quantities are defined as follows :

$$\mu = \mu_{lam} + \mu_{turb}$$

$$\mu_{turb} = C_\mu \rho \frac{k^2}{\varepsilon}$$

$$S^u = \frac{\partial \mu}{\partial x}\left(2\frac{\partial u}{\partial x}\right)+\frac{\partial \mu}{\partial y}\left(\frac{\partial u}{\partial y}+\frac{\partial v}{\partial x}\right)+\frac{\partial \mu}{\partial z}\left(\frac{\partial w}{\partial x}+\frac{\partial u}{\partial z}\right)-\frac{2}{3}\frac{\partial \mu}{\partial x}(\nabla\cdot V)$$

$$S^v = \frac{\partial \mu}{\partial x}\left(\frac{\partial v}{\partial x}+\frac{\partial u}{\partial y}\right)+\frac{\partial \mu}{\partial y}\left(2\frac{\partial v}{\partial y}\right)+\frac{\partial \mu}{\partial z}\left(\frac{\partial v}{\partial z}+\frac{\partial w}{\partial y}\right)-\frac{2}{3}\frac{\partial \mu}{\partial y}(\nabla \cdot V)$$

$$S^w = \frac{\partial \mu}{\partial x}\left(\frac{\partial w}{\partial x}+\frac{\partial u}{\partial z}\right)+\frac{\partial \mu}{\partial y}\left(\frac{\partial w}{\partial y}+\frac{\partial v}{\partial z}\right)+\frac{\partial \mu}{\partial z}\left(2\frac{\partial w}{\partial z}\right)-\frac{2}{3}\frac{\partial \mu}{\partial y}(\nabla \cdot V)$$

$$G_k = \mu\left\{2\left[\left(\frac{\partial u}{\partial x}\right)^2+\left(\frac{\partial v}{\partial y}\right)^2+\left(\frac{\partial w}{\partial z}\right)^2\right]+\left(\frac{\partial u}{\partial y}+\frac{\partial v}{\partial x}\right)^2+\left(\frac{\partial v}{\partial z}+\frac{\partial w}{\partial y}\right)^2 + \left(\frac{\partial u}{\partial z}+\frac{\partial w}{\partial x}\right)^2\right\}$$

$$S^s = \frac{\partial \mu}{\partial x}\frac{\partial s}{\partial x}+\frac{\partial \mu}{\partial y}\frac{\partial s}{\partial y}+\frac{\partial \mu}{\partial z}\frac{\partial s}{\partial z}$$

σ_s = Prandtl-Schmidt number, taken as 0.7

TABLE 2. SELECTED TEST CASES

	CASE 1	*CASE 2*	*CASE 3*	*CASE 4*
Authors	Ha & Lilley	Beer & Chigier	Kamotani & Greber	Kent & Bilger
Fluids (Secondary/Jet)	Air / Air	Air / Air	Air / Air	Air / H_2
Jet Flow Type	Co-flow	Co-flow	Cross-flow	Co-flow
Flow Field	Turbulent Nonreacting	Turbulent Nonreacting	Turbulent Nonreacting	Turbulent Reacting
Flowfield Domain	Unconfined	Unconfined	Unconfined (wind tunnel)	Unconfined (wind tunnel)
Results	Numerical Prediction	Experimental Measurements	Experimental Measurements	Experimental Measurements

TABLE 3. INPUT DATA USED FOR TEST CASES

	CASE 1	*CASE 2*	*CASE 3*	*CASE 4*
Inlet Velocity (m/s)	$U_{jet} = 100$ $U_{sec} = 0$	$U_{jet} = 100$ $U_{sec} = 0$ 25 50	$V_{jet} = -59.8$ $U_{sec} = 6.1$	$U_{jet} = 107.1, 151.1$ $U_{sec} = 21.4, 15.1$
Inlet Density (kg/m^3)	$\rho_{jet} = 1.2$ $\rho_{sec} = 0.3$ 0.6 1.2	$\rho_{jet} = 1.2$ $\rho_{sec} = 1.2$	$\rho_{jet} = 0.746$ $\rho_{sec} = 1.204$	$\rho_{jet} = 0.082$ $\rho_{sec} = 1.18$
Temperature (K)	$T_{jet} = 300$ $T_{sec} = 300$	$T_{jet} = 300$ $T_{sec} = 300$	$T_{jet} = 471$ $T_{sec} = 293$	$T_{jet} = 297$ $T_{sec} = 297$
Internal Grid Mesh	30 x 12 x 12	34 x 12 x 12	26 x 16 x 12	26 x 14 x 14
Grid Sizes (m)	Δx=0.012 Δy=Δz=0.005	Δx=0.008 Δy=Δz=0.005	Δx=0.00635 Δy=0.00794 Δz=0.00249	Δx=0.009 Δy=Δz=0.003377

TABLE 4. INPUT DATA USED FOR CALCULATION OF GENERAL 3-D FLOWS WITH CHEMICAL REACTION

	CASE 5	*CASE 6*
Fuel Injection Type	Co-flow	Cross-flow
Inlet Velocity (m/s)	$U_{jet} = 50$ $U_{sec} = 5, 15, 25$	$V_{jet} = -50$ $U_{sec} = 15, 20, 25$
Inlet Density (kg/m^3)	$\rho_{jet} = 0.65$ $\rho_{sec} = 1.2$	$\rho_{jet} = 0.65$ $\rho_{sec} = 1.2$
Temperature (K)	$T_{jet} = 300$ $T_{sec} = 300$	$T_{jet} = 300$ $T_{sec} = 300$
Internal Grid Mesh	21 x 12 x 12	22 x 12 x 12
Grid Sizes (m)	$\Delta x=0.025$ $\Delta y=\Delta z=0.005$	$\Delta x=0.025$ $\Delta y=0.007$ $\Delta z=0.005$

Where predictions are performed on methane (CH_4) flames in air with the following input data :

AFRs = 17.24

$C_P = 1600$ J/kg-K

$H_{fu} = 50$ MJ/kg

APPENDIX B

FIGURES

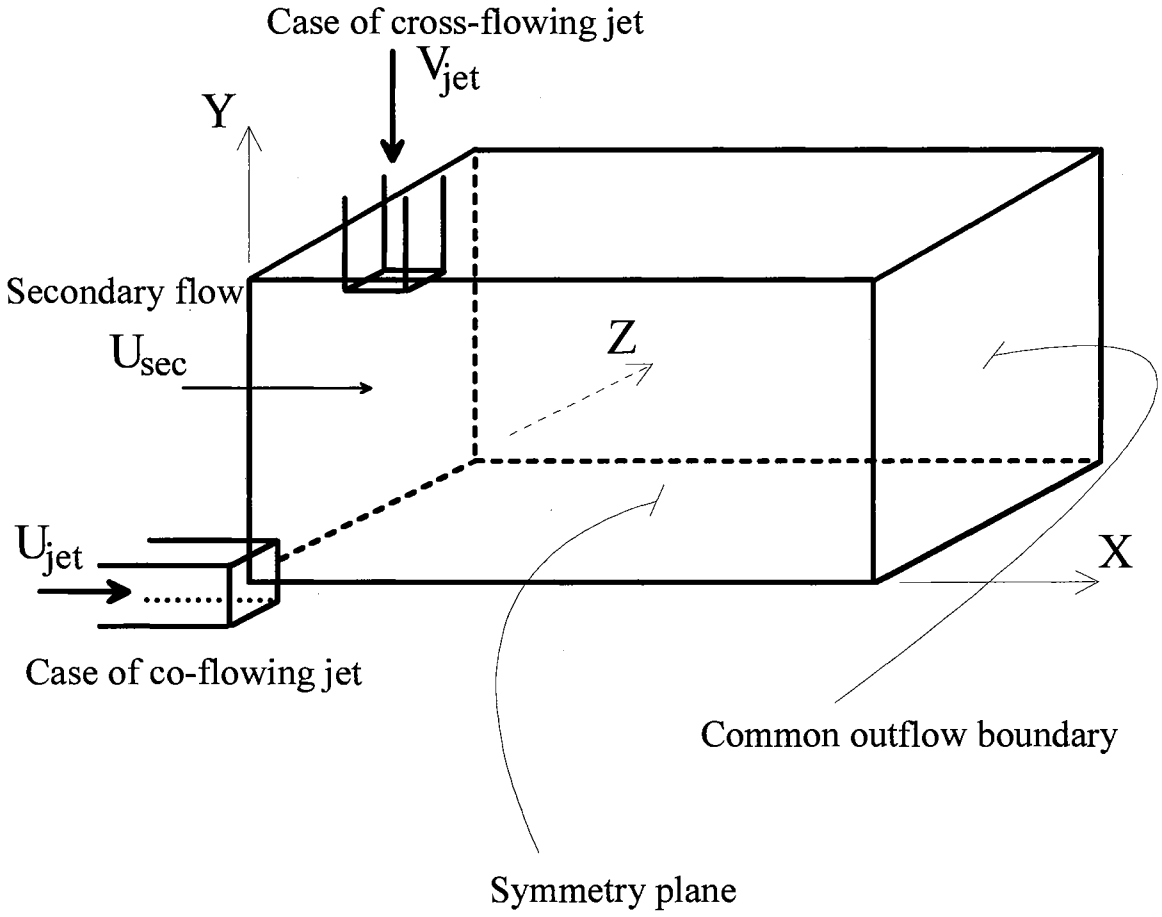

Figure 1. Three Dimensional Physical Domain for Both Co-flowing and Cross-flowing Jet Flows.

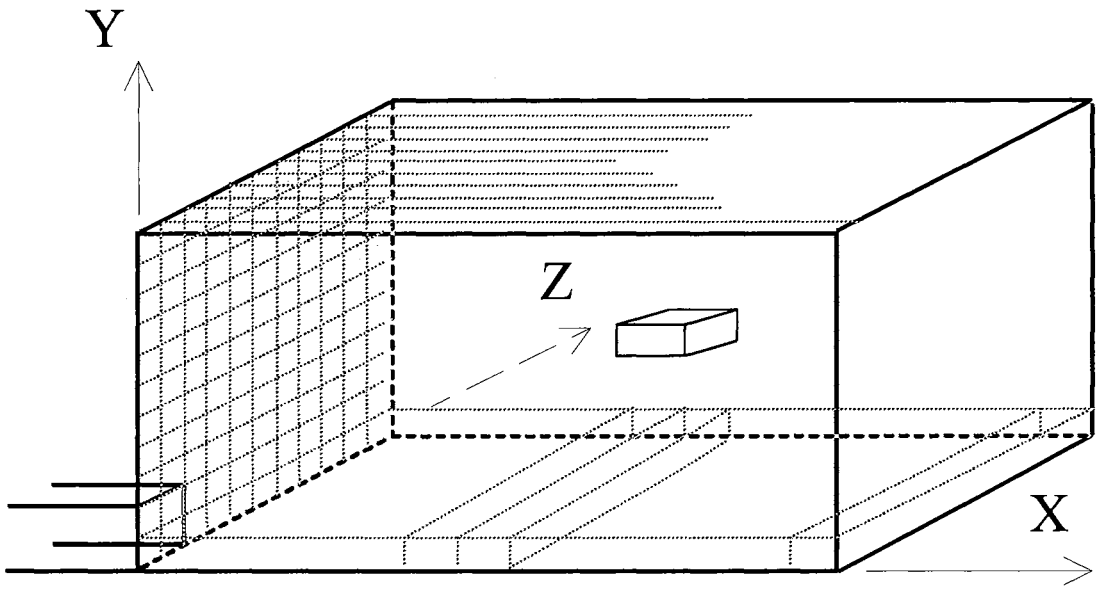

Figure 2. Three-Dimensional Grid System Covering the Flow Domain.

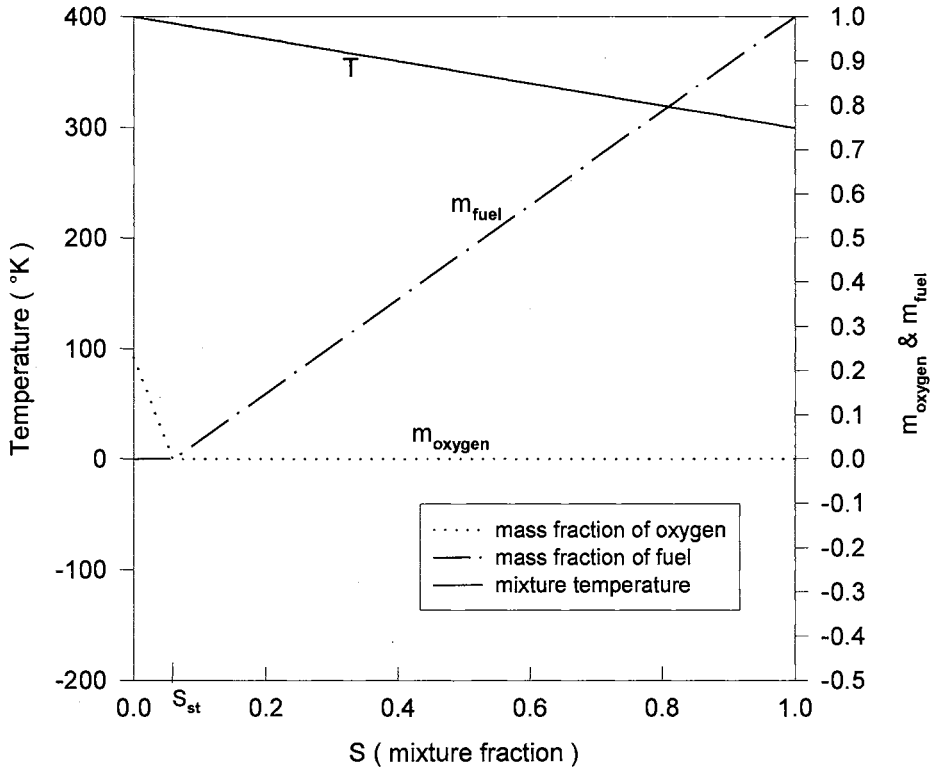

Fuel Jet Flow : Propane (C_3H_8) with $H_{fu} = 0$

Secondary Flow : Air

Inlet Conditions : $T_{air} = 400$ K, $T_{fu} = 300$ K

$\rho_{sec} = 0.879$ kg/m^3 $\rho_{jet} = 1.787$ kg/m^3

$U_{sec} = 30$ m/sec $U_{jet} = 100$ m/sec

Figure 3. Linear Relationships in the SCRS Physically-Controlled Diffusion Flame, With No Chemical Reaction.

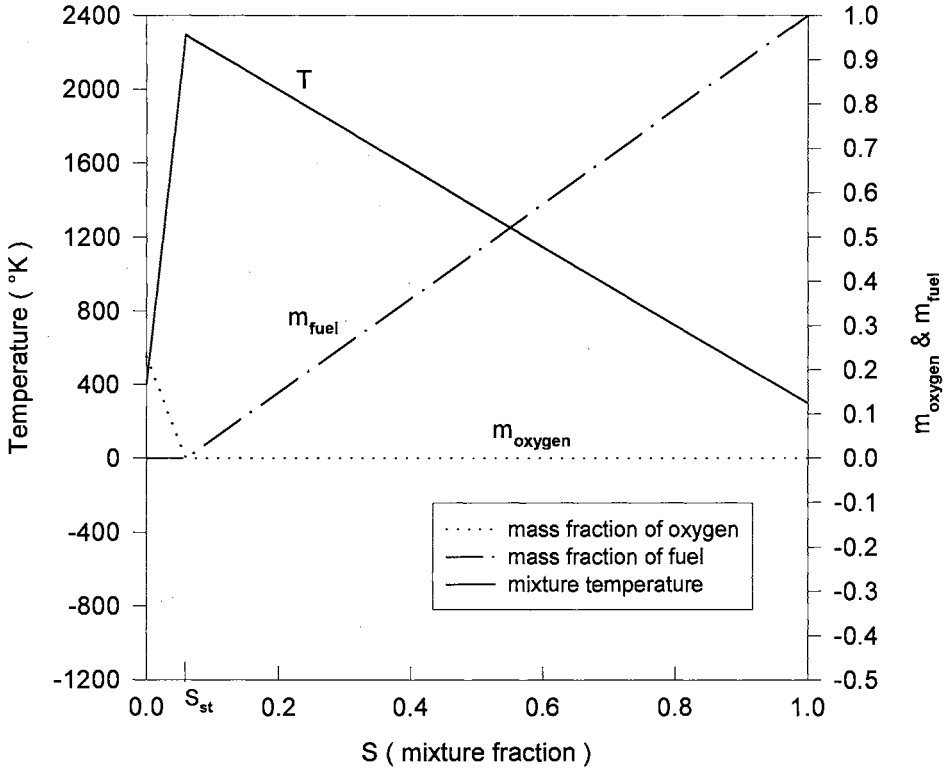

Fuel Jet Flow	: Propane (C_3H_8) with $H_{fu} = 46000$ kJ/kg
Secondary Flow	: Air
Inlet Conditions	: $T_{air} = 400$ K, $T_{fu} = 300$ K
	$\rho_{sec} = 0.879$ kg/m^3 $\rho_{jet} = 1.787$ kg/m^3
	$U_{sec} = 30$ m/sec $U_{jet} = 100$ m/sec

Figure 4. Linear Relationships in the SCRS Physically-Controlled Diffusion Flame, With Chemical Reaction.

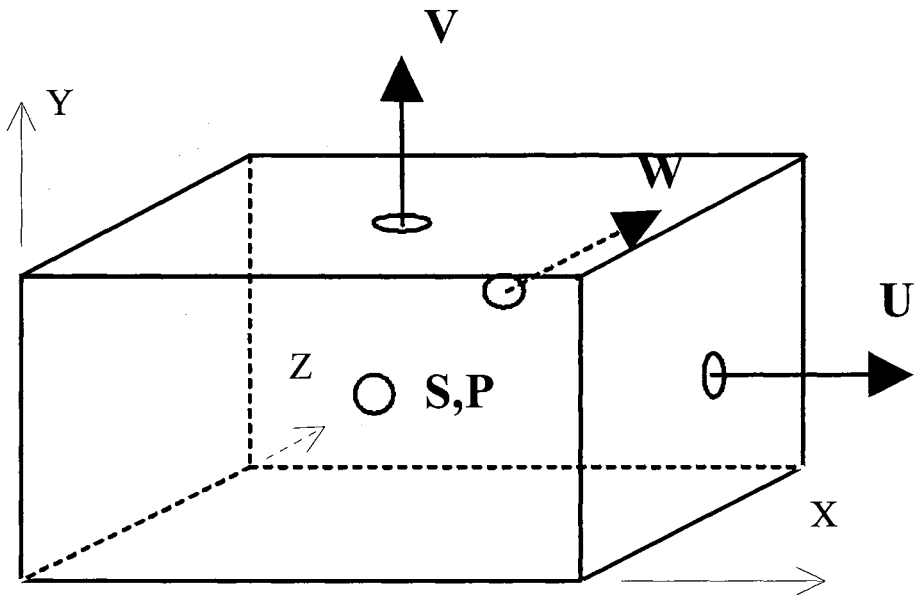

Figure 5. Location of Variables in Typical ijk-Cell.

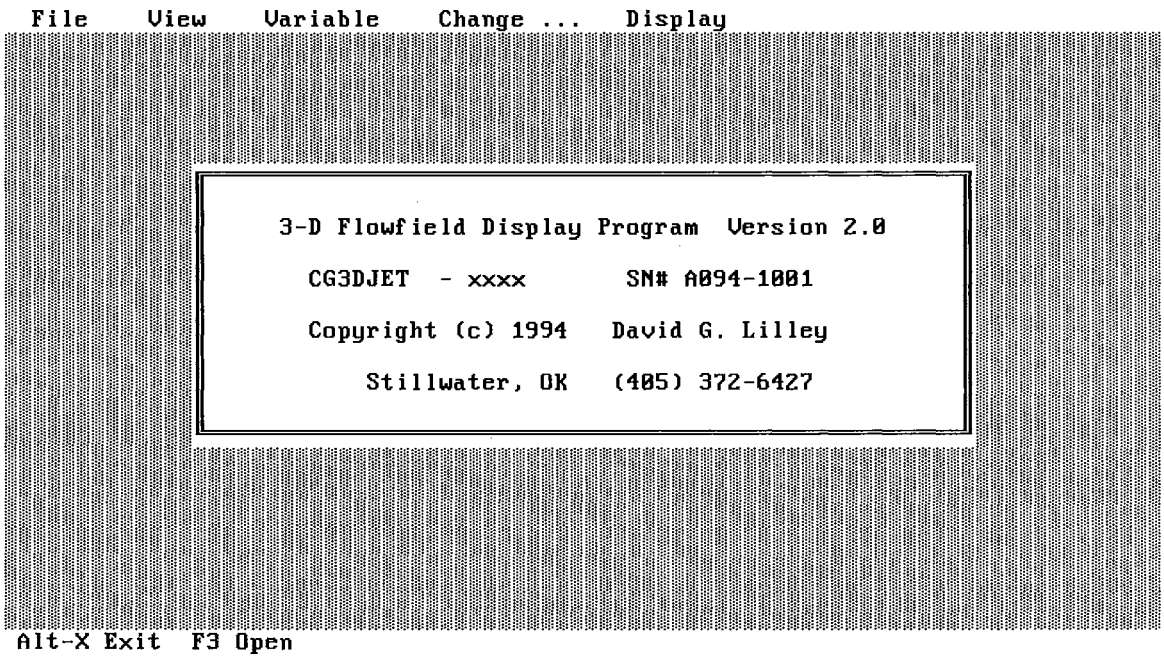

Figure 6. Integrated Environment of Color Display Program.

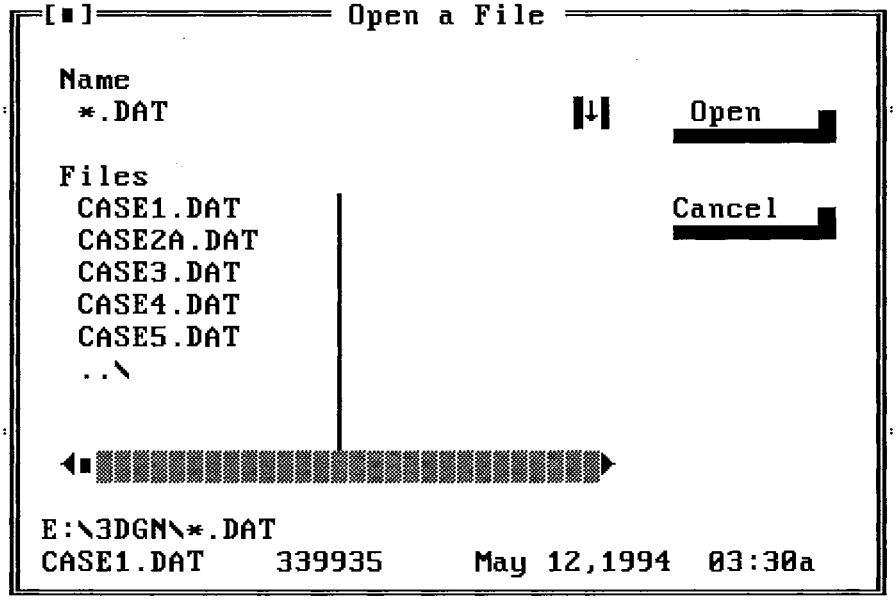

Figure 7. Dialog Box of File-Selection.

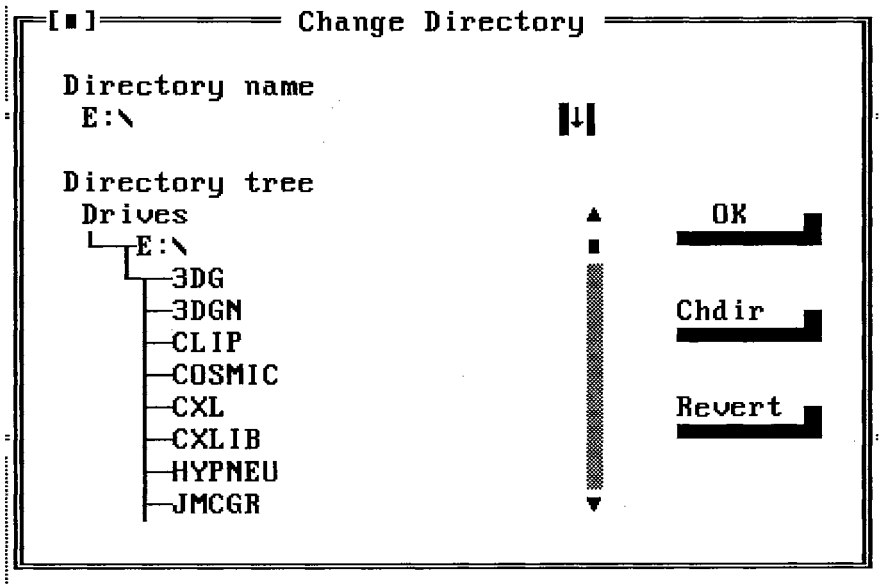

Figure 8. Dialog Box of Change Directory.

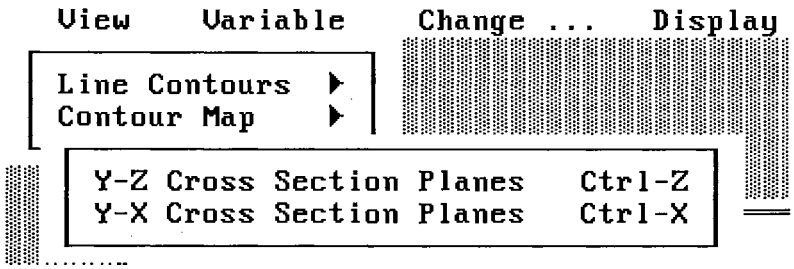

Figure 9. View Menu and its Menu Items with Pop-up Sub-menu.

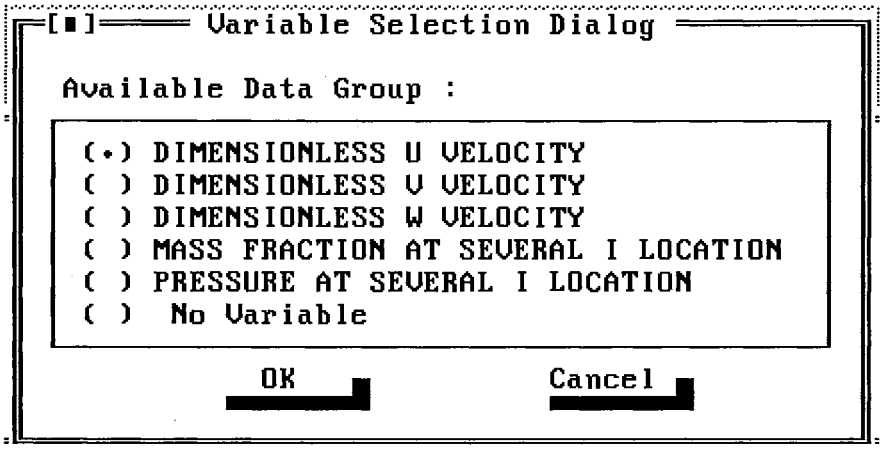

Figure 10. Dialog Box of Variable Selection.

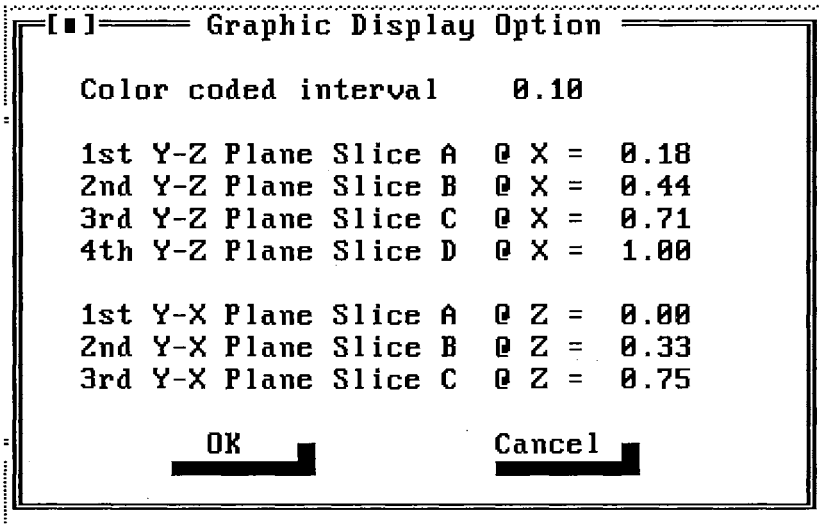

Figure 11. Dialog Box of Graphic Display Option.

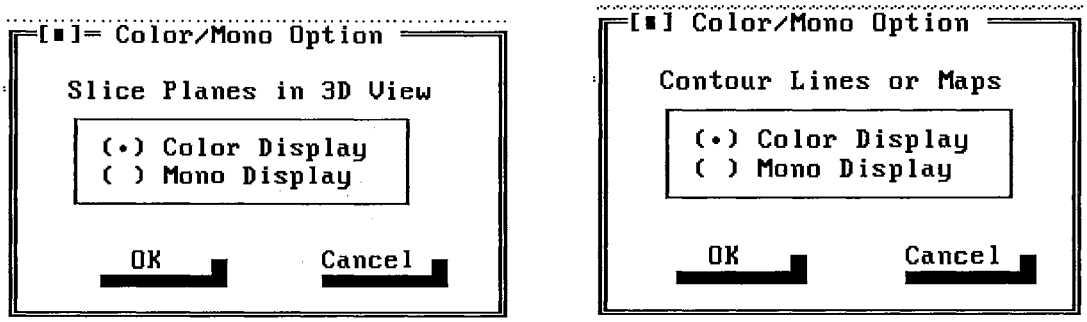

Figure 12. Dialog Box of Color/Mono Display Option for Slice Planes and Contour Plot.

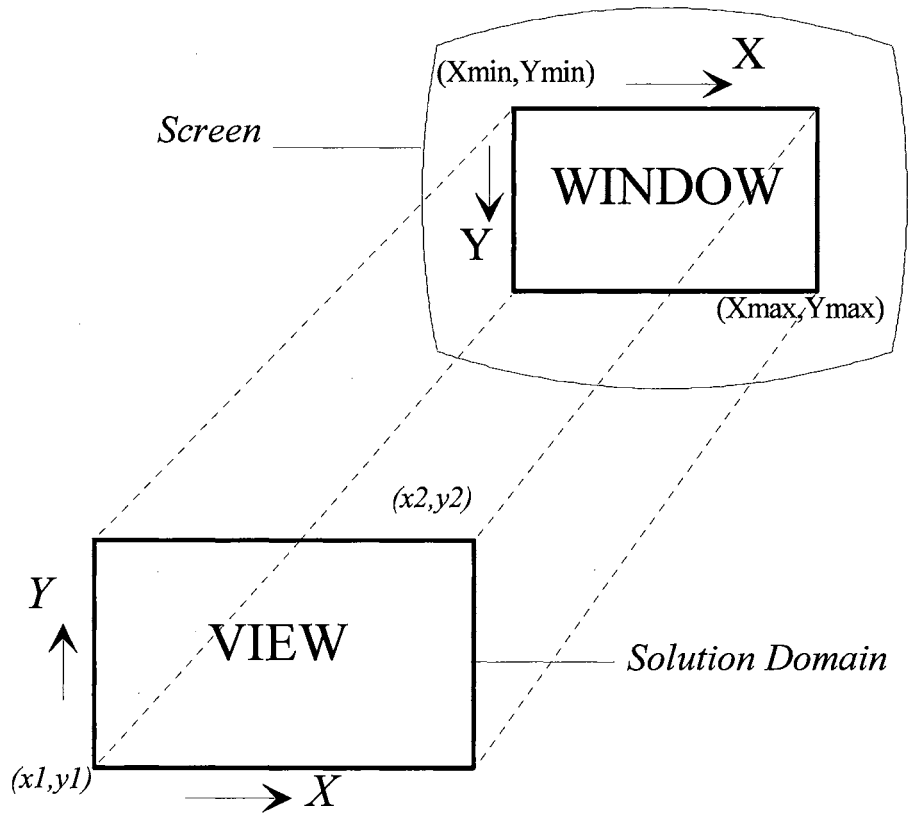

Figure 13. Two Dimensional Mapping between Screen Coordinates and Solution Domain Coordinates.

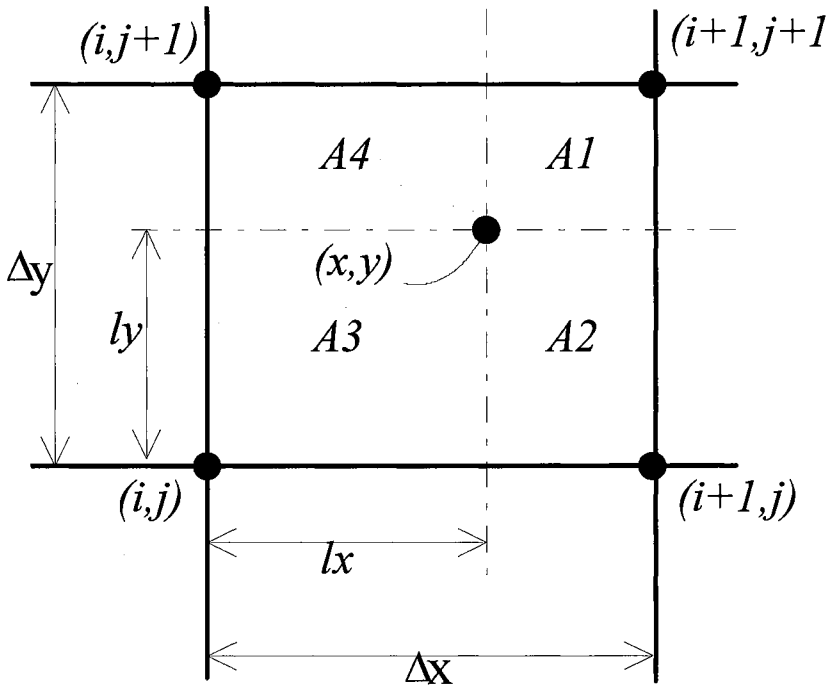

Figure 14. A Typical Point in a Grid Cell.

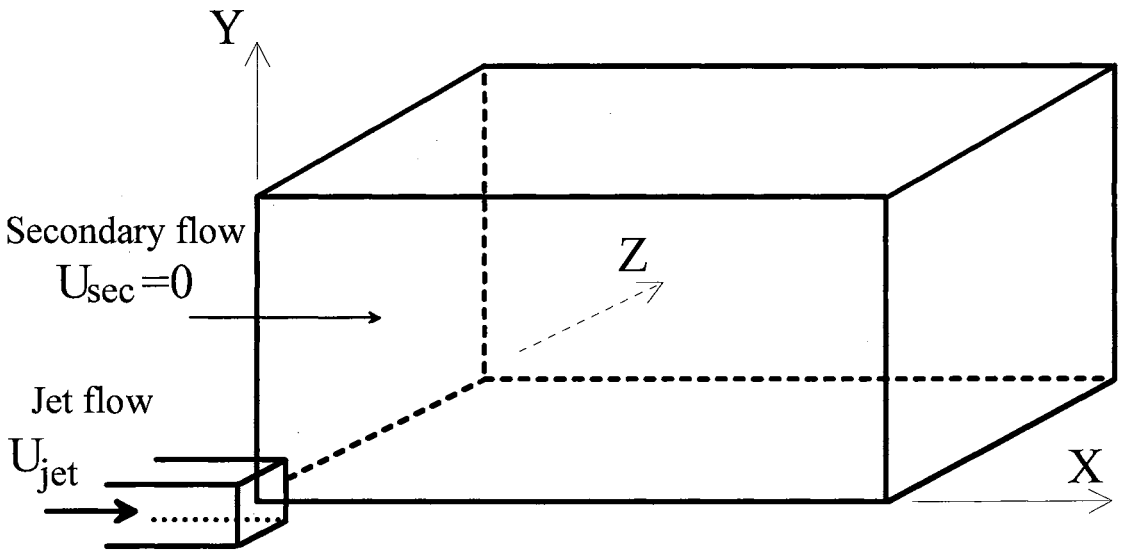

Free Jet of Air into Stagnant Surroundings of Air with Different Density

Solution Domain	: 0.372 x 0.06 x 0.06 m
Jet Diameter	: 0.011 m
Jet Velocity U_{jet}	: 100 m/sec
Jet Density ρ_{jet}	: 1.2 kg/m^3
Surroundings ρ_{sec}	: 0.3, 0.6, 1.2 kg/m^3
Temperature of Air	: 300 K

Figure 15. Schematic for a Free Jet of Air into Stagnant Surroundings of Air with Different Density. (Test Case 1)

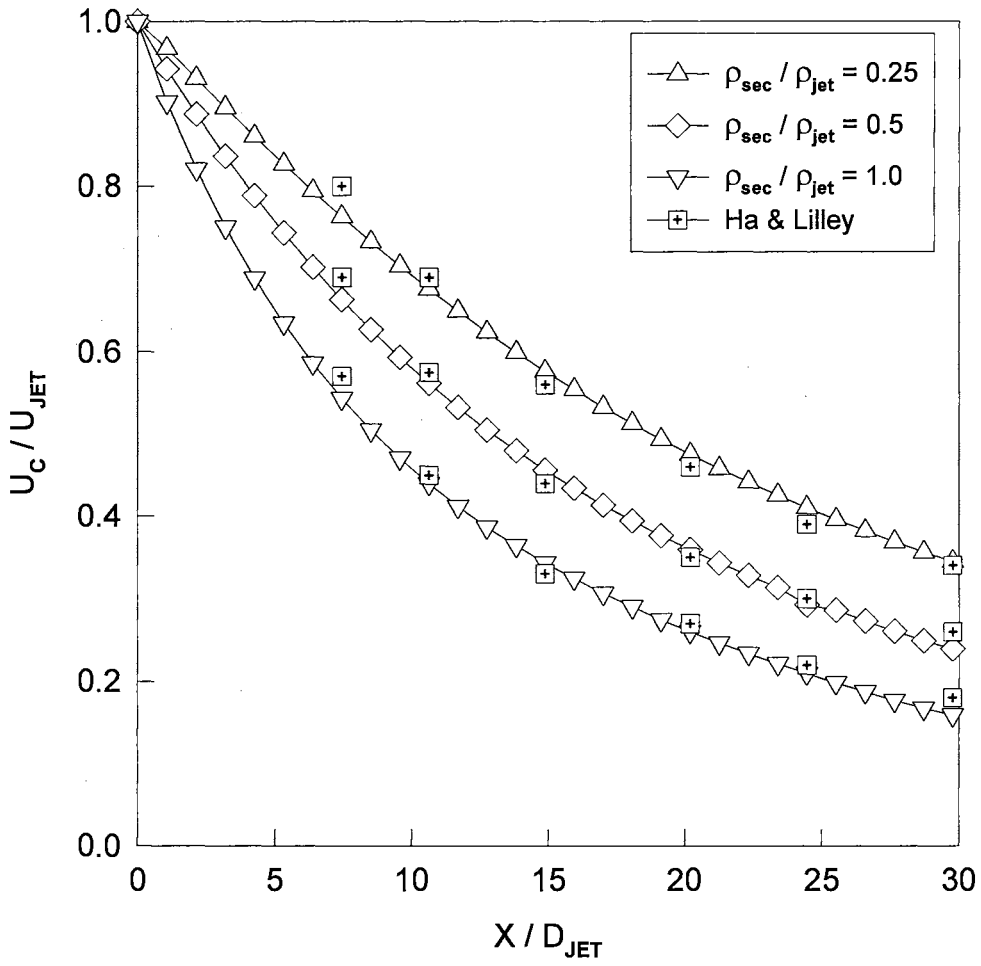

Figure 16. Effect of Density Ratio (Surroundings to Jet) on Axial Velocity Maximum Decay with U_{sec}=0. (Test Case 1)

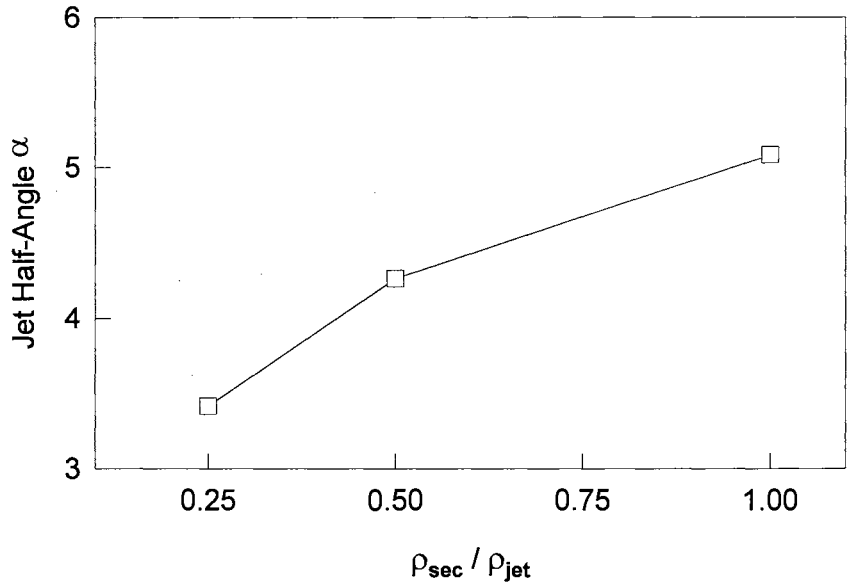

Figure 17. Effect of Density on Jet-Half-Angle α. (Test Case 1)

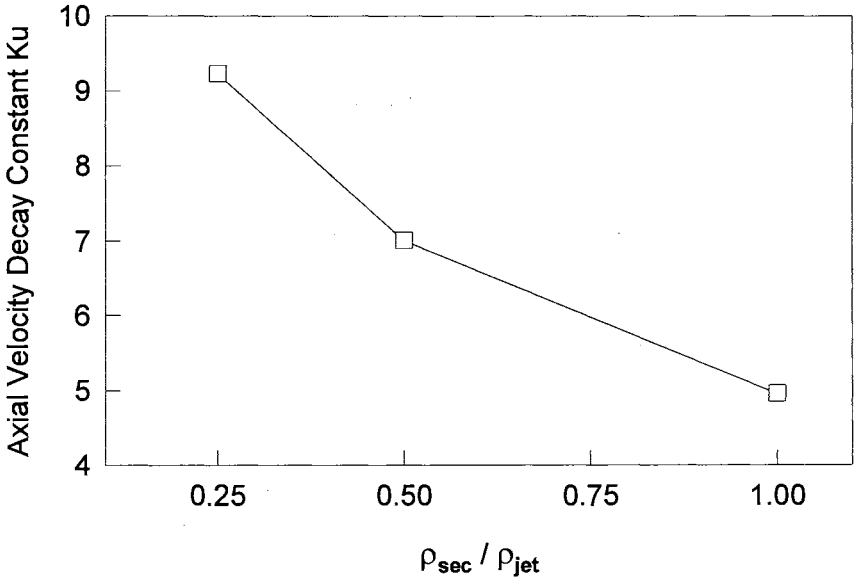

Figure 18. Effect of Density on Axial Velocity Decay Constant K_u. (Test Case 1)

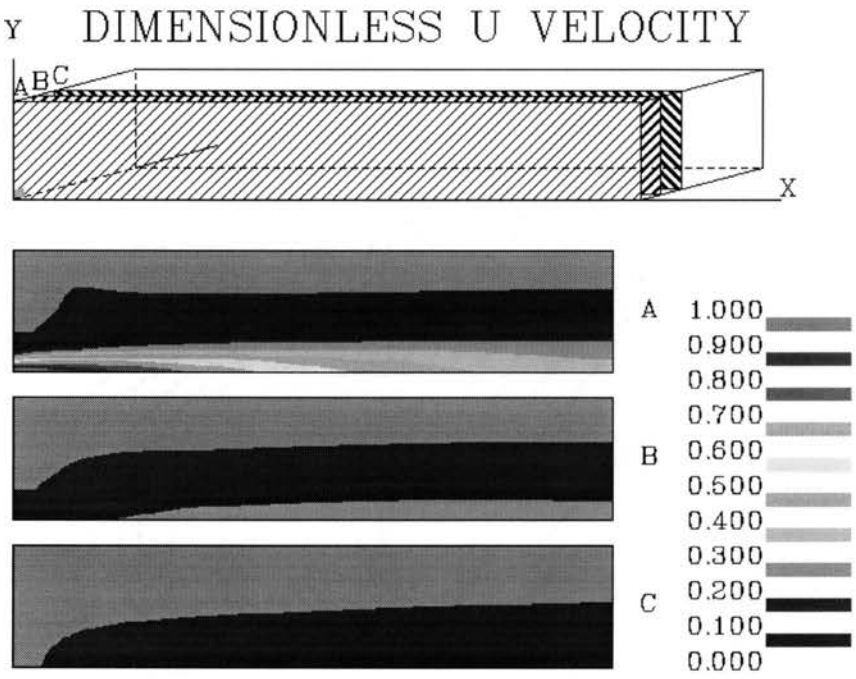

(a) Longitudinal Slices

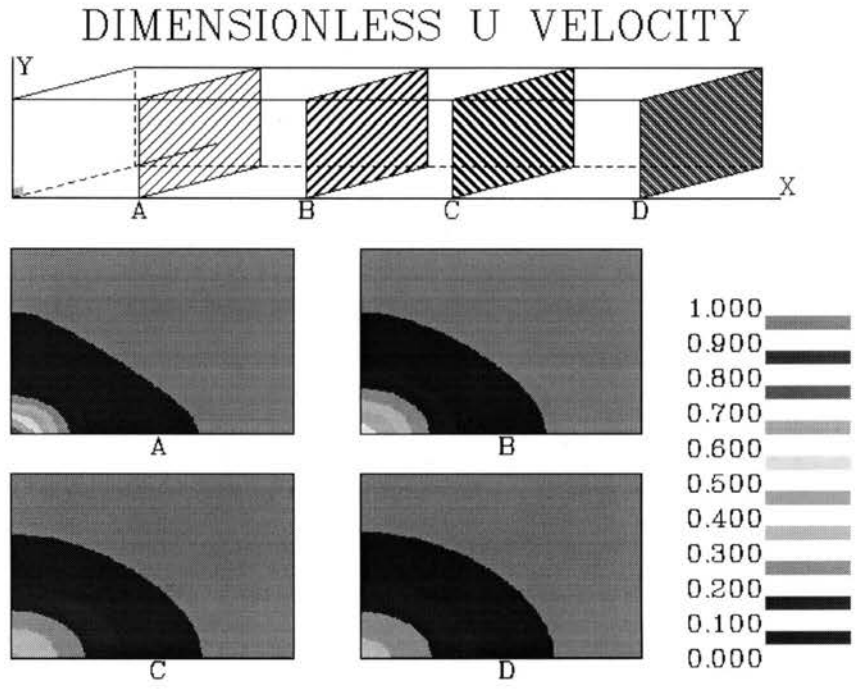

b) Lateral Slices

Figure 19. Dimensionless Axial Velocity for the Different Density Case with $\rho_{sec} / \rho_{jet} = 0.25$. (Test Case 1)

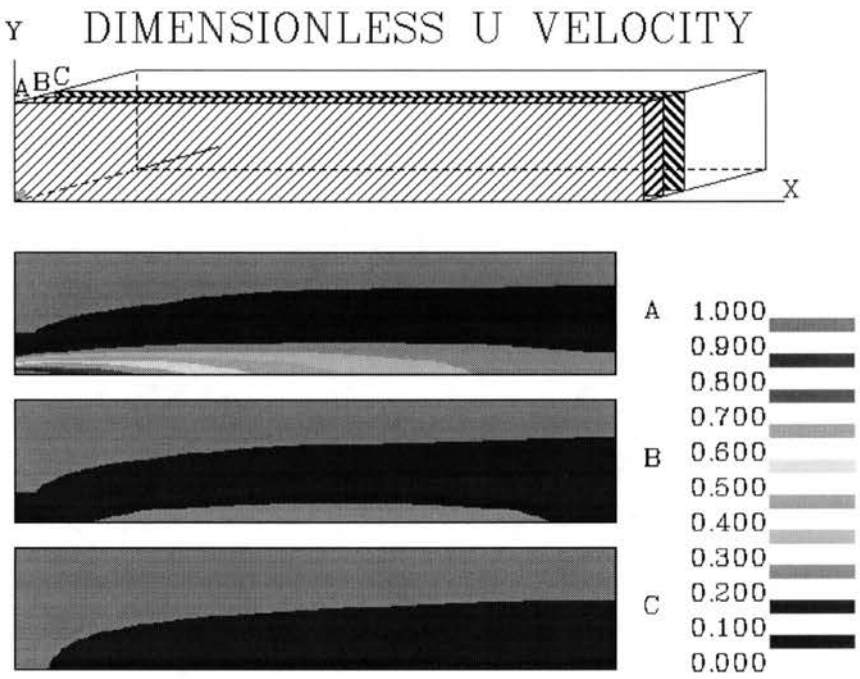

a) Longitudinal Slices

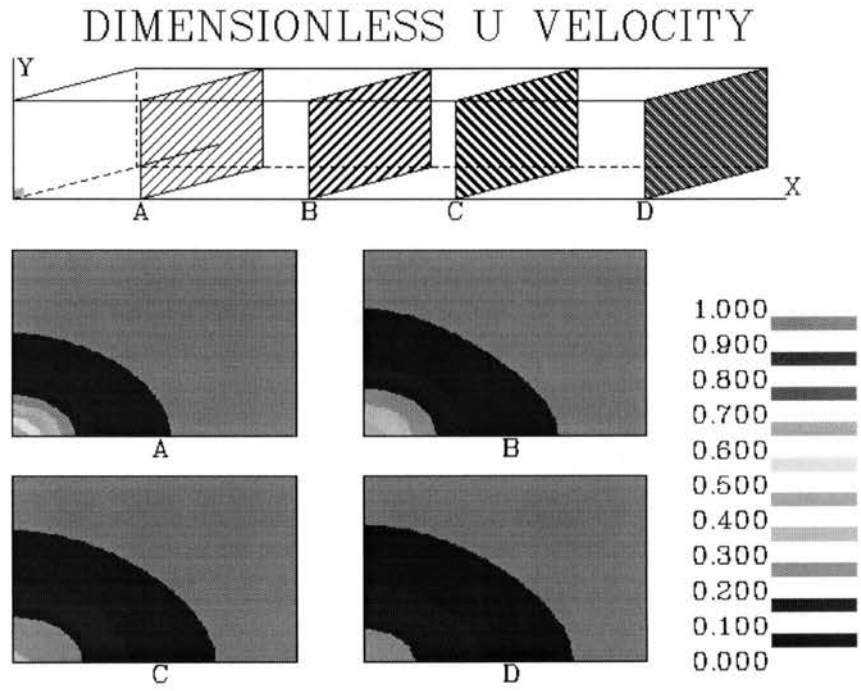

b) Lateral Slices

Figure 20. Dimensionless Axial Velocity for the Different Density Case with $\rho_{sec} / \rho_{jet} = 0.5$. (Test Case 1)

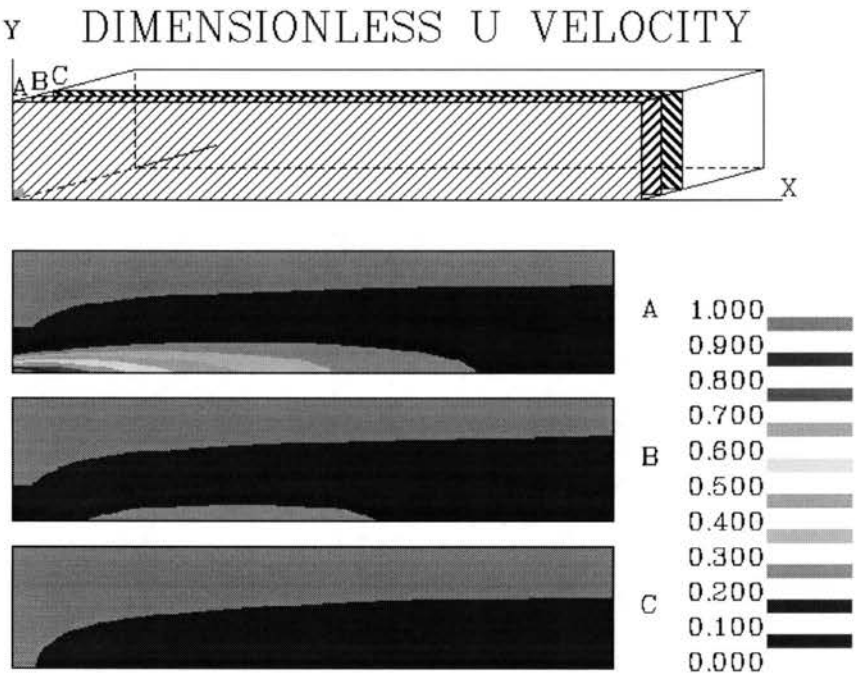

a) Longitudinal Slices

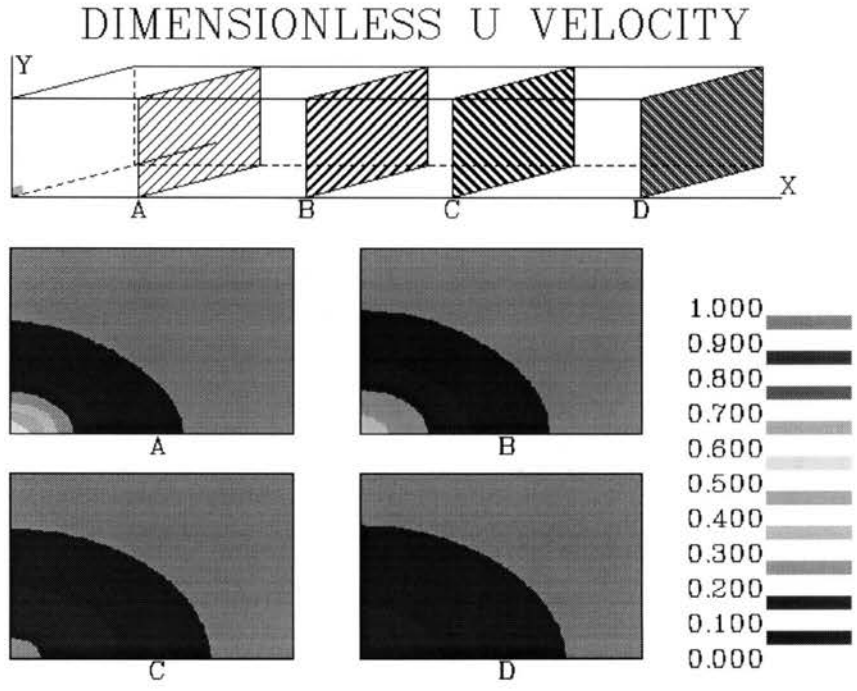

b) Lateral Slices

Figure 21. Dimensionless Axial Velocity for the Different Density Case with $\rho_{sec} / \rho_{jet} = 1.0$. (Test Case 1)

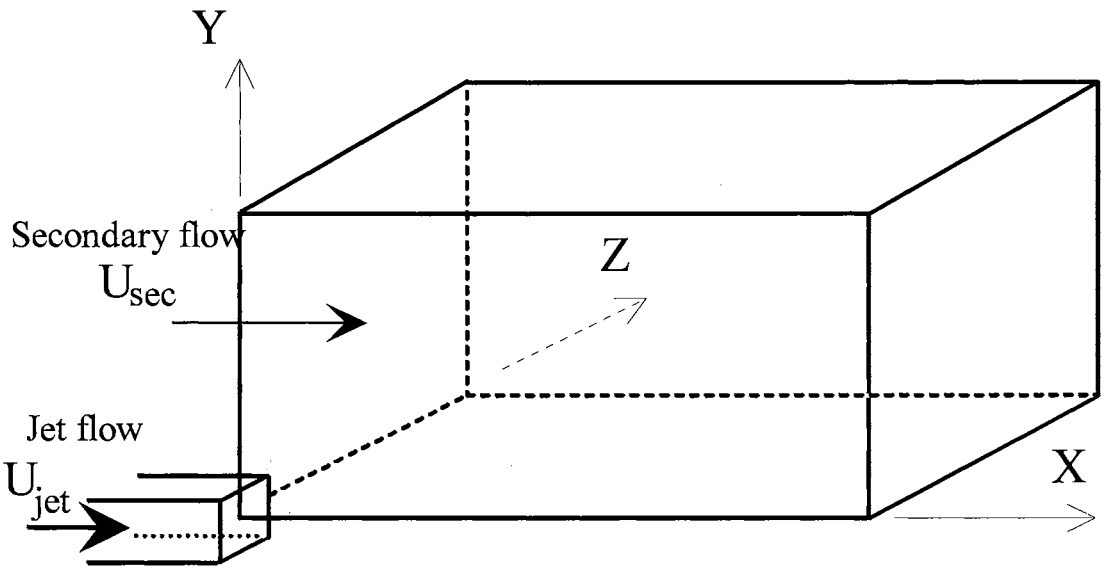

Free Jet of Air into Co-flowing Secondary Flow of Air

Solution Domain	: 0.272 x 0.06 x 0.06 m
Jet Diameter	: 0.011284 m
U_{jet}	: 100 m/sec
U_{sec}	: 0, 25, 50 m/sec
Density of Air	: 1.2 kg/m^3
Temperature of Air	: 300 K

Figure 22. Test Case 2. : Solution Domain for a Free Jet in Co-flowing Surrounding Flow.

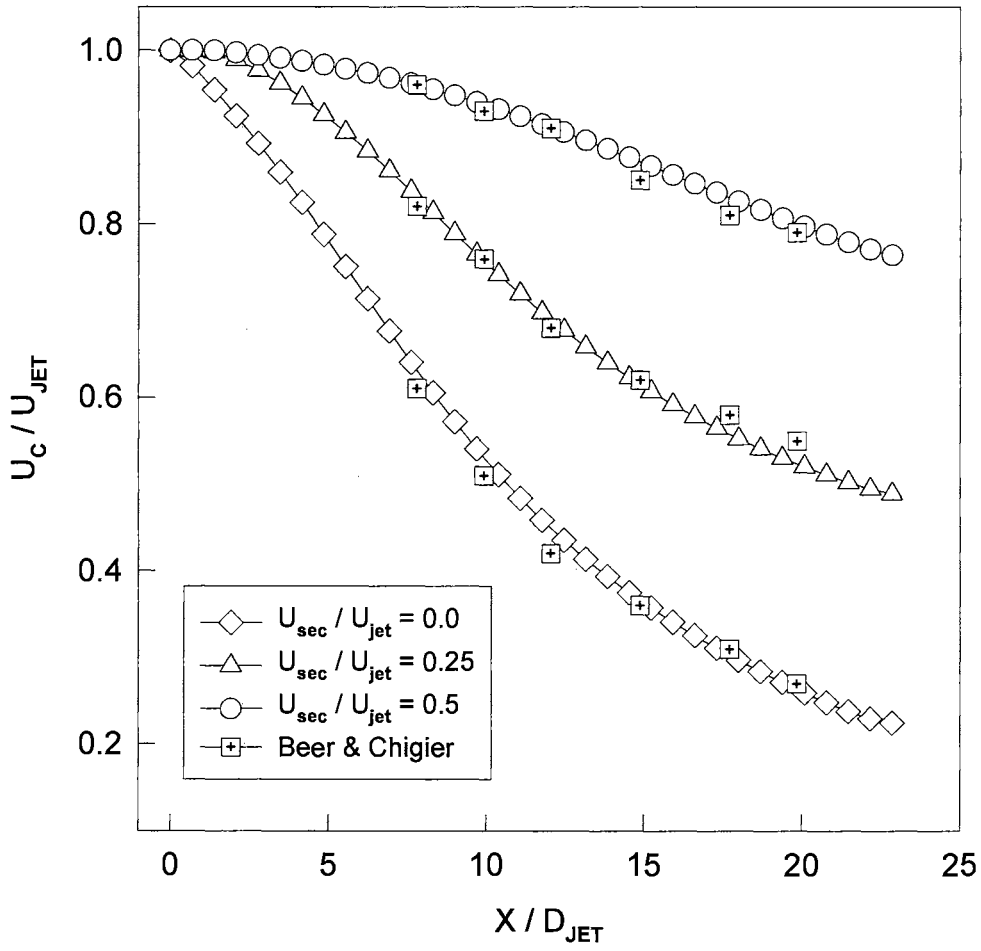

Figure 23. Effect of Velocity Ratio (Secondary to Jet) on Axial Velocity Maximum Decay. (Test Case 2)

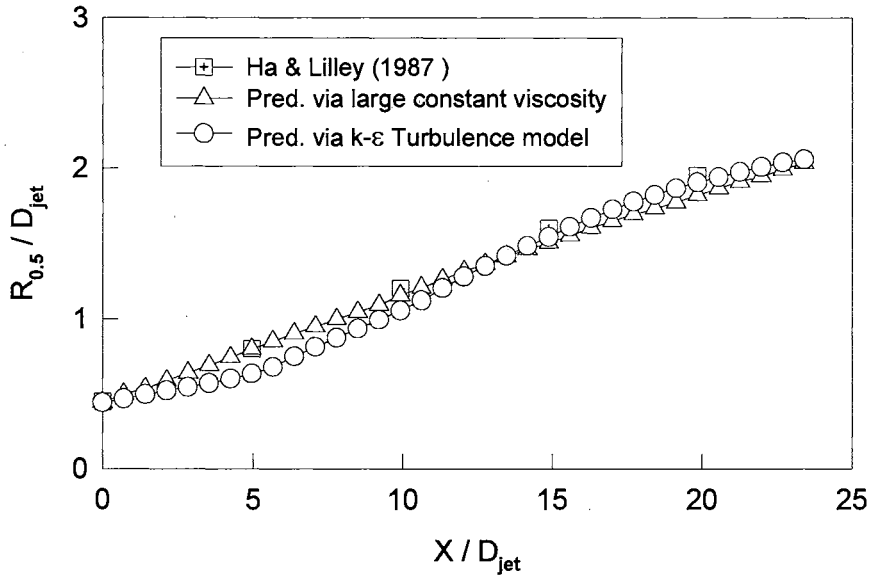

Figure 24. Half Velocity Line for a Free Jet in Stagnant Surroundings. (Test Case 2)

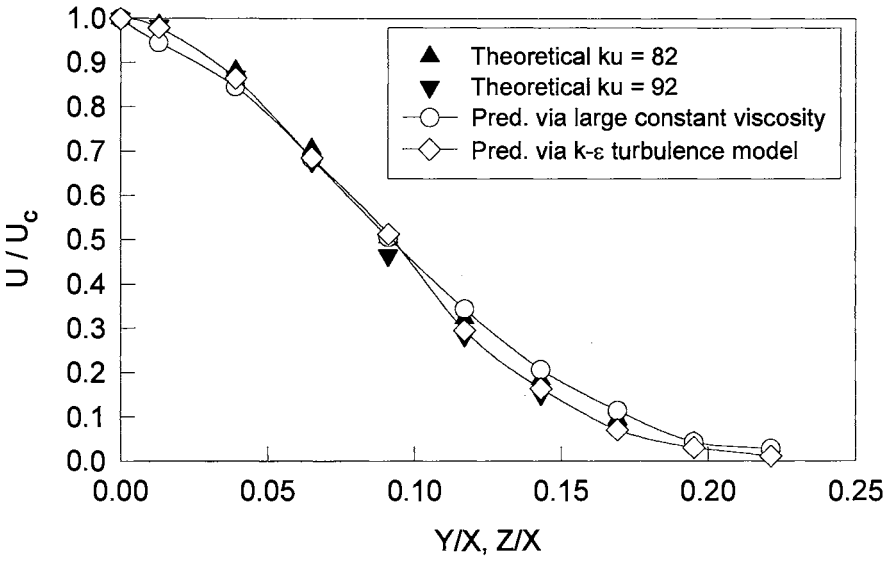

Figure 25. Transverse Profile of Velocity for a Free Jet in Stagnant Surroundings. (Test Case 2)

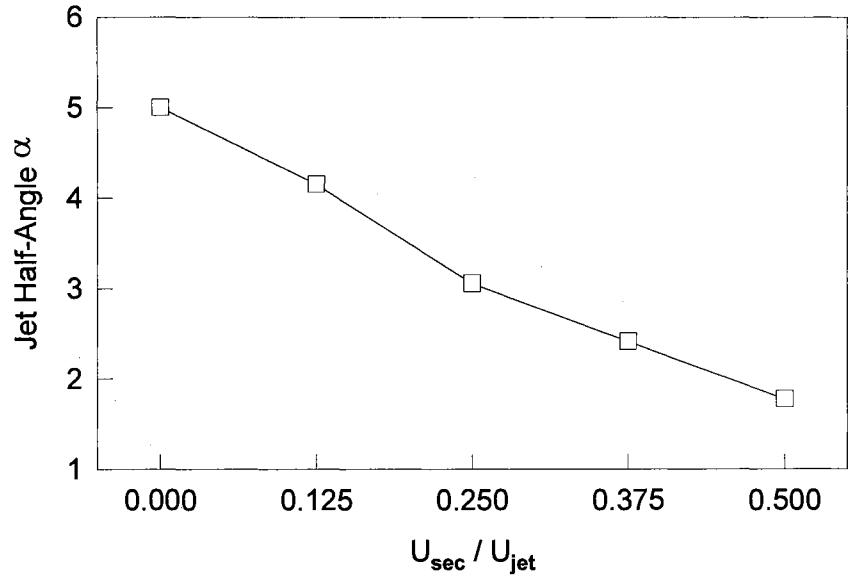

Figure 26. Effect of Velocity Ratio on Jet Half-Angle α. (Test Case 2)

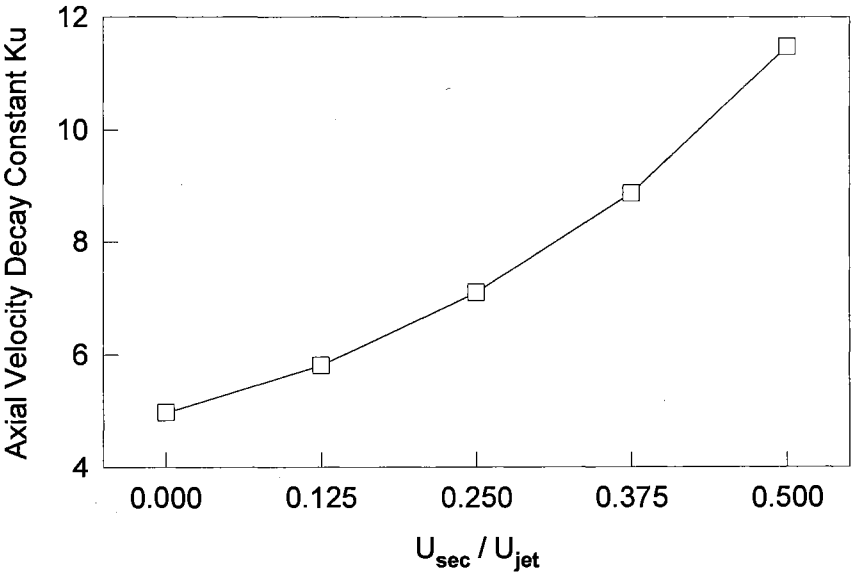

Figure 27. Effect of Velocity Ratio on Axial Velocity Decay Constant K_u. (Test Case 2)

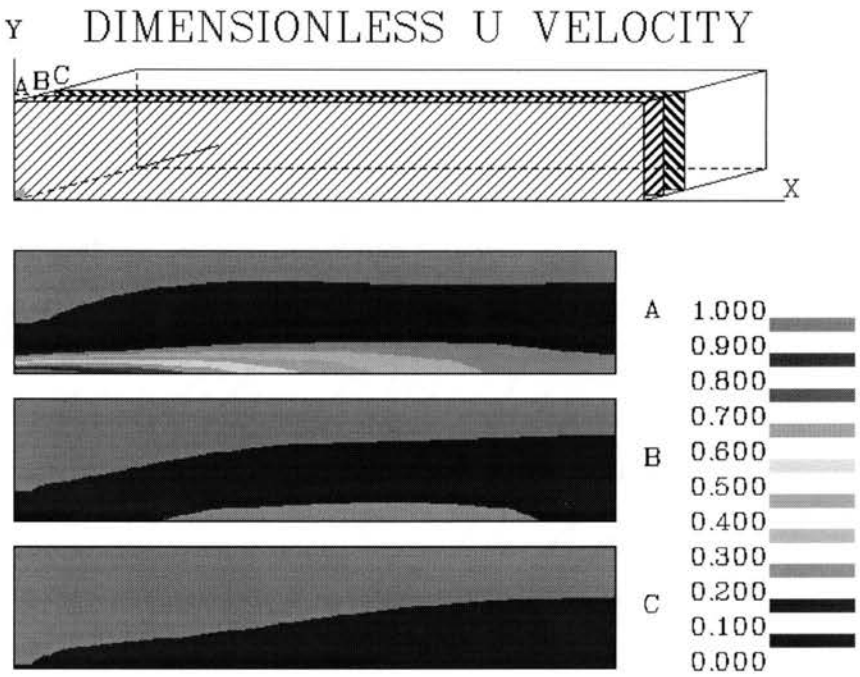

a) Longitudinal Slices

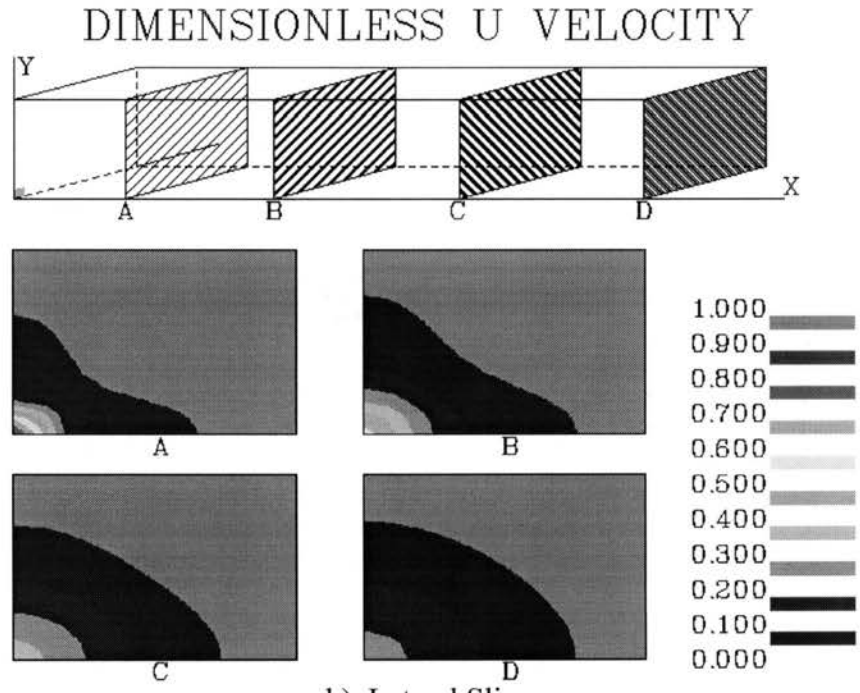

b) Lateral Slices

Figure 28. Dimensionless Axial Velocity for the Stagnant Surroundings Case with VR = 0.

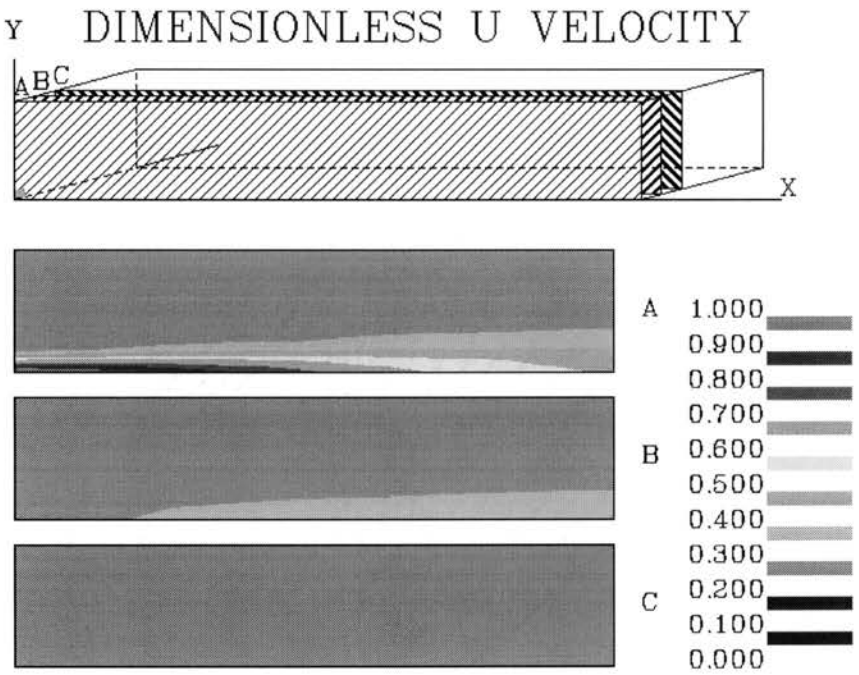

a) Longitudinal Slices

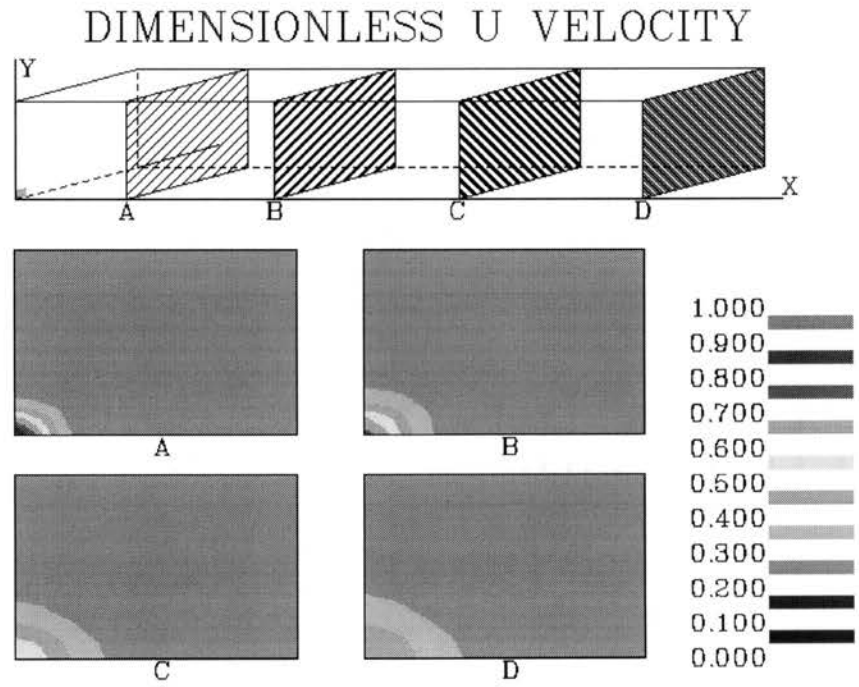

b) Lateral Slices

Figure 29. Dimensionless Axial Velocity for the Co-flowing Case with VR = 0.25. (Test Case 2)

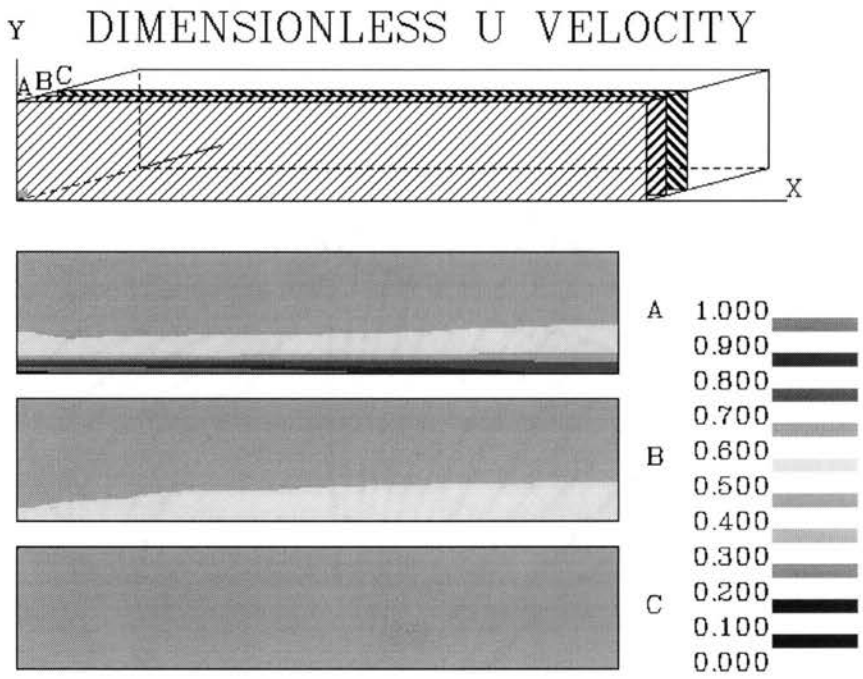

a) Longitudinal Slices

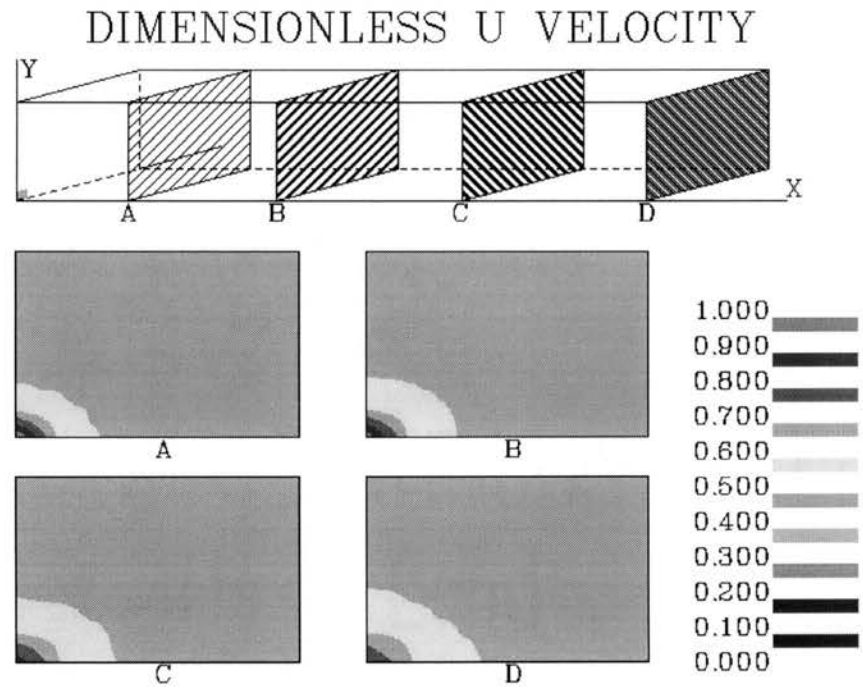

b) Lateral Slices

Figure 30. Dimensionless Axial Velocity for the Co-flowing Case with VR = 0.5. (Test Case 2)

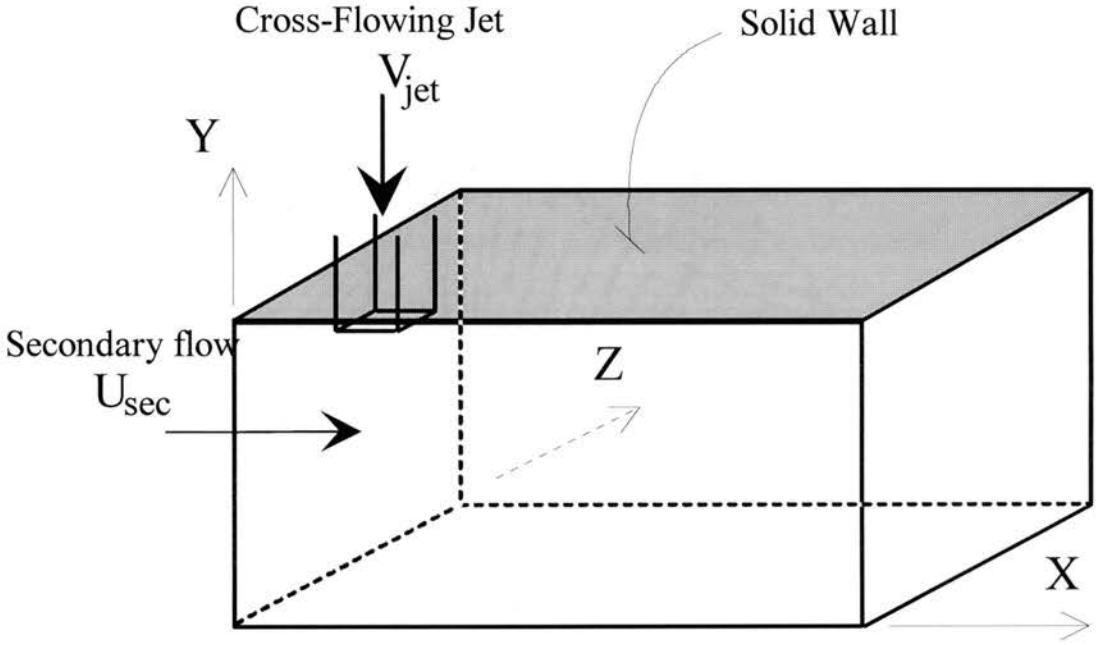

Solution Domain	: 0.165 x 0.127 x 0.0635 m
Jet Diameter	: 0.00635 m
V_{jet}	: 59.79 m/sec
ρ_{jet} (Density)	: 0.746 kg/m^3
T_{jet} (Temperature)	: 471 K
U_{sec}	: 6.096 m/sec
ρ_{sec} (Density)	: 1.204 kg/m^3
T_{sec} (Temperature)	: 293 K

Figure 31. Test Case 3. : Solution Domain for a Jet in Cross-flowing Flow.

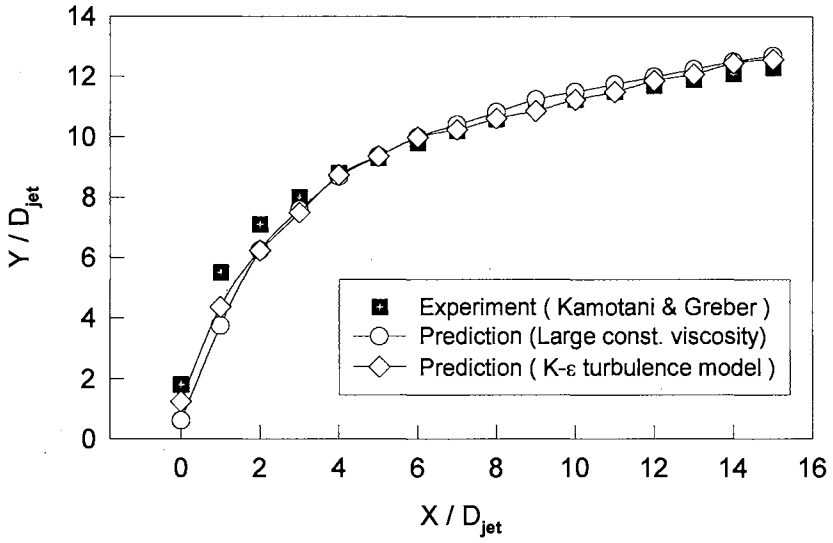

Figure 32. Maximum Temperature Centerline Location. (Test Case 3)

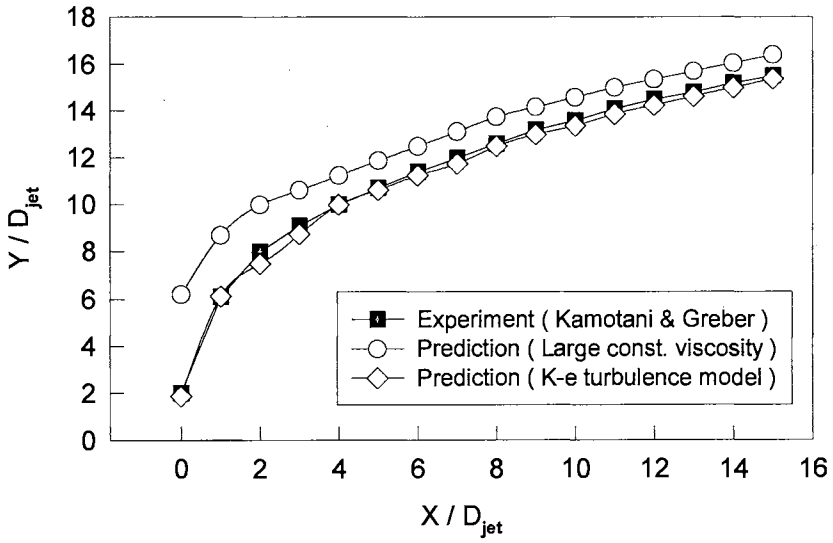

Figure 33. Maximum Velocity Centerline Location. (Test Case 3)

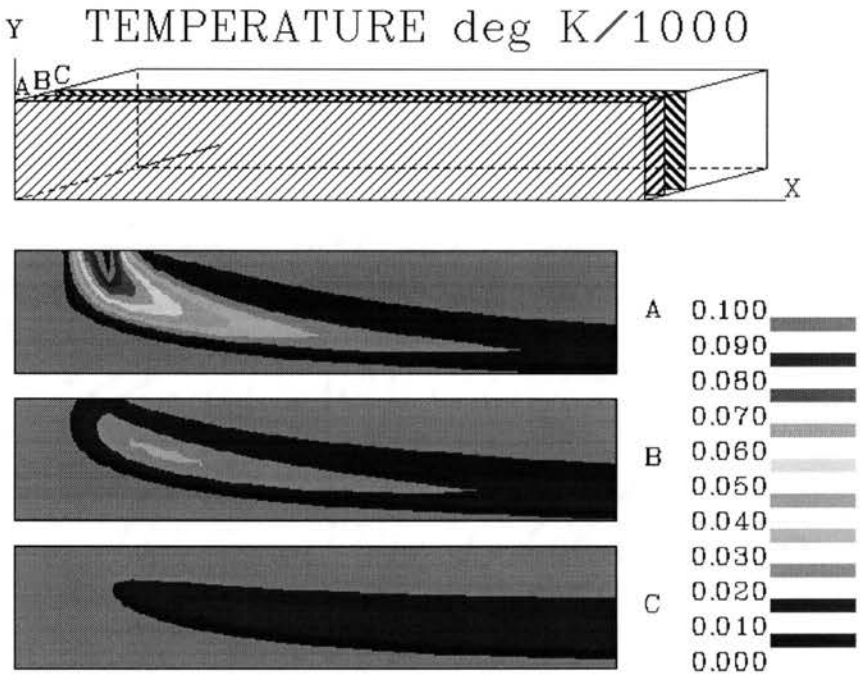

a) Longitudinal Slices

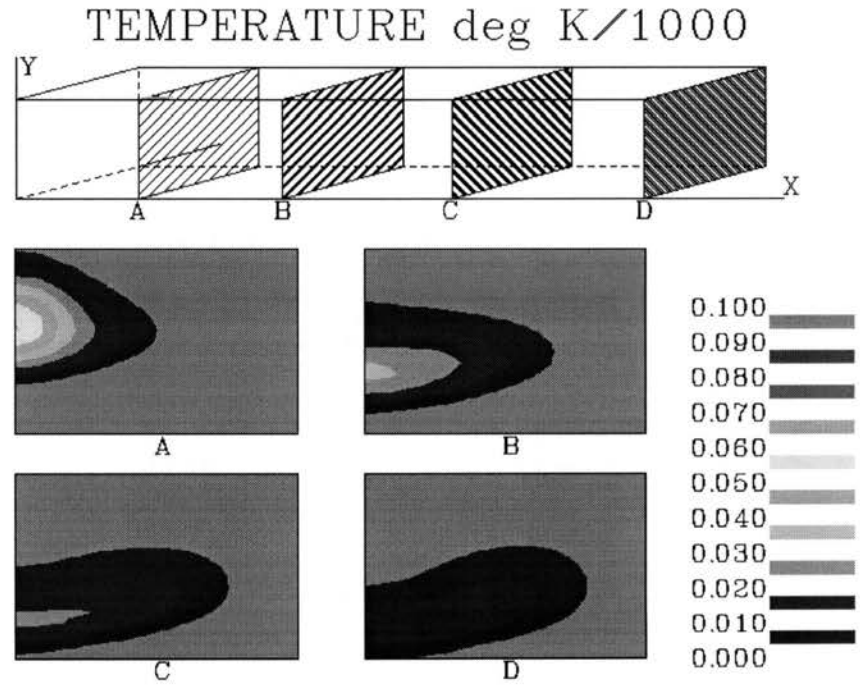

b) Lateral Slices

Figure 34. Temperature Distribution for a Jet in Cross-flowing flow. (Test Case 3)

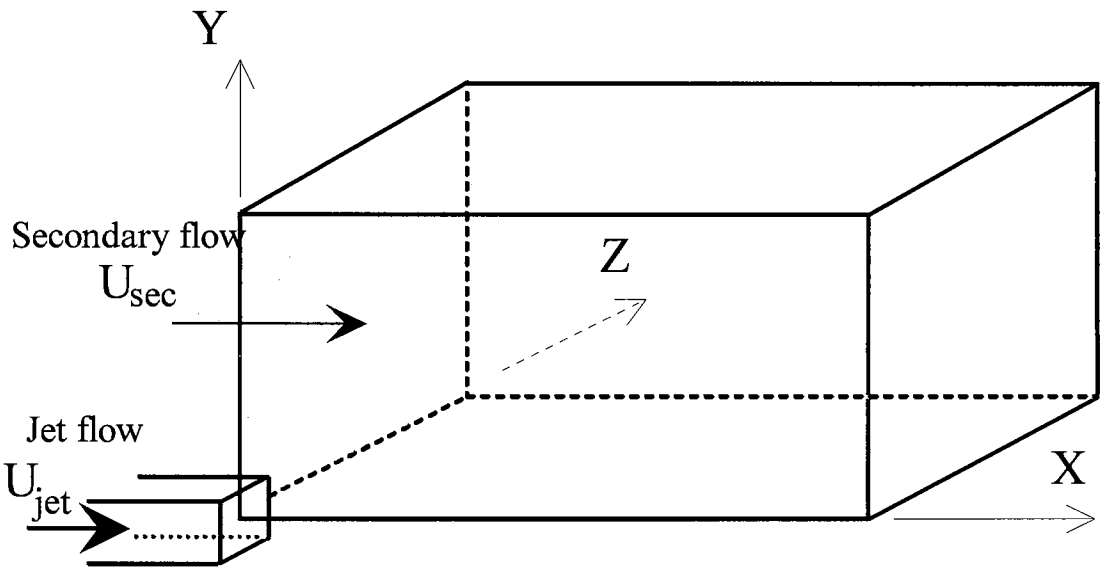

Free Jet of H_2 Emerging into Co-flowing Flow of Air at 300 K

Solution Domain	: 0.396 x 0.0473 x 0.0473 m
Jet Diameter	: 0.00762 m
$U_{sec} / U_{jet} = 0.2$	: $U_{jet} = 107.1$ m/sec, $U_{sec} = 21.4$ m/sec
$U_{sec} / U_{jet} = 0.1$	: $U_{jet} = 151.1$ m/sec, $U_{sec} = 15.1$ m/sec
Density of Air	: 1.2 kg/m^3
Temperature of Air	: 300 K

Figure 35. Solution Domain for Diffusion Flames of a Round Jet of Hydrogen in a Co-flowing Stream of Air. (Test Case 4)

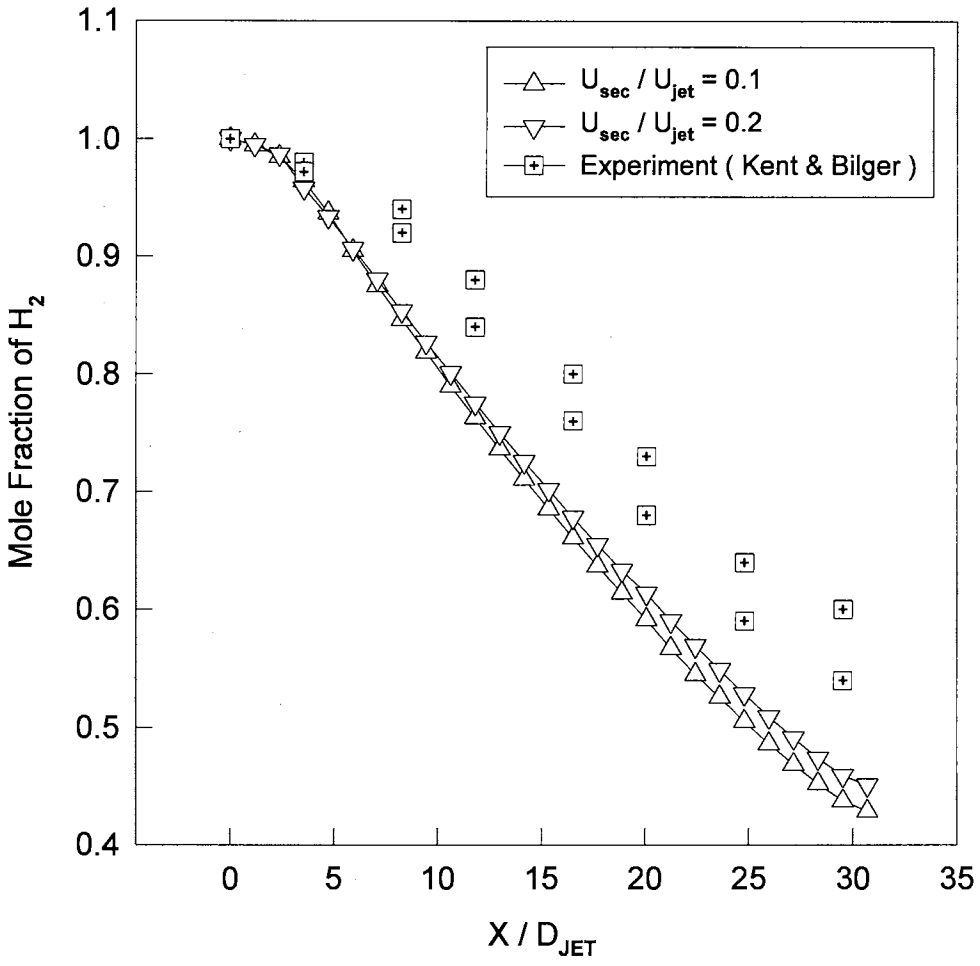

Figure 36. Axial Distribution of H_2-composition .
(Prediction via constant viscosity)
(Test Case 4)

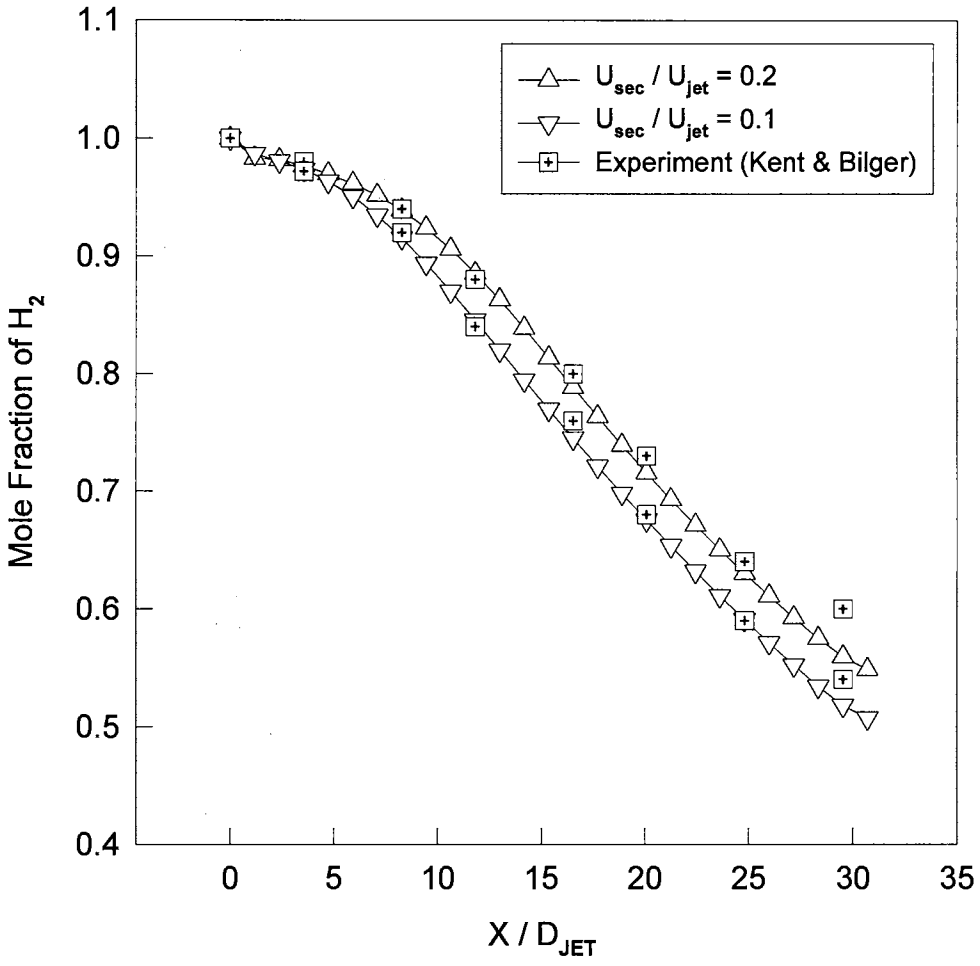

Figure 37. Axial Distribution of H_2-composition.
(Prediction via k-ε turbulence model)
(Test Case 4)

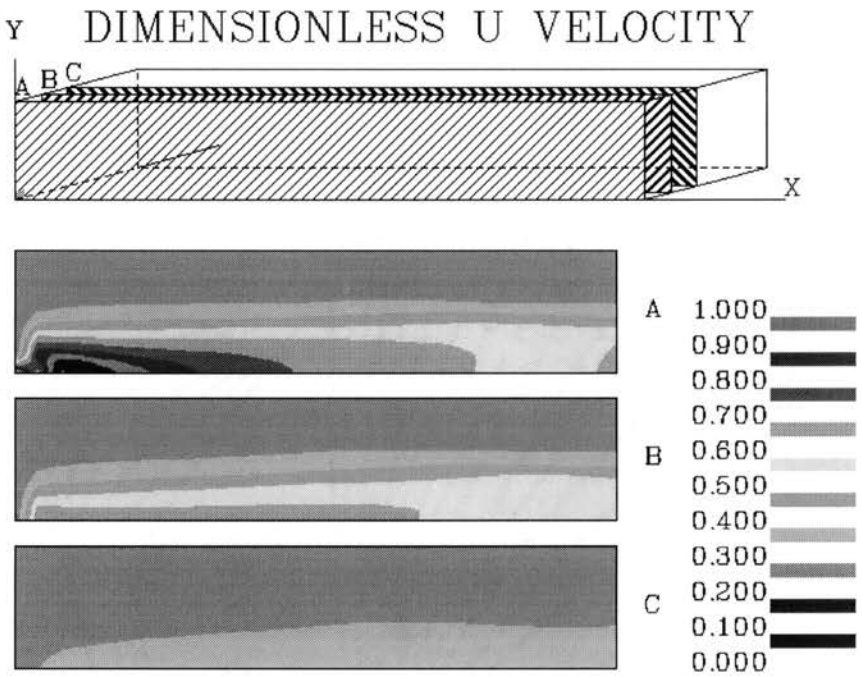

(a) Longitudinal Slices

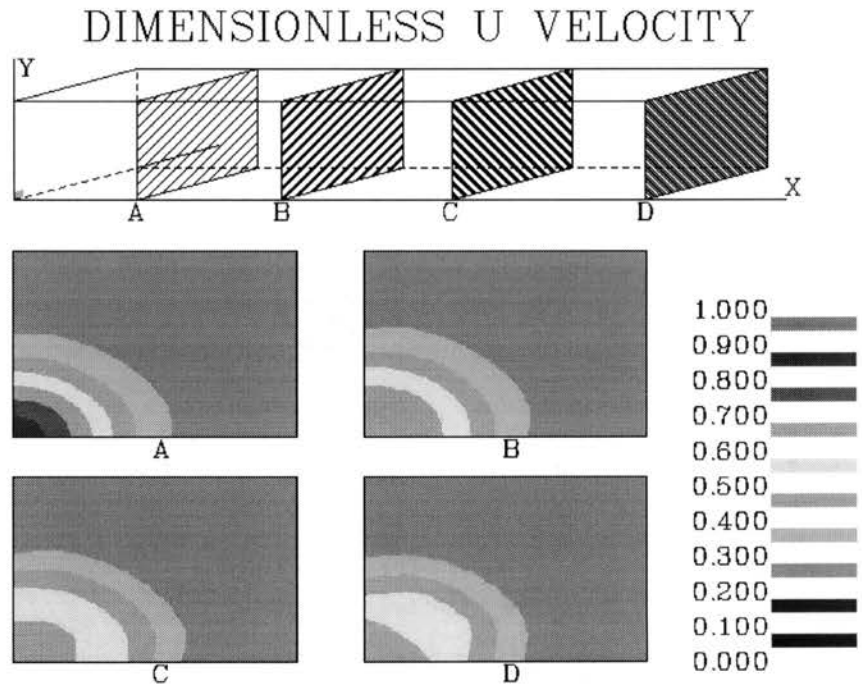

b) Lateral Slices

Figure 38. Dimensionless Axial Velocity for the VR=0.2 Reacting Jet. (Test Case 4)

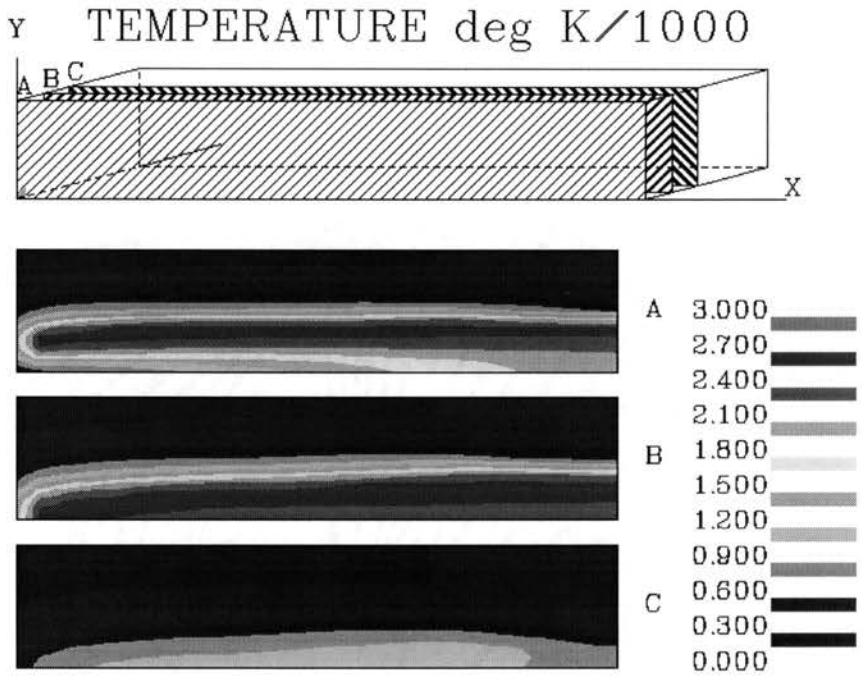

(a) Longitudinal Slices

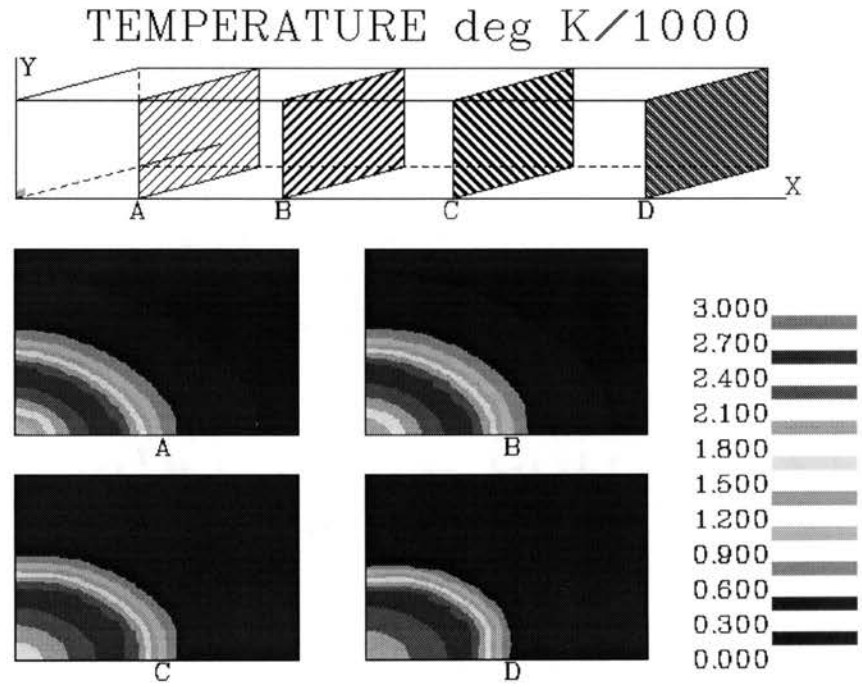

b) Lateral Slices

Figure 39. Temperature Distribution for the VR=0.2 Reacting Jet. (Test Case 4)

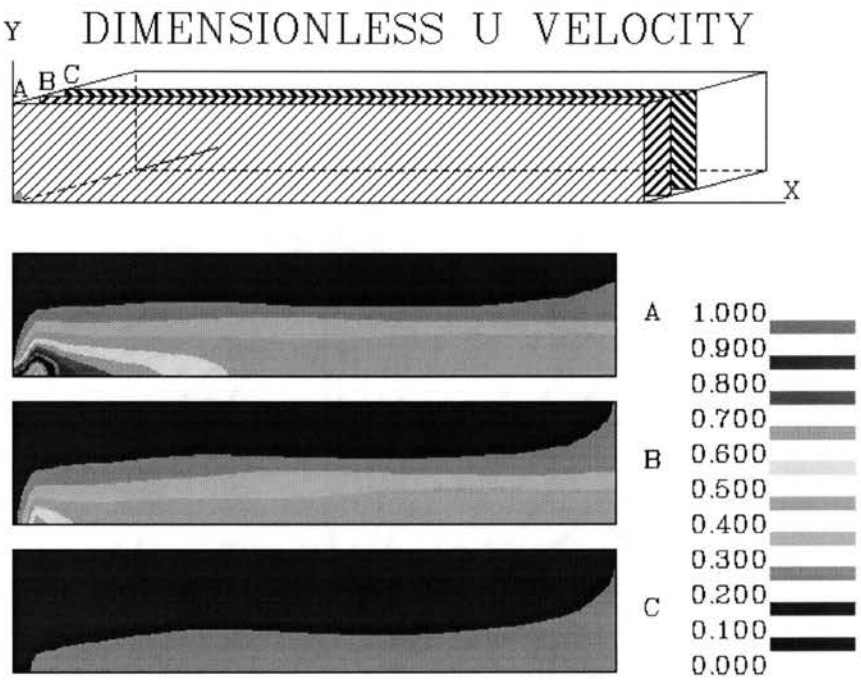

(a) Longitudinal Slices

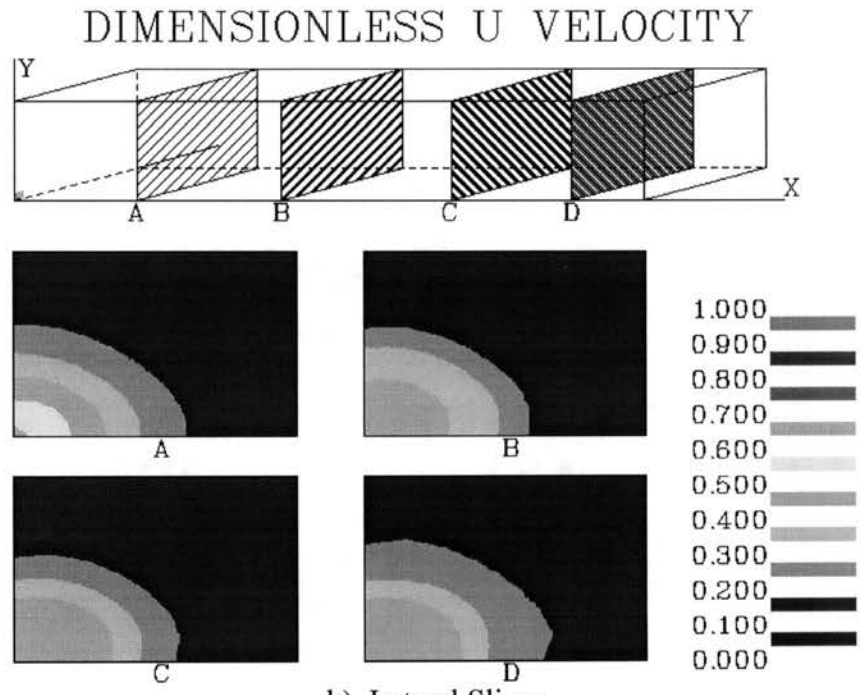

b) Lateral Slices

Figure 40. Dimensionless Axial Velocity for the VR=0.1 Reacting Jet. (Test Case 4)

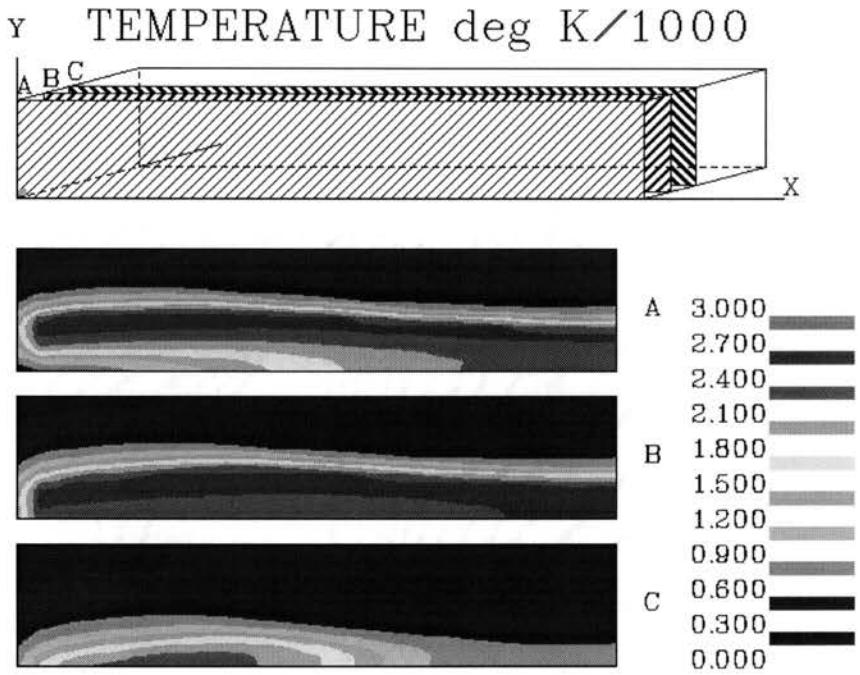

(a) Longitudinal Slices

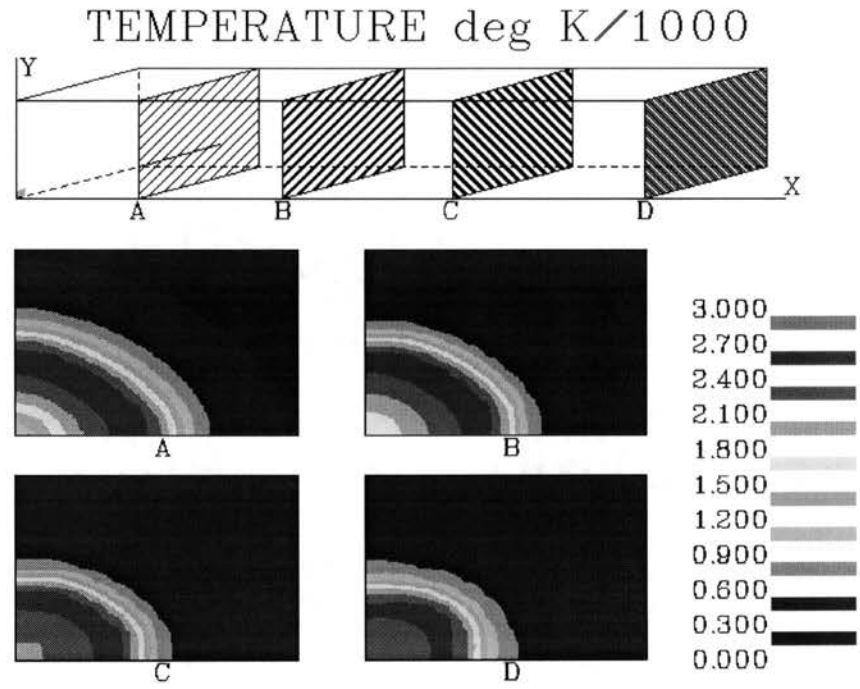

b) Lateral Slices

Figure 41. Temperature Distribution for the VR=0.1 Reacting Jet. (Test Case 4)

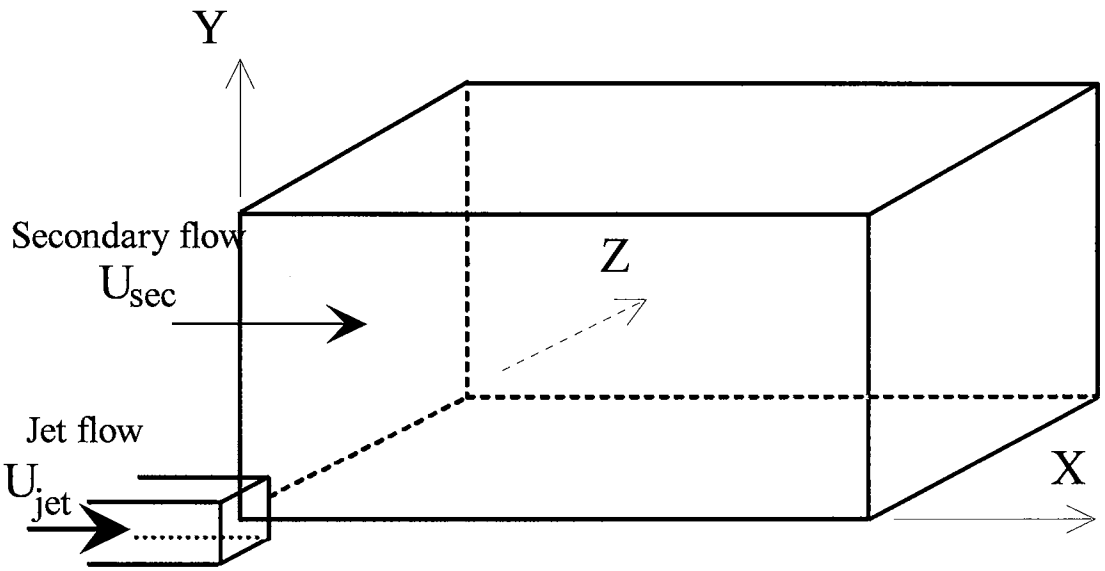

Free Jet of CH_4 Emerging into Co-flowing Flow of Air at 300 K

Solution Domain	: 0.525 x 0.06 x 0.06 m	
Jet Diameter	: 0.01155 m	
$U_{sec} / U_{jet} = 0.1$	: $U_{jet} = 50$ m/sec,	$U_{sec} = 5$ m/sec
$U_{sec} / U_{jet} = 0.3$	: $U_{jet} = 50$ m/sec,	$U_{sec} = 15$ m/sec
$U_{sec} / U_{jet} = 0.5$	: $U_{jet} = 50$ m/sec,	$U_{sec} = 25$ m/sec
ρ_{jet} (Density of CH_4)	: 0.65 kg/m^3	
ρ_{sec} (Density of Air)	: 1.2 kg/m^3	
Temperature of Air	: 300 K	

Figure 42. Solution Domain for Diffusion Flames of a Round Jet of Methane in a Co-flowing Stream of Air. (Test Case 5)

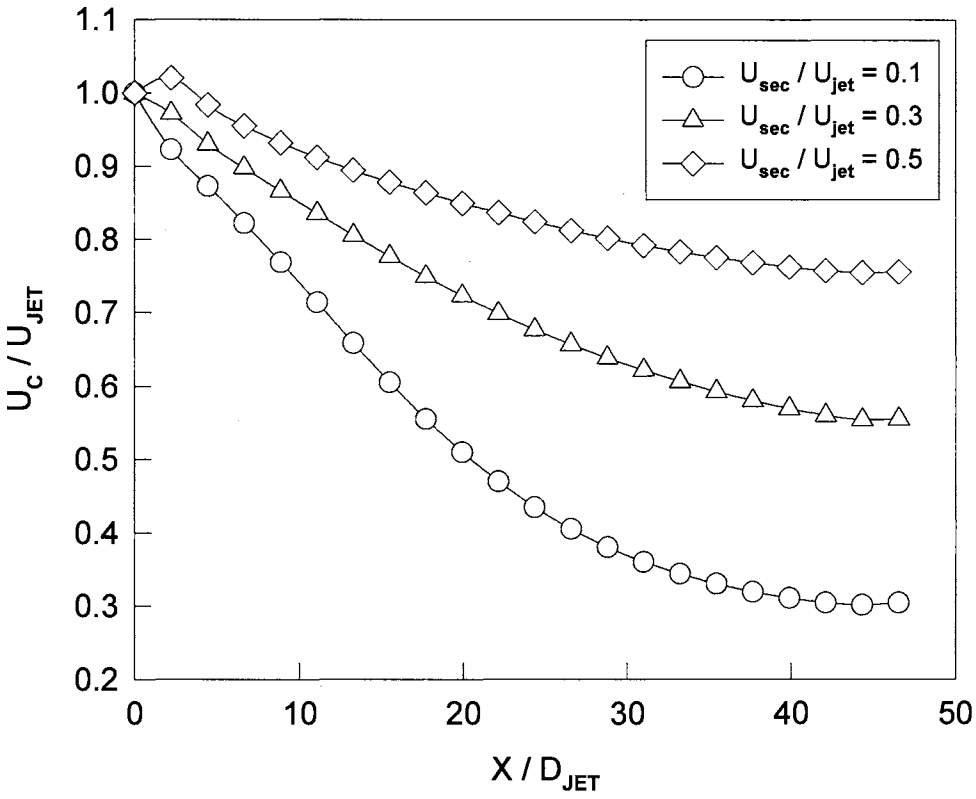

Figure 43. Effect of Velocity Ratio on Centerline Velocity Decay. (Test Case 5)

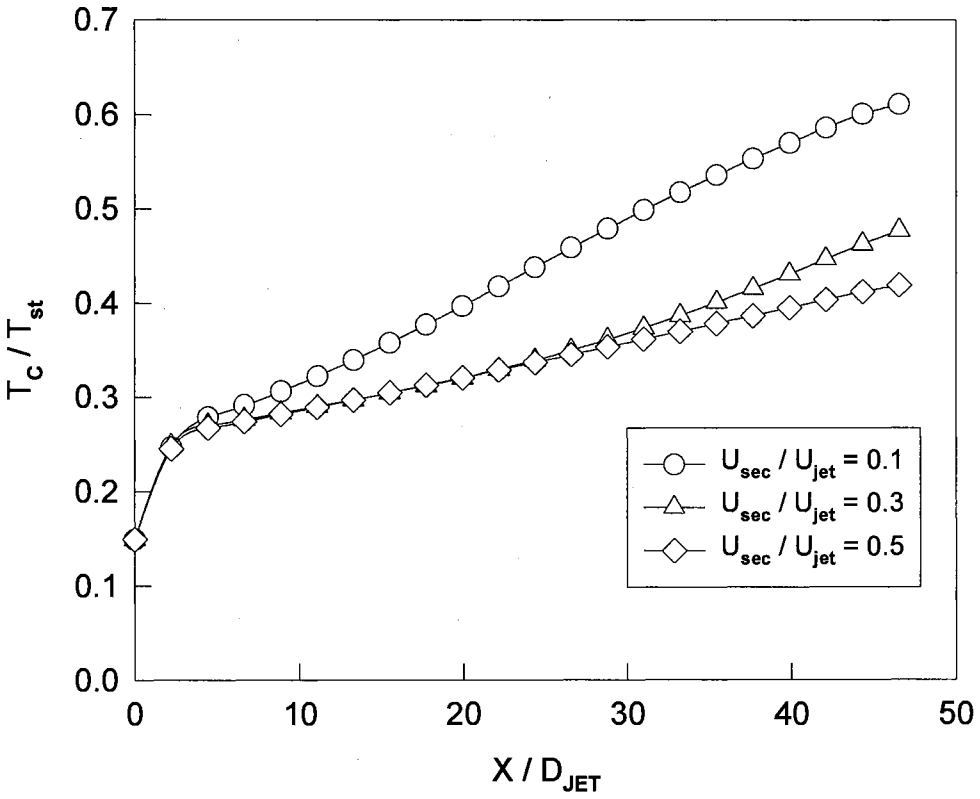

Figure 44. Effect of Velocity Ratio on Centerline Temperature Decay. (Test Case 5)

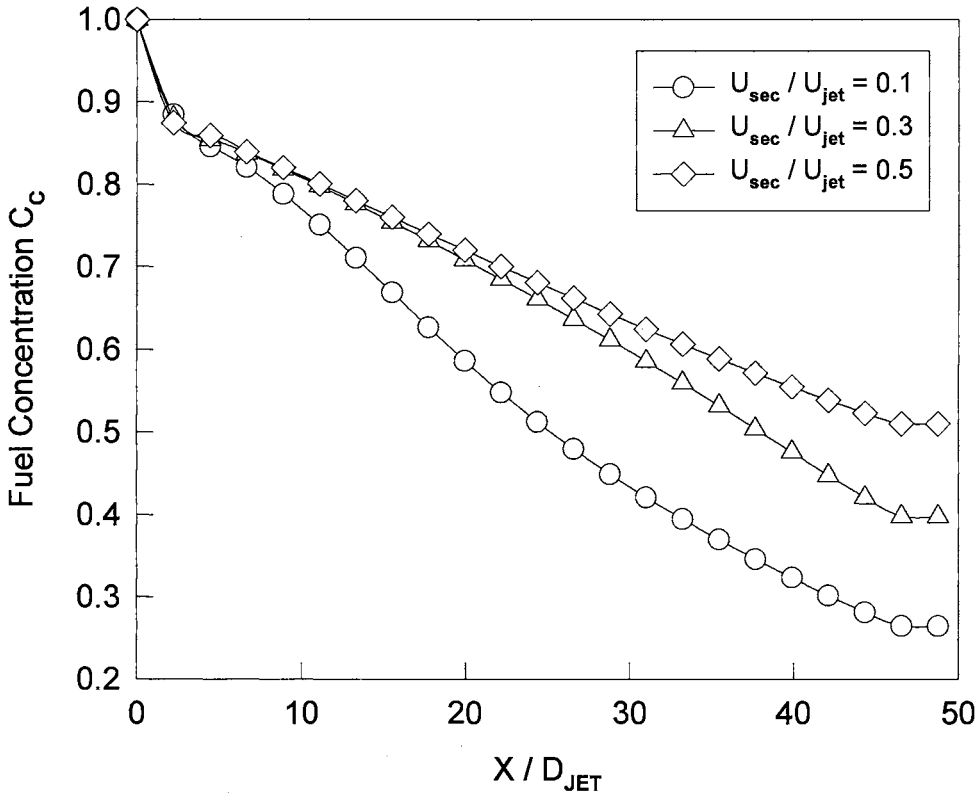

Figure 45. Effect of Velocity Ratio on Centerline Unburned Fuel Fraction . (Test Case 5)

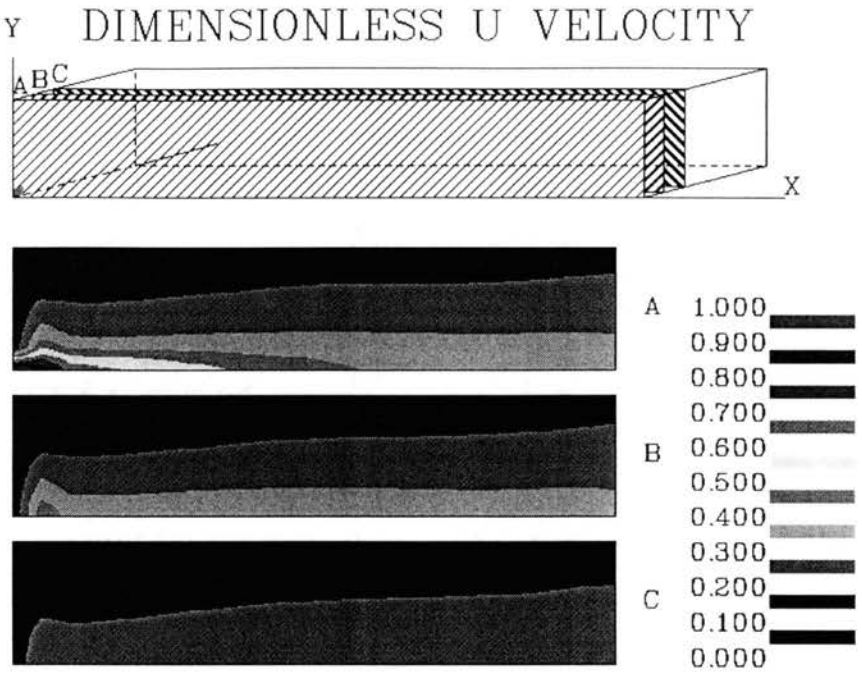

(a) Longitudinal Slices

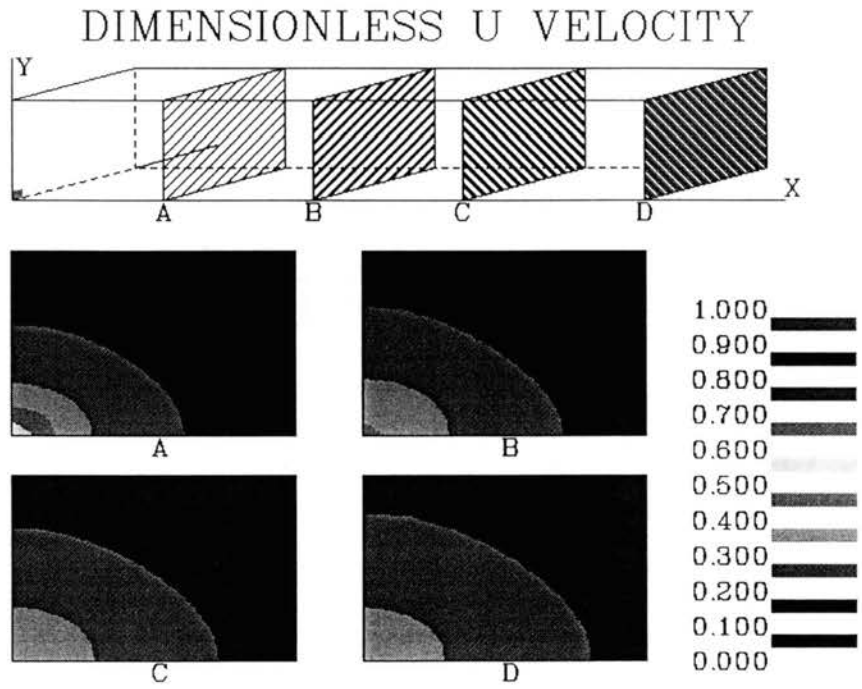

b) Lateral Slices

Figure 46. Dimensionless Axial Velocity for the VR=0.1 Reacting Jet Case. (Test Case 5)

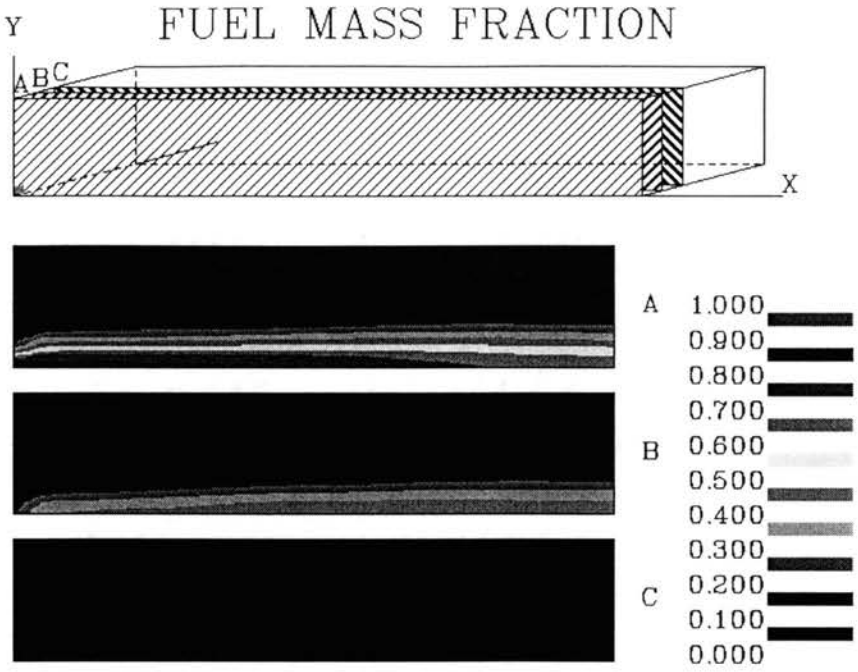

(a) Longitudinal Slices

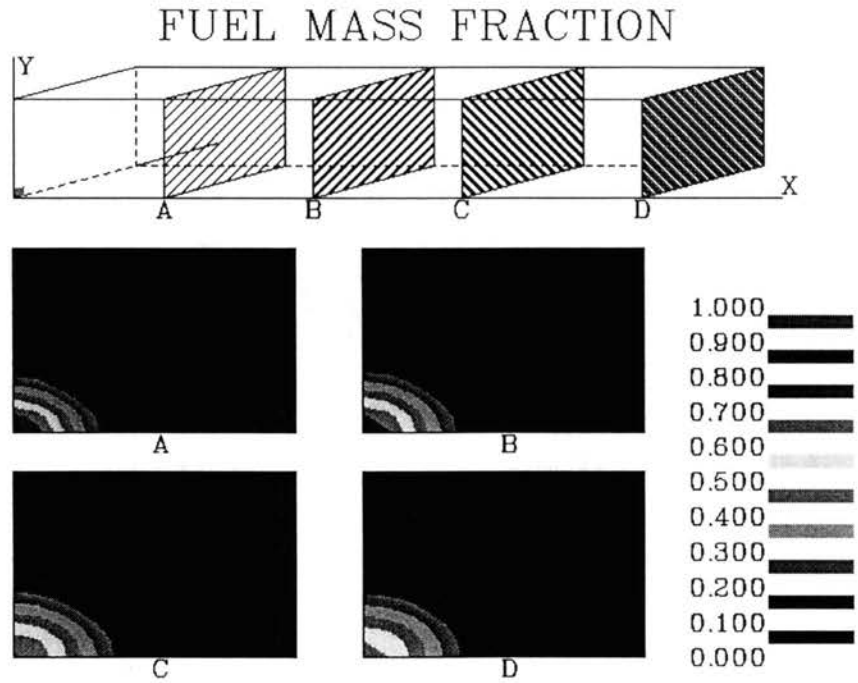

b) Lateral Slices

Figure 47. Unburned Fuel Mass Fraction for the VR=0.1 Reacting Jet Case. (Test Case 5)

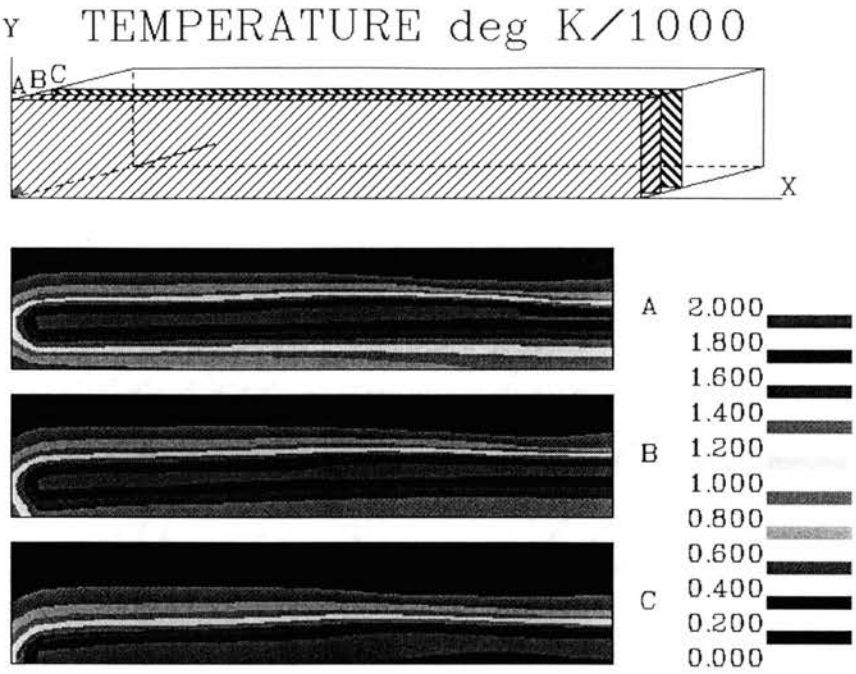

(a) Longitudinal Slices

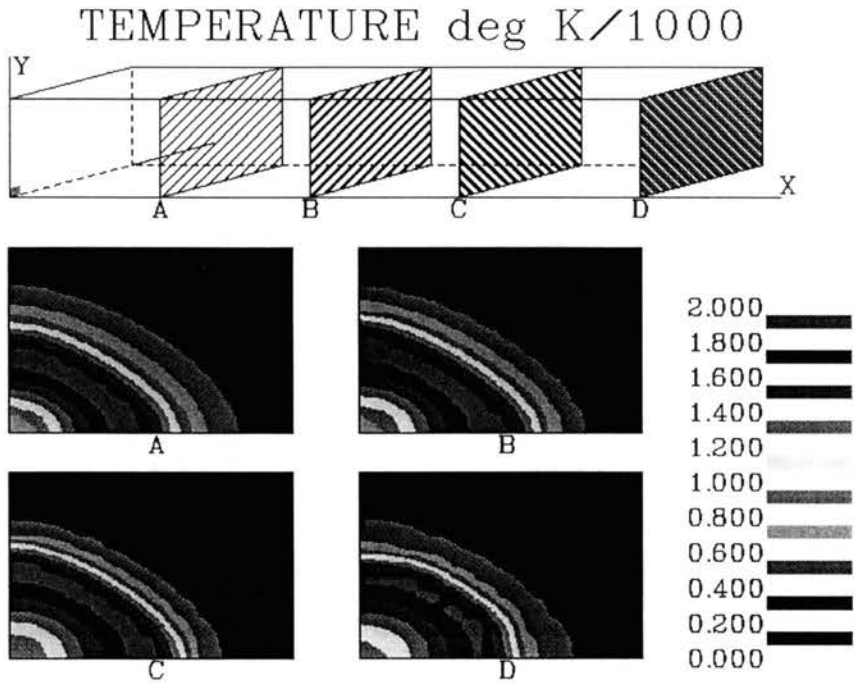

b) Lateral Slices

Figure 48. Temperature Distribution for the VR=0.1 Reacting Jet Case. (Test Case 5)

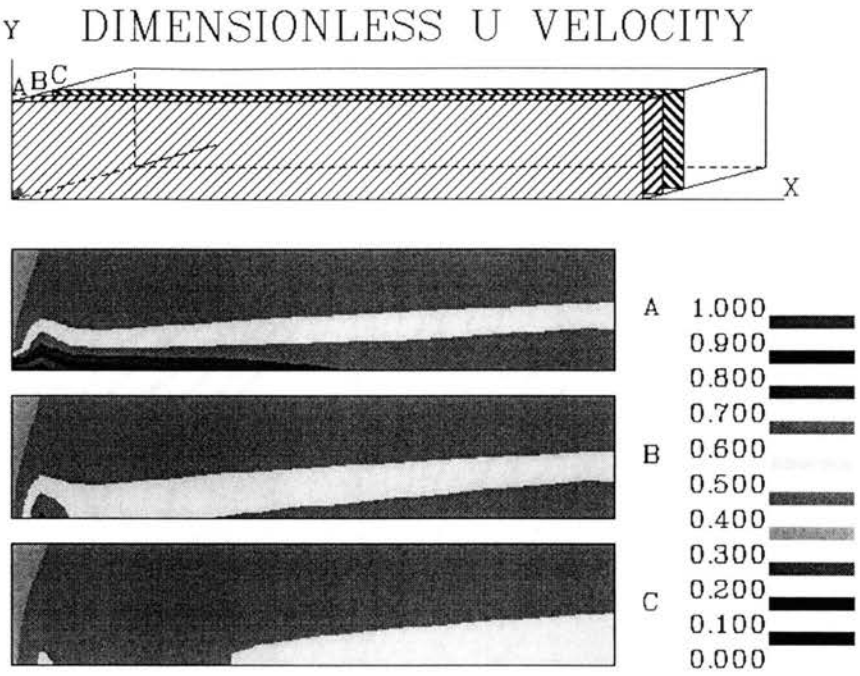

(a) Longitudinal Slices

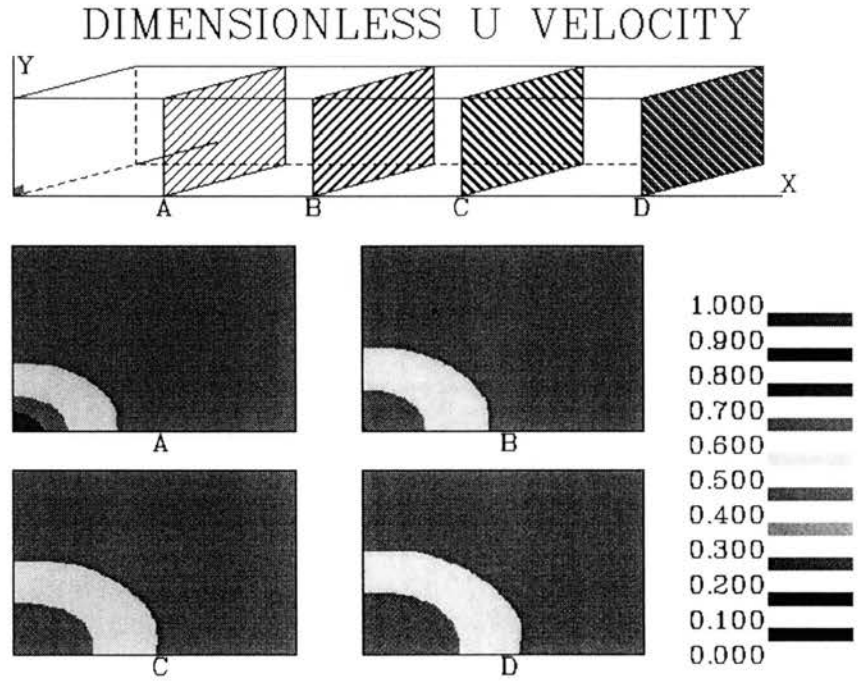

b) Lateral Slices

Figure 49. Dimensionless Axial Velocity for the VR=0.3 Reacting Jet Case. (Test Case 5)

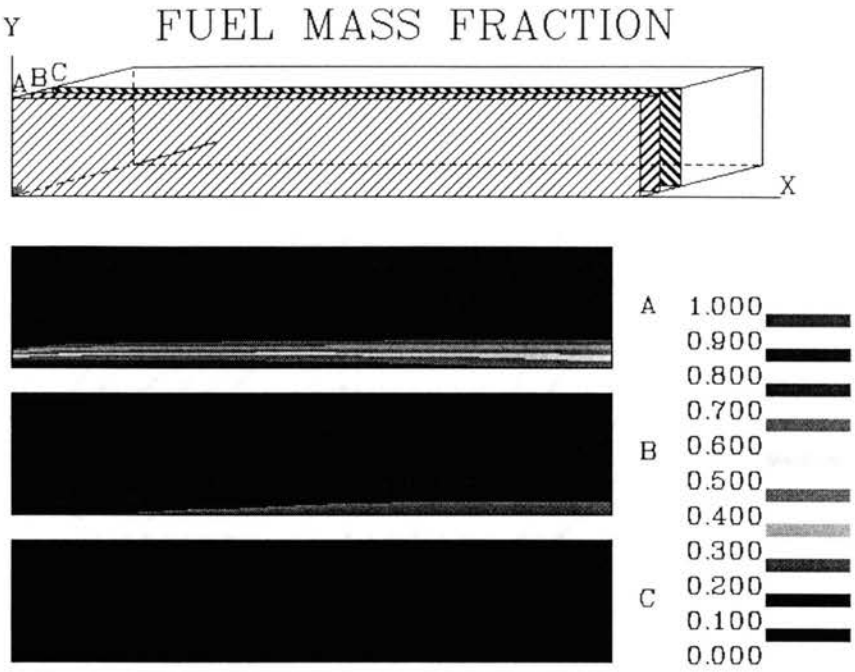

(a) Longitudinal Slices

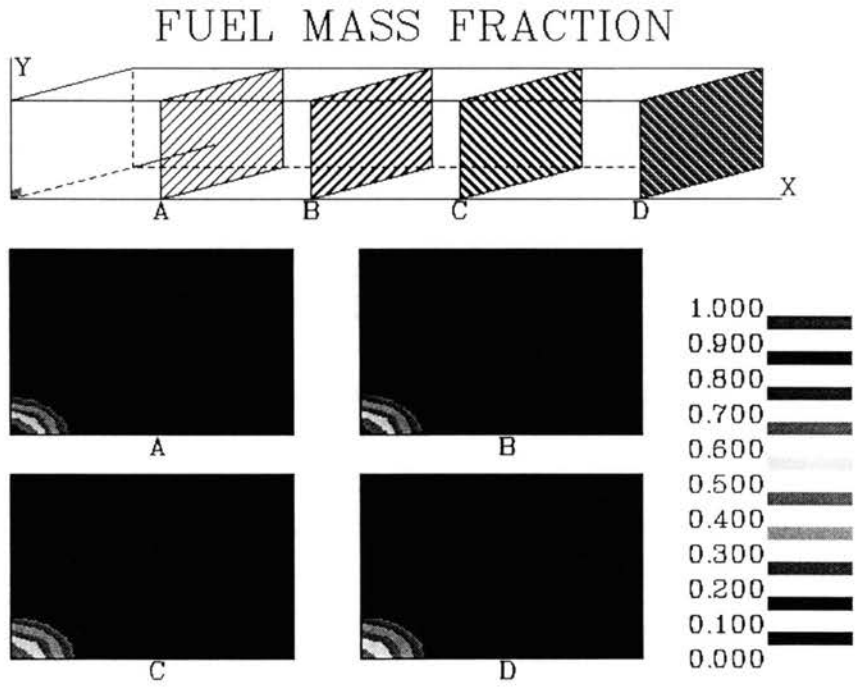

b) Lateral Slices

Figure 50. Unburned Fuel Mass Fraction for the VR=0.3 Reacting Jet Case. (Test Case 5)

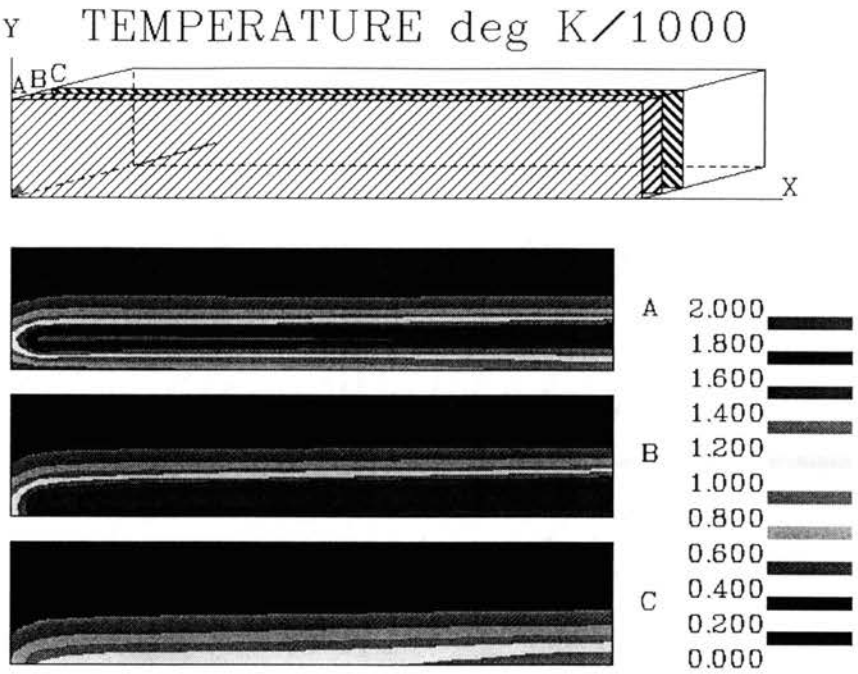

(a) Longitudinal Slices

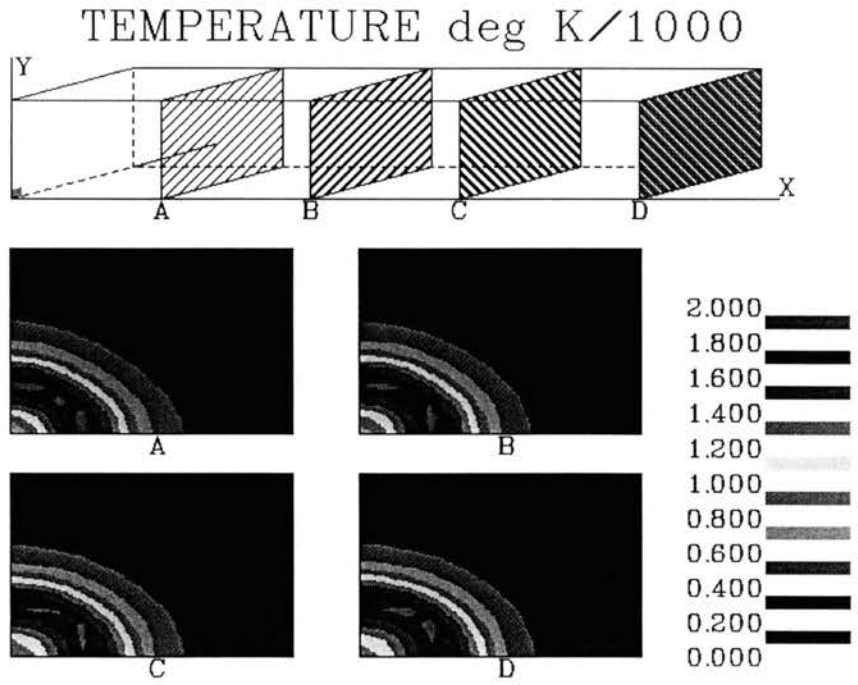

b) Lateral Slices

Figure 51. Temperature Distribution for the VR=0.3 Reacting Jet Case. (Test Case 5)

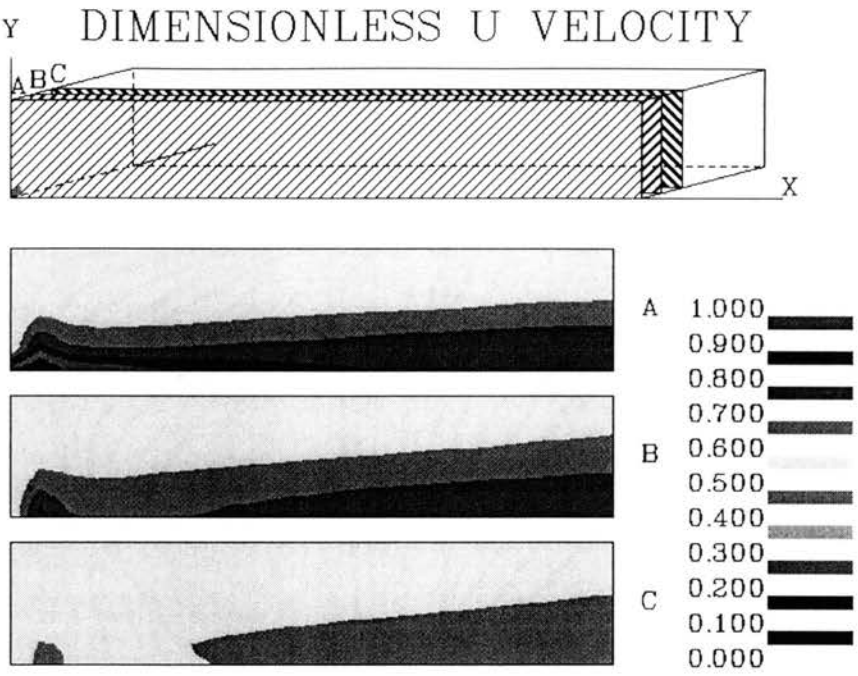

(a) Longitudinal Slices

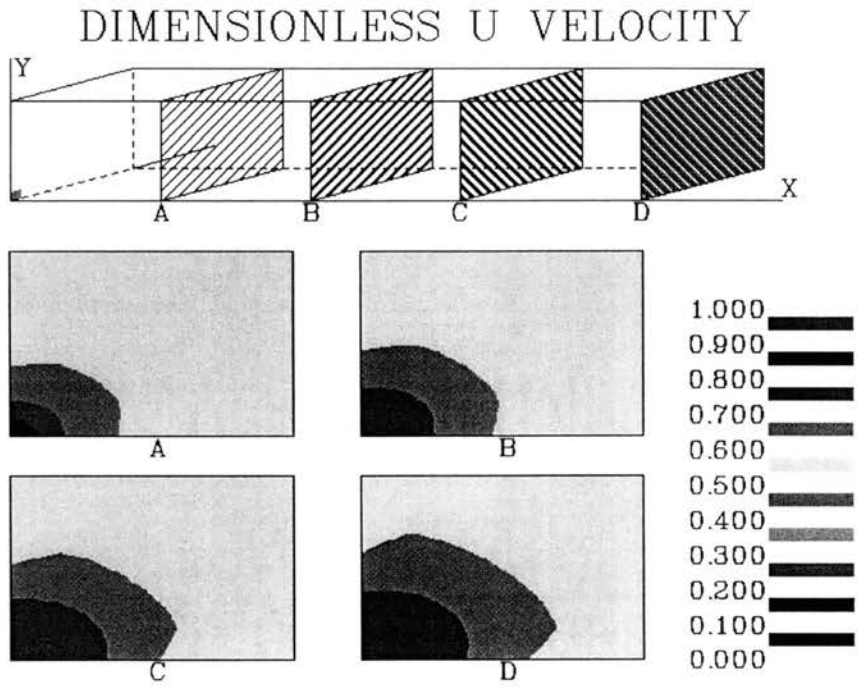

b) Lateral Slices

Figure 52. Dimensionless Axial Velocity for the VR=0.5 Reacting Jet Case. (Test Case 5)

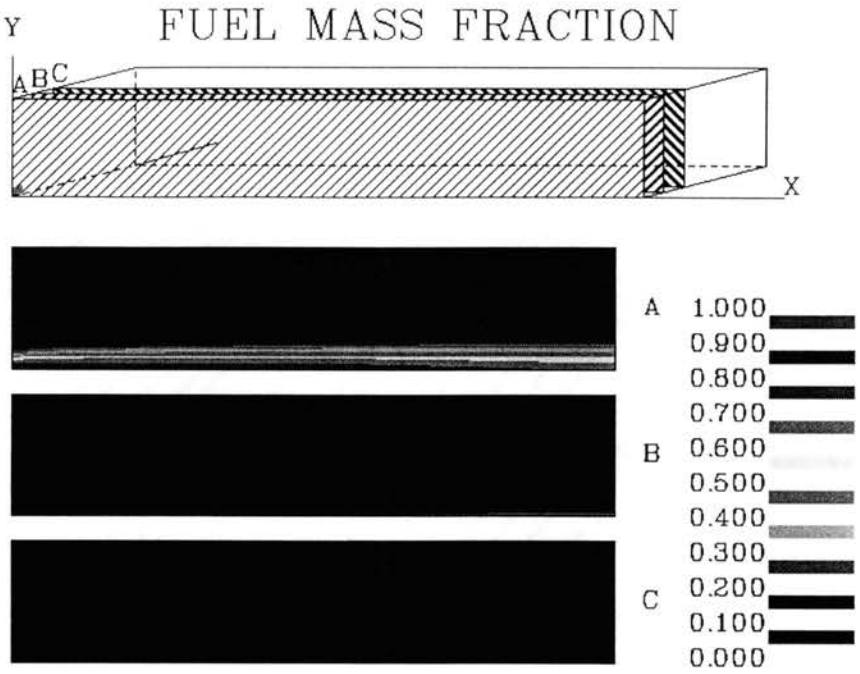

(a) Longitudinal Slices

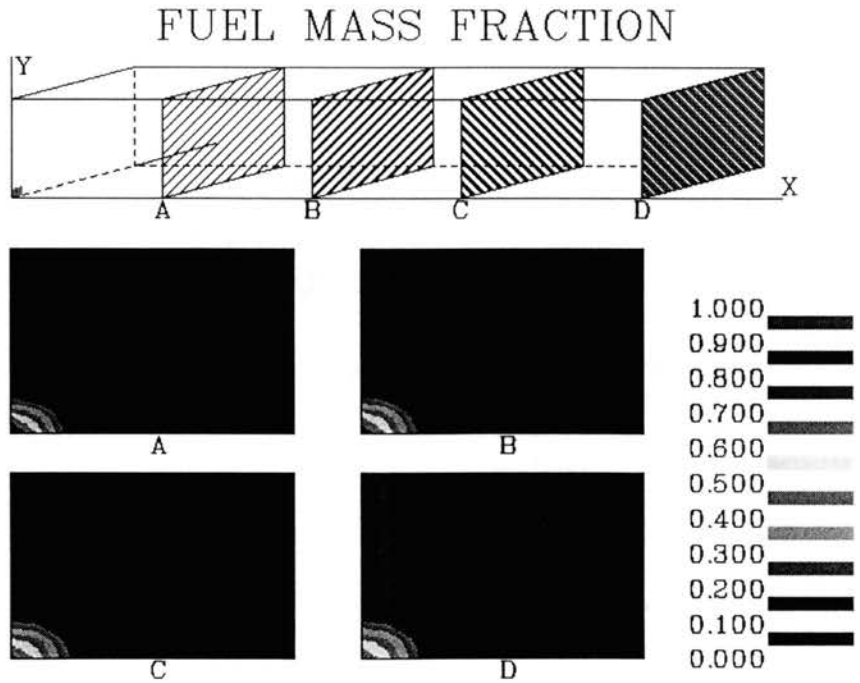

b) Lateral Slices

Figure 53. Unburned Fuel Mass Fraction for the VR=0.5 Reacting Jet Case. (Test Case 5)

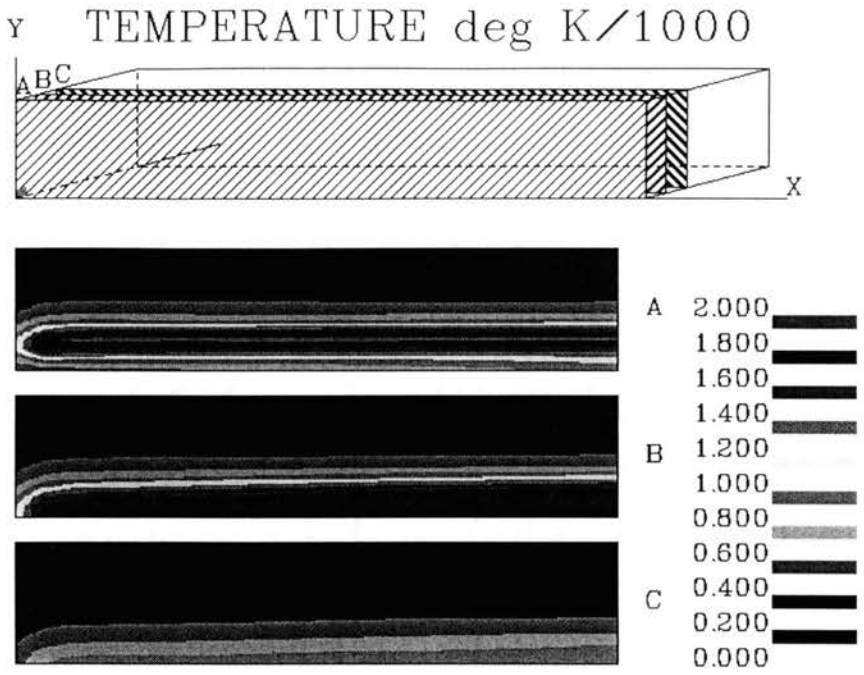

(a) Longitudinal Slices

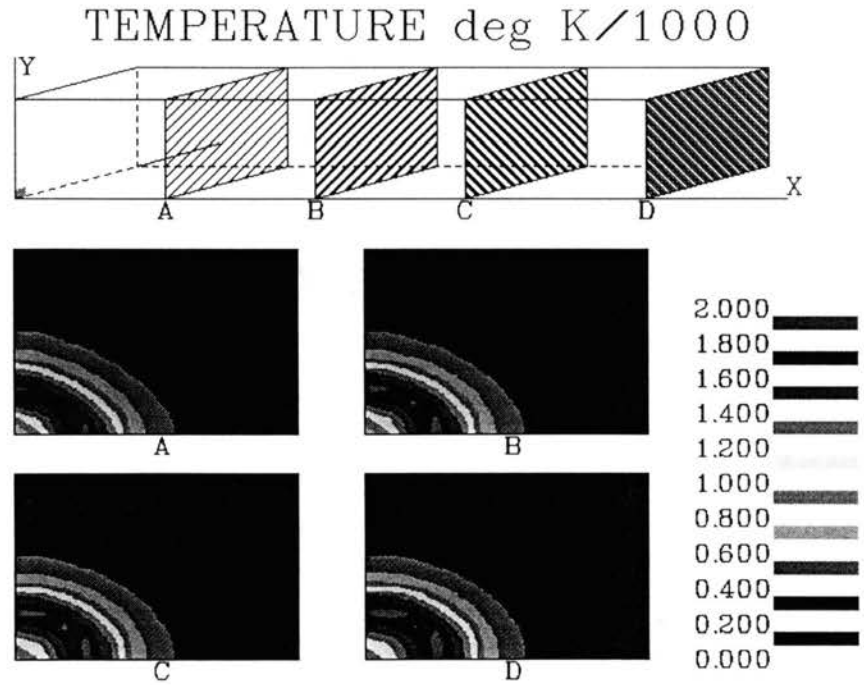

b) Lateral Slices

Figure 54. Temperature Distribution for the VR=0.5 Reacting Jet Case. (Test Case 5)

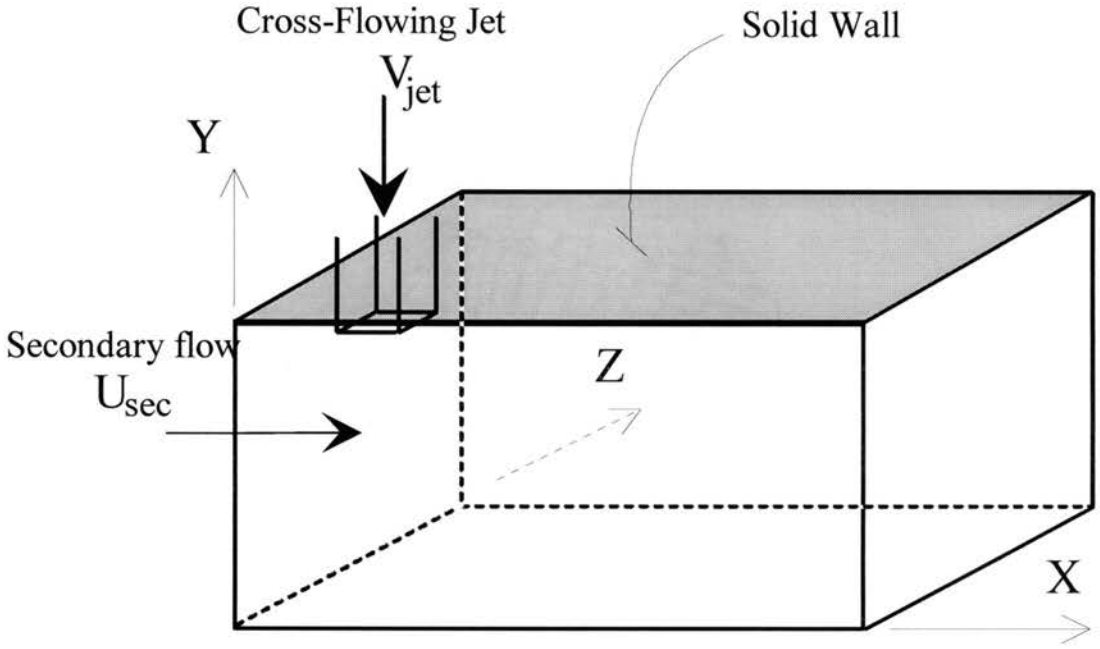

Free Jet of CH_4 Emerging into Cross-flowing Flow of Air at 300 K

Solution Domain	: 0.55 x 0.084 x 0.06 m
Jet Diameter	: 0.01826 m
V_{jet}	: 50 m/sec
ρ_{jet} (Density)	: 0.65 kg/m^3
T_{jet} (Temperature)	: 300 K
U_{sec}	: 15, 20, 25 m/sec
ρ_{sec} (Density)	: 1.2 kg/m^3
T_{sec} (Temperature)	: 300 K

Figure 55. Solution Domain for Diffusion Flames of a Round Jet of Methane in a Cross-flowing Stream of Air. (Test Case 6)

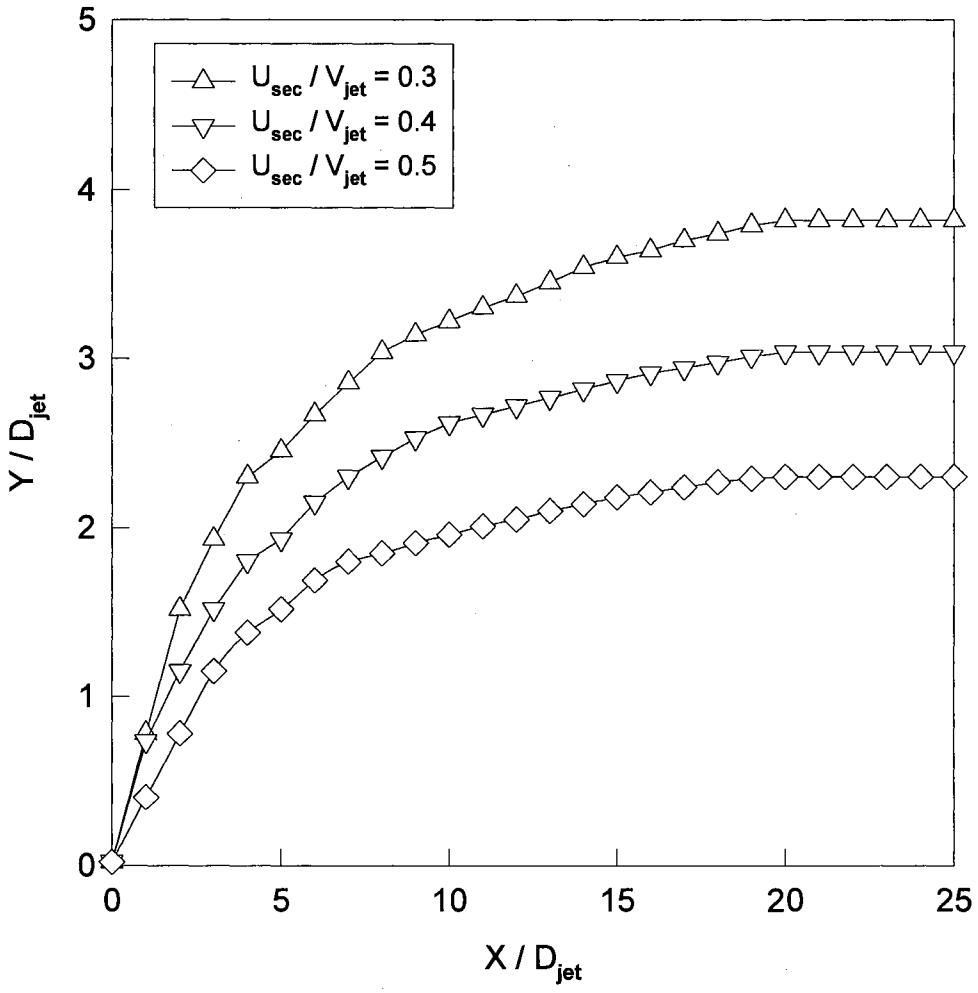

Figure 56. Effect of Cross-flow Velocity Ratio on Maximum Velocity Centerline Location. (Test Case 6)

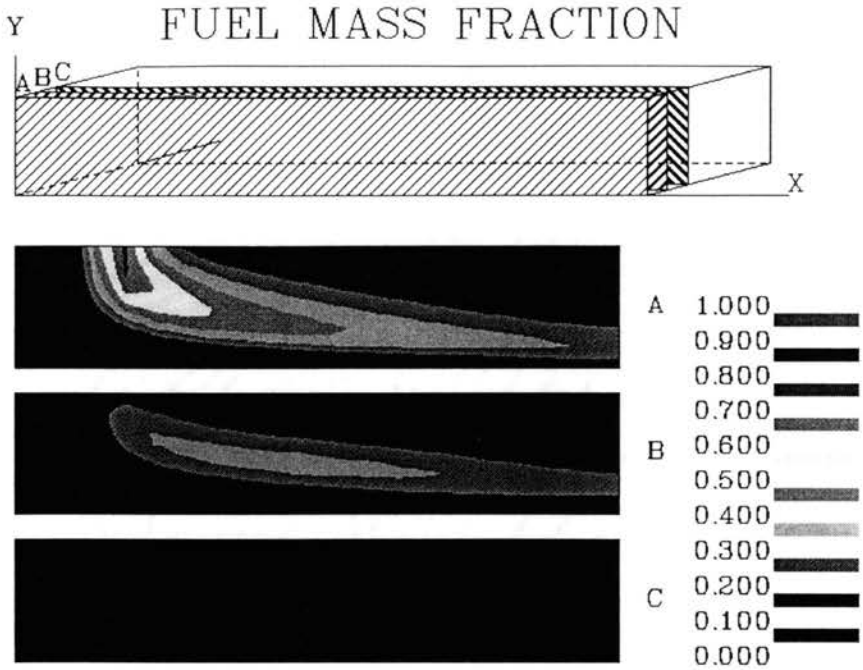

(a) Longitudinal Slices

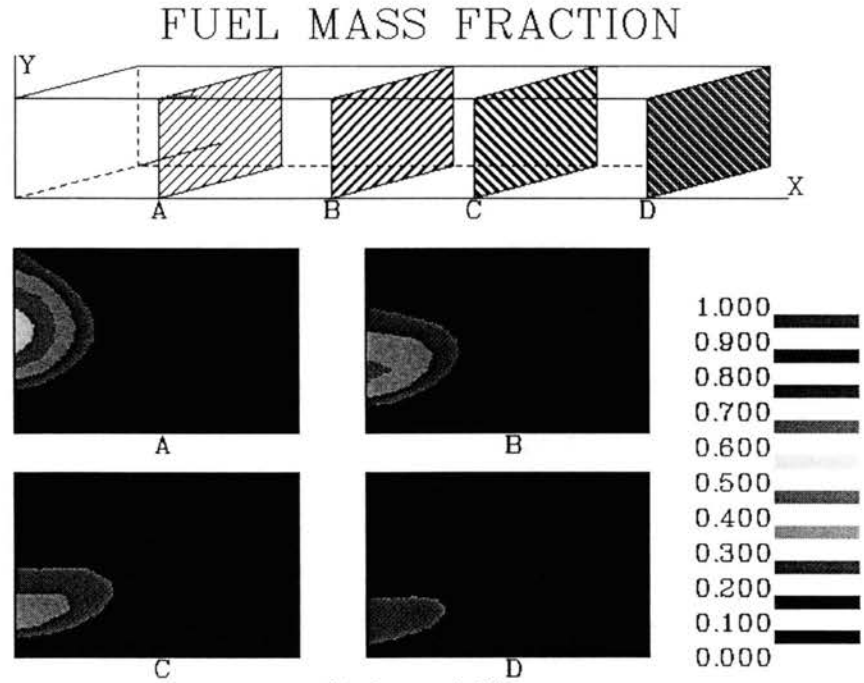

b) Lateral Slices

Figure 57 Unburned Fuel Mass Fraction for the VR=0.3 Reacting Jet Case. (Test Case 6)

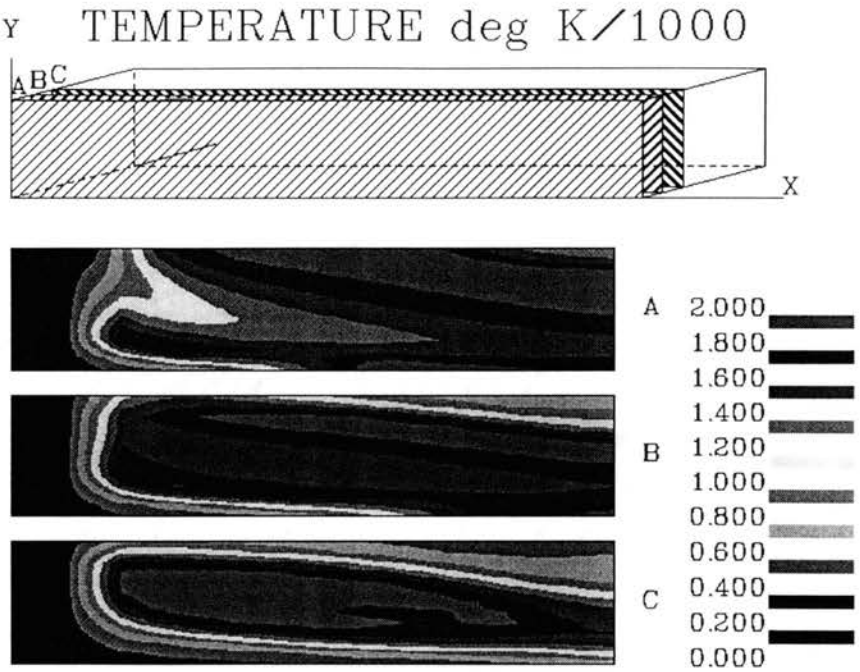

(a) Longitudinal Slices

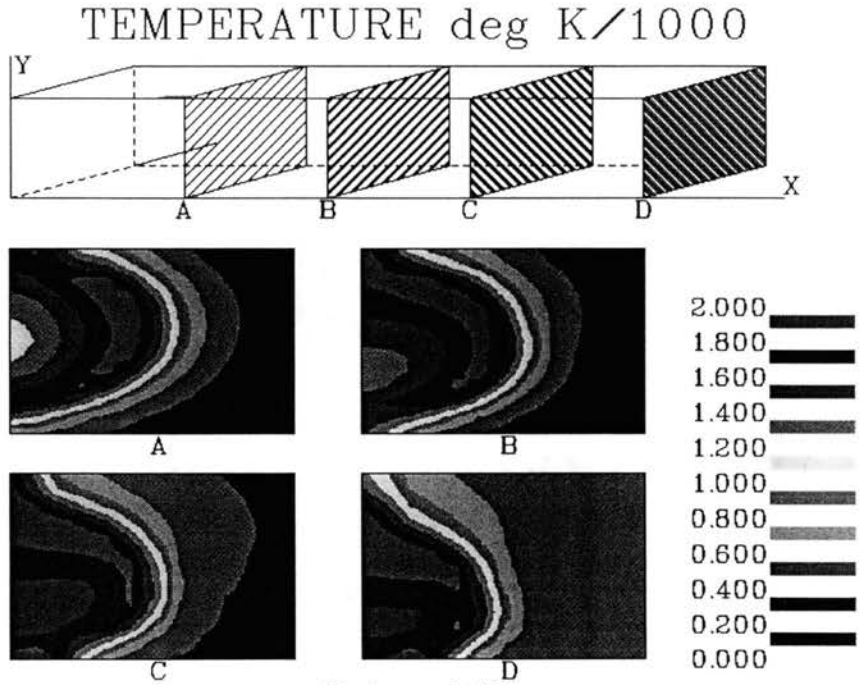

b) Lateral Slices

Figure 58 Temperature Distribution for the VR=0.3 Reacting Jet Case. (Test Case 6)

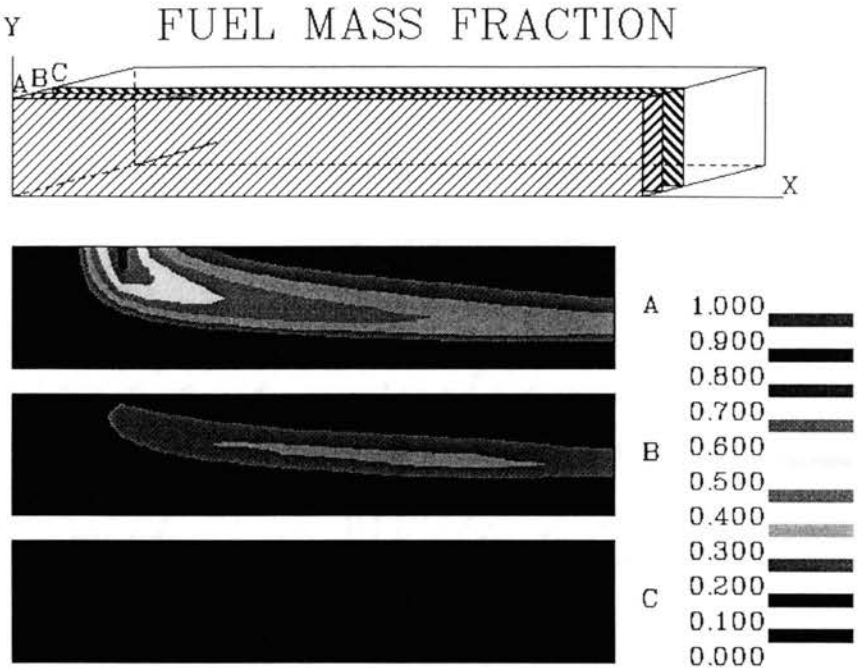

(a) Longitudinal Slices

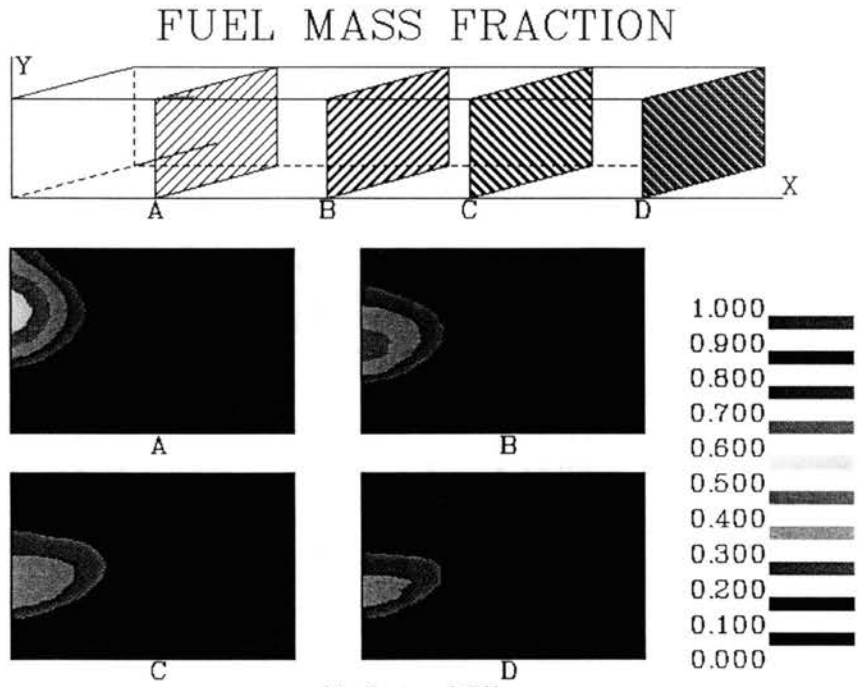

b) Lateral Slices

Figure 59 Unburned Fuel Mass Fraction for the VR=0.4 Reacting Jet Case. (Test Case 6)

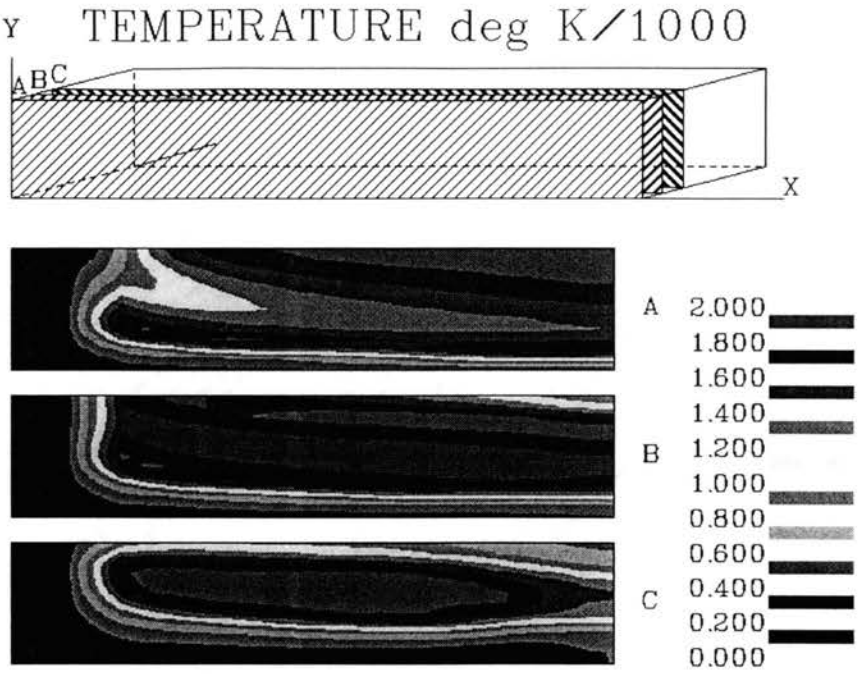

(a) Longitudinal Slices

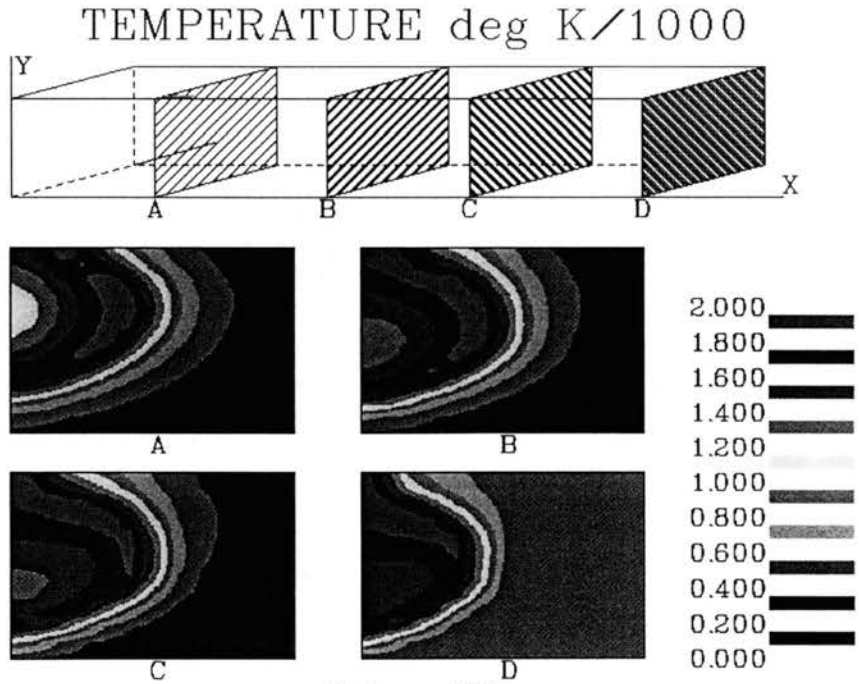

b) Lateral Slices

Figure 60. Temperature Distribution for the VR=0.4 Reacting Jet Case. (Test Case 6)

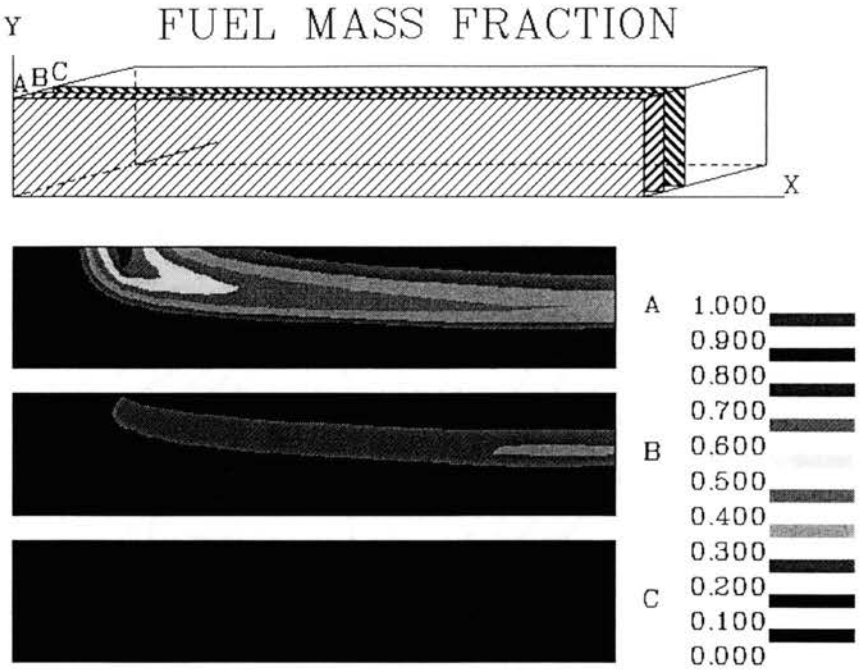

(a) Longitudinal Slices

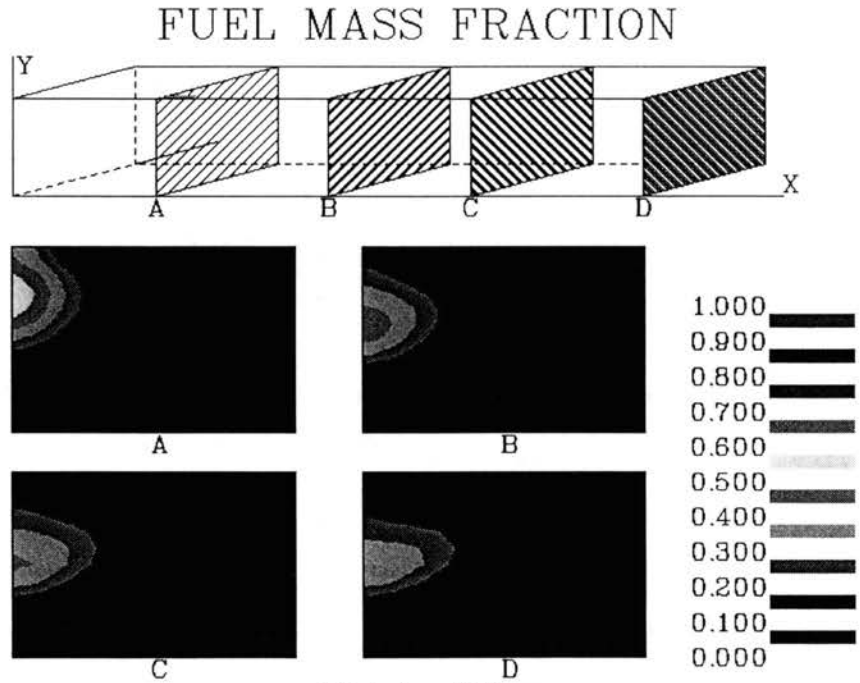

b) Lateral Slices

Figure 61. Unburned Fuel Mass Fraction for the VR=0.5 Reacting Jet Case. (Test Case 6)

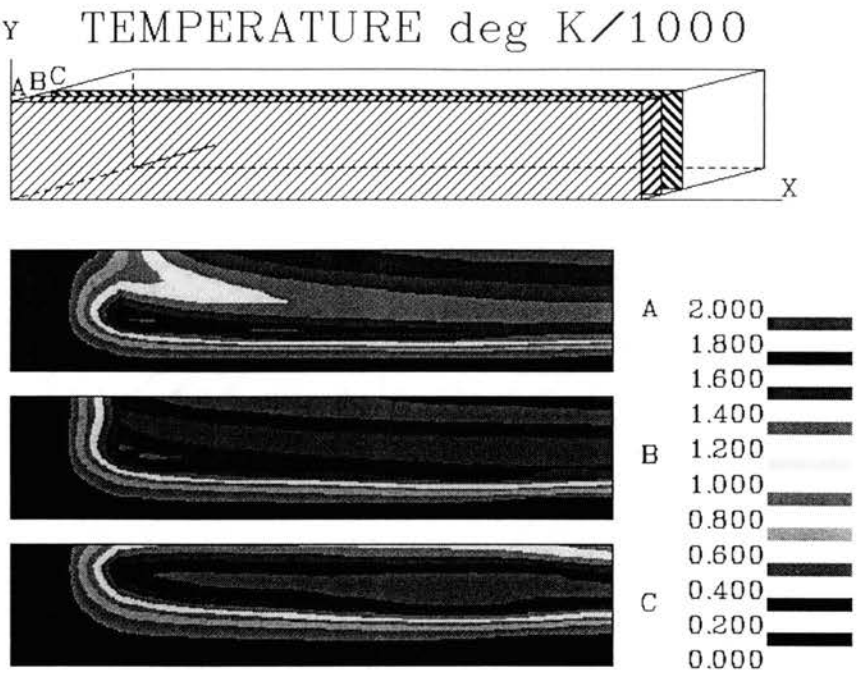

(a) Longitudinal Slices

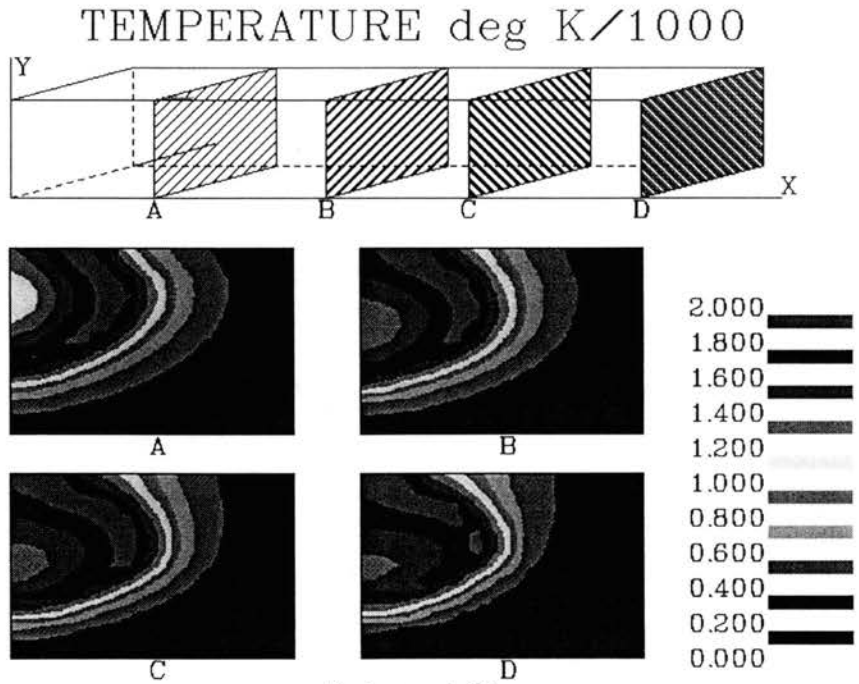

b) Lateral Slices

Figure 62. Temperature Distribution for the VR=0.5 Reacting Jet Case. (Test Case 6)

APPENDIX C

LIST OF A TYPICAL DATA FILE

36	14	14	.272000E+00	.600000E-01	.600000E-01	
.0000E+00	.8000E-02	.1600E-01	.2400E-01	.3200E-01	.4000E-01	.4800E-01
.5600E-01	.6400E-01	.7200E-01	.8000E-01	.8800E-01	.9600E-01	.1040E+00
.1120E+00	.1200E+00	.1280E+00	.1360E+00	.1440E+00	.1520E+00	.1600E+00
.1680E+00	.1760E+00	.1840E+00	.1920E+00	.2000E+00	.2080E+00	.2160E+00
.2240E+00	.2320E+00	.2400E+00	.2480E+00	.2560E+00	.2640E+00	.2720E+00
.0000E+00	.5000E-02	.1000E-01	.1500E-01	.2000E-01	.2500E-01	.3000E-01
.3500E-01	.4000E-01	.4500E-01	.5000E-01	.5500E-01	.6000E-01	
.0000E+00	.5000E-02	.1000E-01	.1500E-01	.2000E-01	.2500E-01	.3000E-01
.3500E-01	.4000E-01	.4500E-01	.5000E-01	.5500E-01	.6000E-01	
DIMENSIONLESS U VELOCITY						
.7530E+00	.5000E+00	.0000E+00	.0000E+00	.0000E+00	.0000E+00	.0000E+00
.0000E+00	.0000E+00	.0000E+00	.0000E+00	.0000E+00	.0000E+00	
.5000E+00	.2500E+00	.0000E+00	.0000E+00	.0000E+00	.0000E+00	.0000E+00
.0000E+00	.0000E+00	.0000E+00	.0000E+00	.0000E+00	.0000E+00	
-.1857E-02	-.1843E-02	-.1807E-02	-.1756E-02	-.1699E-02	-.1641E-02	-.1588E-02
-.1541E-02	-.1502E-02	-.1472E-02	-.1449E-02	-.1434E-02	-.1429E-02	
-.1776E-02	-.1765E-02	-.1736E-02	-.1695E-02	-.1648E-02	-.1600E-02	-.1555E-02
-.1516E-02	-.1482E-02	-.1455E-02	-.1434E-02	-.1421E-02	-.1416E-02	
-.1749E-02	-.1739E-02	-.1712E-02	-.1674E-02	-.1631E-02	-.1586E-02	-.1544E-02
-.1507E-02	-.1475E-02	-.1449E-02	-.1429E-02	-.1416E-02	-.1412E-02	
...	...	...	...	...	...	...
...	...	...	...	...	...	...
DIMENSIONLESS V VELOCITY						
.0000E+00	.0000E+00	.0000E+00	.0000E+00	.0000E+00	.0000E+00	.0000E+00
.0000E+00	.0000E+00	.0000E+00	.0000E+00	.0000E+00	.0000E+00	
.5764E-02	-.4639E-02	-.1207E-01	-.6982E-02	-.3788E-02	-.2159E-02	-.1314E-02
-.8519E-03	-.5858E-03	-.4279E-03	-.3353E-03	-.2865E-03	-.2712E-03	

-.2481E-01	-.2180E-01	-.1526E-01	-.9387E-02	-.5683E-02	-.3527E-02	-.2275E-02
-.1532E-02	-.1080E-02	-.8021E-03	-.6354E-03	-.5463E-03	-.5182E-03	
-.1987E-01	-.1772E-01	-.1321E-01	-.9069E-02	-.6075E-02	-.4084E-02	-.2795E-02
-.1965E-02	-.1429E-02	-.1084E-02	-.8721E-03	-.7565E-03	-.7198E-03	
-.1396E-01	-.1287E-01	-.1040E-01	-.7813E-02	-.5677E-02	-.4082E-02	-.2948E-02
-.2160E-02	-.1620E-02	-.1259E-02	-.1029E-02	-.9020E-03	-.8613E-03	
-.9888E-02	-.9333E-02	-.7986E-02	-.6409E-02	-.4956E-02	-.3763E-02	-.2844E-02
-.2161E-02	-.1669E-02	-.1326E-02	-.1102E-02	-.9762E-03	-.9354E-03	
-.7150E-02	-.6853E-02	-.6092E-02	-.5122E-02	-.4150E-02	-.3288E-02	-.2578E-02
-.2020E-02	-.1601E-02	-.1298E-02	-.1096E-02	-.9796E-03	-.9419E-03	
-.5226E-02	-.5058E-02	-.4610E-02	-.4004E-02	-.3356E-02	-.2747E-02	-.2217E-02
-.1782E-02	-.1443E-02	-.1191E-02	-.1018E-02	-.9183E-03	-.8855E-03	
-.3791E-02	-.3692E-02	-.3420E-02	-.3037E-02	-.2609E-02	-.2187E-02	-.1805E-02
-.1480E-02	-.1219E-02	-.1020E-02	-.8823E-03	-.8012E-03	-.7745E-03	
-.2649E-02	-.2590E-02	-.2425E-02	-.2186E-02	-.1910E-02	-.1628E-02	-.1366E-02
-.1137E-02	-.9483E-03	-.8028E-03	-.7002E-03	-.6393E-03	-.6192E-03	
-.1683E-02	-.1649E-02	-.1555E-02	-.1415E-02	-.1250E-02	-.1078E-02	-.9143E-03
-.7688E-03	-.6472E-03	-.5521E-03	-.4845E-03	-.4441E-03	-.4307E-03	
-.8177E-03	-.8025E-03	-.7592E-03	-.6946E-03	-.6173E-03	-.5360E-03	-.4576E-03
-.3871E-03	-.3276E-03	-.2808E-03	-.2473E-03	-.2273E-03	-.2206E-03	
...	...	...	...	...	...	...
...	...	...	...	...	...	...

VITA

TZER-KUN LIN

Candidate for the Degree of

Doctor of Philosophy

Thesis : THREE-DIMENSIONAL COMBUSTION CALCULATIONS AND GRAPHIC DISPLAY

Major Field : Mechanical Engineering

Biographical :

Personal Data : Born in Hsin-Chu, Taiwan, Republic of China, May 21, 1963, the son of Mr. Lin, Ging-Long and Mrs. Lin Chang, Li-Hua. Married to Lee, Chian-Huat on Sep. 4, 1991.

Education : Graduated form Hsin-Chu Senior High School, Taiwan, R. O. C., in June, 1981; received Bachelor of Science degree in Mechanical Engineering from National Taiwan Cheng Kung University in June, 1985; received Master of Science degree in the School of Mechanical and Aerospace Engineering from Oklahoma State University, Stillwater, Oklahoma, in December, 1990; completed requirements for the Doctor of Philosophy degree with a major in Mechanical and Aerospace Engineering at Oklahoma State University, in December, 1995.

Professional Experience : Teaching Assistant, Department of Mechanical Engineering, Oklahoma State University, August 1990 to May 1994. Research Assistant, Fluid Engineering Services Inc., Stillwater, Oklahoma, January 1991 to August 1994.